Identifying Mineralogical and Geochemical Vectors towards the Epithermal Au-Ag Correnso Mine, Waihi

A thesis

submitted in partial fulfilment

of the requirements for the degree

of

Masters of Science in Earth Sciences

at

The University of Waikato

by

Ravinder Sardul Singh

THE UNIVERSITY OF
WAIKATO
Te Whare Wānanga o Waikato

2015

Abstract

The Au-Ag rich Correnso vein is a low sulphidation epithermal deposit located east of Waihi and is named after the clay mineral correnside. Hydrothermally altered andesitic and dacitic host rocks of the Waipupu Formation, informally subdivided into Upper Andesite and Lower Andesite units, contain Au-Ag rich quartz veins. The interaction of hot, dominantly meteoric water with the host rocks causes mineralogical and geochemical changes. Hydrothermal alteration manifested as mineralogical alteration and geochemical signatures can help in identifying vectors to constrain potential areas of enhanced mineralization for exploration purposes. Hydrothermal alteration has been suggested to have potential as exploration vector for epithermal deposits in particular as alteration halos can extend up to considerable distances (Christie et al., 2001; Simpson and Mauk, 2004).

Visual core logging, petrography, pXRF, and Aqua-Regia/2-Acid Digest (ICP-MS) analysis were used in this study to analyse and quantify alteration zonation patterns and trace element metasomatism in order to identify vectors towards the mineralisation. Results suggest a clear mineralogical and geochemical alteration zonation pattern around the vein system with elevated concentrations of As, Sb, Zn, Pb, Se, and K. The unaltered, moderately altered and highly altered rocks are often adjacent to one another, implying that hydrothermal fluids have migrated through the host rocks in a highly heterogeneous fashion. The migration of fluids is likely controlled by both primary and secondary (e.g. fault/fracture) permeability. The overall mineralogical pattern can be described as quartz ± adularia ± sericite assemblage which is similar to the adjacent deposits of the Waihi area. Alteration zonation in the host rocks consists of potassic alteration proximal to the vein system surrounded by sericitic alteration, with illite-smectite dominated argillic assemblage overprinting both alteration types. Propylitic alteration is more prominent to the outward zones and distal to the mineralisation. Geochemical analysis shows enrichment of pathfinder elements such as As, Sb, Zn, Pb, Se, and K and depletion of Cu, Te and Se.

Acknowledgements

I would like to thank many people who helped and supported me to successfully finish this project. Firstly I would like to thank my chief supervisor Dr Shaun Barker for his immense support and guidance throughout the timeline of this project. Special thanks to Roger Briggs who shared his invaluable advice and knowledge besides helping me with the optical mineralogy. I would also like to thank David Lowe for his help and support for completing this project. Thanks to the technical staff of the department especially; Renat Radosinky, Annette Rodgers and Xu Ganqing for their help with thin slide preparation, XRF, and XRD analysis.

I would also like to thank Lorrance Tockler and Jackie Hobbins of Newmont Waihi Gold for providing significant logistical support, including access to the drill core samples and exploration data. This study was funded by University of Waikato School of Science Masters Research scholarship, AusIMM NZ Branch Education Endowment Trust Scholarship and SGS Waihi Analytical Support Scholarship.

I would like to thank my parents and family back home, and my friends in New Zealand at the university and in Auckland for their kind love and support. This study would not have been possible without the constant encouragement and support from my father.

Table of Contents

List of Figures

List of Tables

Chapter One

1. Introduction

1.1. Introduction

The Coromandel Volcanic Zone (CVZ), which hosts the Hauraki Goldfield, contains approximately 50 low-sulphidation (adularia-sericite) epithermal Au-Ag vein deposits and porphyry Cu deposits (Brathwaite et al. 1989). The Correnso deposit is part of the Waihi epithermal system together with the world class Martha Hill, Golden Cross, Favona, Moonlight, Union, and Trio deposits (Figure 1). It is a high grade, "blind" Au-Ag deposit, discovered recently in 2009 and is named after the clay mineral corrensite. The corrensite is associated with Au-Ag mineralisation in the deeper parts of the Waihi epithermal vein system (Hobbins et al., 2012). The regional occurrence of hydrothermal alteration in this area has the potential to be used to identify various mineralogical and geochemical vectors which can be used to vector towards Au-Ag epithermal veins.

This thesis is based on the results obtained through visual core logging, portable XRF (pXRF), Aqua-Regia (ICP-MS) analysis, and petrographical study describing mineralogy, hydrothermal alteration, and geochemistry of rocks around the deposit. The results indicate that the deposit has undergone intense hydrothermal alteration and exhibit alteration zonation patterns and distinct geochemical signatures which are in par with the classic low sulphidation epithermal deposits found in other places.

1.2. Study Objectives

The principal objective of this thesis is to study the mineralogy and geochemistry of the rocks around the Correnso epithermal vein system. This will give a better understanding of the distribution of mineralogical alteration halos and nature of the mineralization of these deposits, further assisting in identifying the factors

controlling the proximal or distal alteration zonation to the epithermal Au-Ag deposits.

1.3. Methodology

This study involved thorough understanding of the composition and nature of the rocks around the Correnso vein system. Drillcore logging and sample collection was done at Newmont Waihi Gold core shed. This involved recording and taking photos of all the visible features like alteration intensity and style, visible mineralogy, and weathering intensity. The samples were selected at 10 metre intervals throughout the length of the drill cores for geochemical and mineralogical analysis.

The laboratory analysis for the samples was done in stages. Firstly, portable XRF (p-XRF) analysis was carried on the whole rock samples. The rocks were then cut into small chips for the preparation of thin sections for optical mineralogy. The left over rock samples were crushed and powdered for p-XRF and XRD analysis. Powdered samples were also sent to SGS Waihi laboratory for ICP-MS and Aqua-Regia/2-Acid analysis. The detailed methodology is described in detail in the concerning analysis chapters.

1.4. Mine Location

The Waihi town is situated 140 kilometres southeast of Auckland and 75 kilometres east of Hamilton city on State Highway 2. The high grade Au-Ag Correnso deposit is part of the Waihi epithermal system together with the world class Martha Hill, Golden Cross, Favona, Moonlight, Union, and Trio deposits (Figure 1.1A & B). It is a “blind” underground deposit located east of Waihi town. The mine is currently operated by Newmont Waihi Gold, owned by Newmont Corporation. Correnso lies between Union Hill-Trio deposit to the south and the eastern end of the Martha vein to the north with surface coordinates being 396350 E and 396650 E. The drillcore samples are currently stored in Moresby Avenue coreshed which is situated within the Newmont Waihi Gold office.

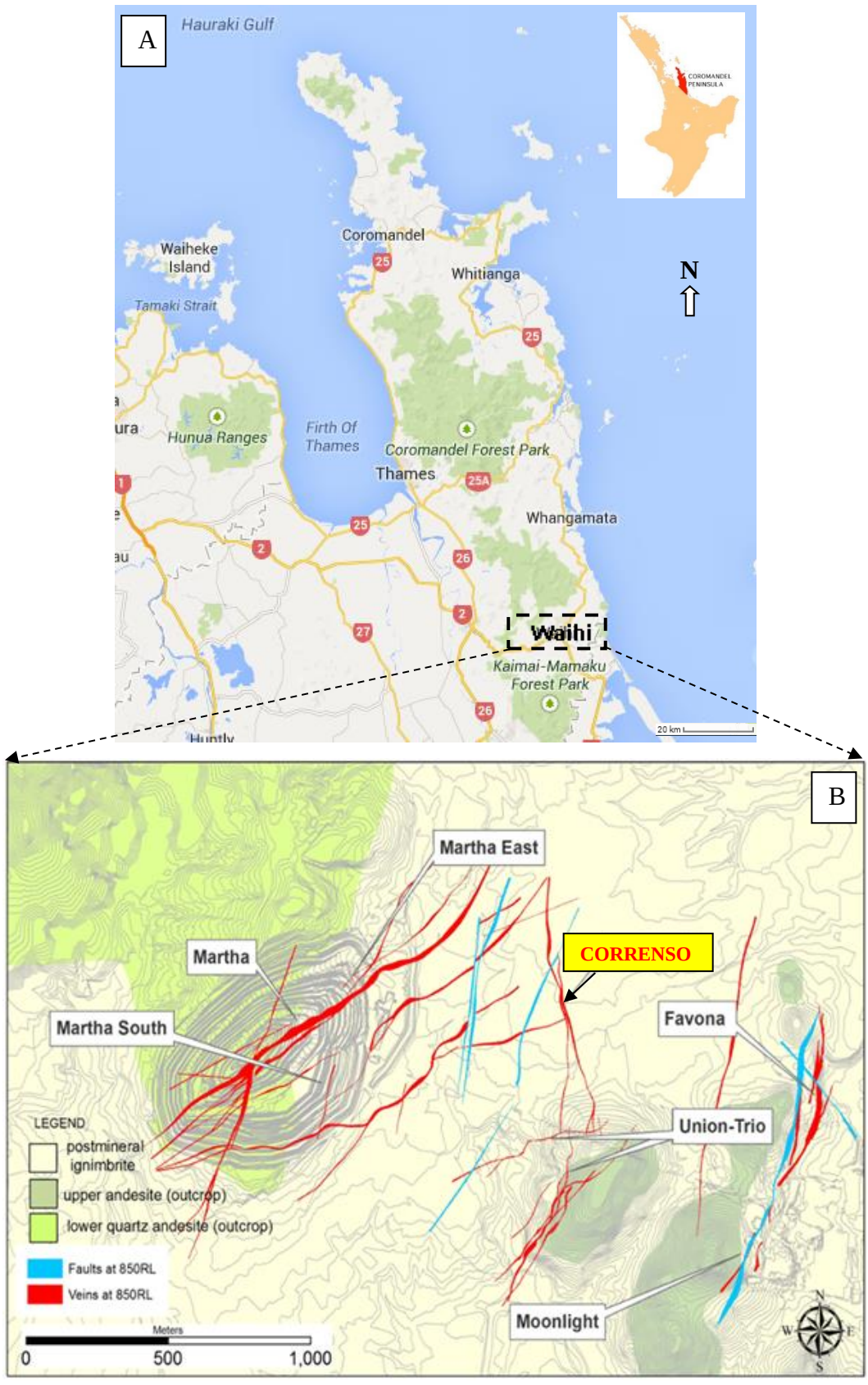

Figure 1.1. **(A)** Regional Map of Coromandel Peninsula (Google Earth, 2014). **(B)** Location and extent of Correnso Vein in Waihi, New Zealand and other veins (Adapted from Newmont, Waihi 2014).

2. Previous Work and Literature Review

2.1. Introduction

This chapter deals with the exploration history and previous work published on the epithermal deposits in the Coromandel Volcanic Zone. A brief literature review on the work done specific to Waihi area and Correnso deposit is also presented in this chapter. Also, the overall general description of epithermal deposits and their characteristics, hydrothermal alteration and review on the previous and current work done and published around the world specific to epithermal deposits and hydrothermal alteration is also described in detail.

2.2. Epithermal Deposits

The word epithermal is a combination of two Greek words 'epi' and 'thermal' meaning 'shallow heat'. The term is derived from the genetic classification scheme for hydrothermal ore deposits proposed by Swedish-American geologist Waldemar Lindgren in his book "Mineral deposits" in 1933.The classification was based on the stratigraphic relationships in volcanic sequences and the occurrence of metal and mineral deposits in active hydrothermal systems (Simmons et al., 2005). These deposits form at shallow depths as compared to porphyry Cu-Au systems and commonly associated with the hydrothermal alteration (Corbett, 2002). The significance of epithermal deposits is evident from the fact that nearly 6% of all gold and 16% of all silver mined have come from epithermal deposits. Epithermal deposits can cover areas that range from <10 to >100 km² and can occur in a diversity of shapes reflecting the influence of structural and lithological controls (Simmons et al., 2005).

2.2.1. Classification of Epithermal deposits

Lindgren's classification scheme was based on stratigraphic relationships in volcanic sequences and by analogy with metal and mineral occurrences and mineral textures in active hydrothermal systems; he inferred that these deposits were formed at certain depths (<200°C and pressures (~100 bars). The classic paper by White (1955) paved the way for future work on the relation between hydrothermal environments with epithermal deposits. Most important work and investigations done extensively on epithermal deposits started in late 1970's. The earliest work on the characteristics of the geology and mineralisation of low sulphidation epithermal deposits and their relationship with hydrothermal systems was done by Browne (1970, 1978), Buchanan (1981), Heald et al (1987), Sillitoe (1994, 1999). The broad classification of these deposits in detail was presented by White and Hedenquist (1990) in their paper on epithermal deposits.

Epithermal deposits are further classified into low and high sulphidation on the basis of alteration, gangue mineral assemblages, metal contents, sulphide contents, sulphide mineral assemblages, and water-host rock interaction (Corbett, 2002). The low sulphidation deposits are derived from reduced, near pH, dilute fluids developed by the entrainment of magmatic components within deep circulating groundwaters and these deposits are characterised by sulphur species reduced to H_2S (Corbett & Leach, 1998). The dilution of hydrothermal fluids can result into different deposit and mineralisation styles because of the addition of increased quantities of ground waters during migration of fluids away from the source of heat (magmatic source) to higher crustal levels (Figure 2.1) (Corbett, 2002).

In comparison, High sulphidation epithermal deposits are generated in both the epithermal and the upper parts of the underlying porphyry environments up to 2 km in vertical depths. These are often generated in advanced argillic lithocaps as the result of absorption of significant amounts of magmatic volatiles by groundwater, generating significant volumes of acidic fluid (Sillitoe, 1999). These are characterised by pyrite rich high suphidation-state sulphide assemblages

typified by enargite, luzonite, digenite and advanced argillic alteration assemblages of quartz, alunite, kaolinite/dickite and massive sulphide bodies of replacement origin dominated by pyrite, melnikovite, and marcasite (Figure 2.1) (Arribas, 1995). Examples of high sulphidation epithermal deposits around the world include Yanacocha, Pierina, El Indio, La Coipa, Lepanto, Chinkuashish, Nansatsu, and Wafi. These types of deposits are also characterised by zoned alteration (Figure 2.1) which is formed as the result of the progressive cooling and neutralization of the hot acidic fluids by reaction with host rocks and ground waters (Corbett, 2002).

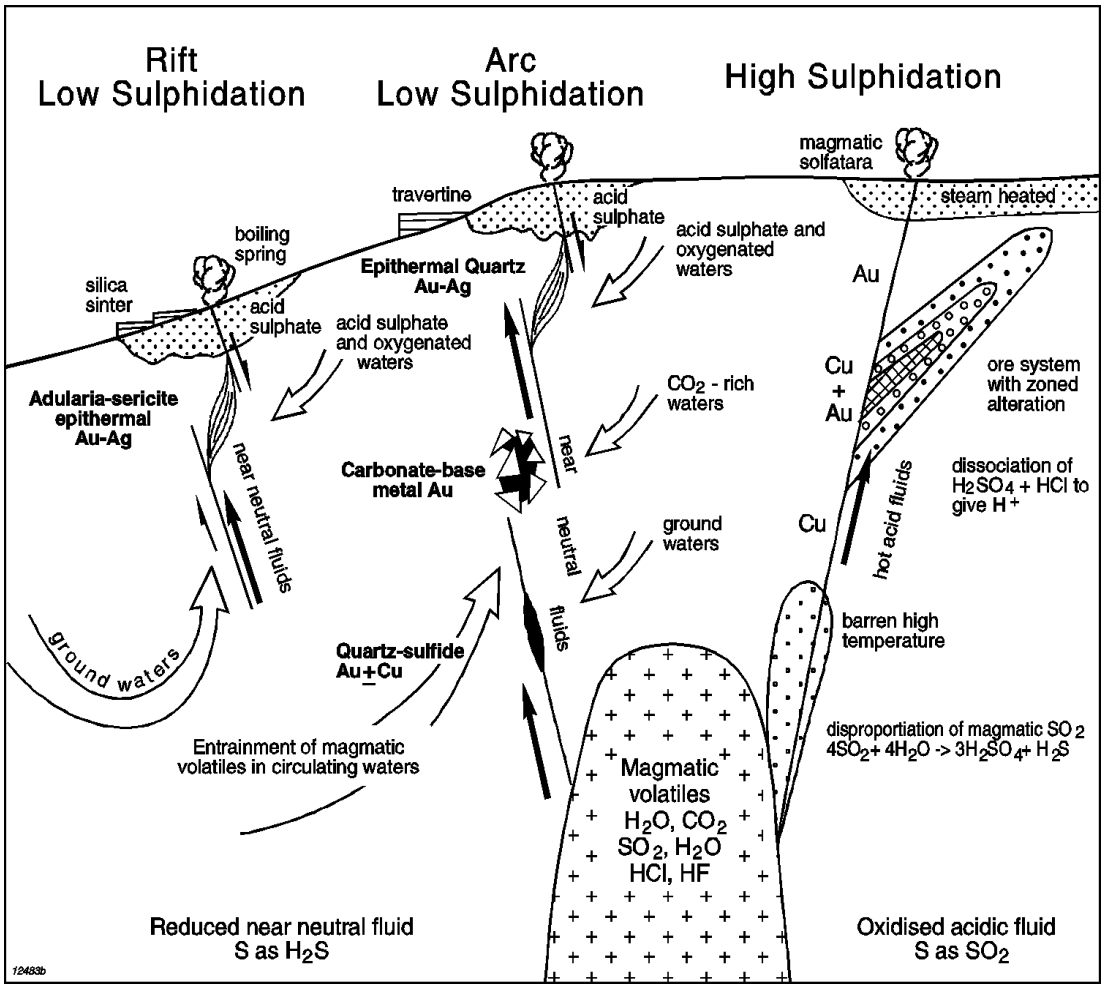

Figure 2.1. Derivation of low and high sulphidation fluids including arc and rift low sulphidation (Corbett, 2002).

Table 2.1. Common differences between low sulphidation and high sulphidation deposits with examples (White & Hendenquist, 1995).

EXAMPLES OF EPITHERMAL GOLD DEPOSITS	
LOW SULFIDATION	**HIGH SULFIDATION**
McLaughlin, California, USA	Goldfield, Nevada, USA
Round Mountain, Nevada, USA	Summitville, Colorado, USA
Hishikari, Japan	Iwato, Kasuga and Akeshi, Japan
Emperor, Fiji	La Coipa, Chile
Golden Cross, New Zealand	El Indio, Chile
Waihi, New Zealand	Pueblo Viejo, Dominican Republic
Lebong Tandai, Indonesia	Chinkuashih, Taiwan
Porgera Zone VII, Papua New Guinea	Lepanto, Philippines
Pajingo, Australia	Lahóca, Hungary
FORM OF DEPOSITS	
LOW SULFIDATION (Adularia-sericite)	**HIGH SULFIDATION** (Acid sulfate)
Open-space veins dominant	Veins subordinate, locally dominant
Disseminated ore mostly minor	Disseminated ore dominant
Replacement ore minor	Replacement ore common
Stockwork ore common	Stockwork ore minor

HYDROTHERMAL ALTERATION		
	LOW SULFIDATION	**HIGH SULFIDATION**
DEEP, MINERALIZING FLUID	near-neutral pH	acid (pH <1 to >3)
MINERAL ASSEMBLAGE	illite (sericite)	alunite, kaolinite, pyrophyllite,
	interstratified clays	diaspore, zoned out to illite

2.2.2. Low Sulphidation Epithermal (LSE) deposits

This research project deals with low sulphidation epithermal deposits and therefore focus of this literature review is on low sulphidation rather than other form of deposits. The low sulphidation deposits are further classified into arc low sulphidation and rift low sulphidation on the basis of their associations with magmatic source rocks and input of meteoric geothermal waters (Figure 2.1). The arc-low sulphidation deposits are characteristic of strong field associations with intrusive rocks and these are further categorized into different types (Quartz-sulphide gold $\pm$ copper, polymetalic gold-silver veins, carbonate base metal gold) on the basis of varying ore, gangue, and wall rock mineralogies relating to formation at shallow crustal levels. The rift low sulphidation deposits are characterised by adularia-sericite epithermal gold-silver ores (Figure 2.1) and occur as veins with gangue mineralogies which are deposited by circulating dilute,

commonly meteoric, geothermal waters typically confined to rifts within arc or back arc environments (Corbett, 2002). Some of the major low sulphidation deposits are McLaughlin deposits of California, Round Mountain (Nevada), Golden Cross and Martha (Waihi), Emperor (Fiji), Porgera Zone VII (Papua New Guinea), Lebong Tandai and Kelian (Indonesia), Hishikari (Japan), El Penon, Midas, Pajingo (Australia).

2.2.2.1. Characteristics of Low Sulphidation Epithermal Deposits

In low sulphidation epithermal environments, the dominant circulating meteoric waters absorb most of the acid magmatic gases such as CO_2, SO_2, and HCl. These fluids equilibrate with their host rocks in a low sulphidation environment and become reduced developing into a near-neutral pH (Giggenbach, 1991). The boiling of near-neutral pH solutions at shallow depths as the result of drop in pressure and temperature conditions causes the generation of CO_2 and H_2S rich vapours. This results in the formation of steam heated acid-sulphate waters near the Earth's surface with decreasing pH because of condensation of these vapours in the vadose zone above the water table. The eventual loss of H_2S from the solution at depth due to boiling causes the solubility of gold to decrease, thus leading to its precipitation (Henley et al., 1984). The areas of high mineralisation have been identified by studying the common environments and settings for these deposits across the world. Geologic settings, hydrology, structure, and hydrothermal alteration defined by pressure, temperature and fluid geochemistry are the main factors controlling the localisation and style of mineralisation.

2.2.2.1.1. Geologic and Tectonic Controls on Mineralisation

Low sulphidation epithermal deposits are formed at higher crustal levels than porphyry type of deposits, at temperatures < 300°C and typically < 1 km (Corbett, 2002). Andesitic to dacitic volcanic settings host most of the epithermal deposits known and are rarely found in basic volcanoes (Mitchell and Garson, 1981; in White and Hedenquist, 1990). The deposits are found in number of geological and tectonic settings but are most commonly associated with intra-arc or back-arc rifts (such as the Taupo Volcanic Zone and the Coromandel Peninsula) within

continental or island arcs, typical of convergent tectonic settings. Volcanism is the main factor controlling the localisation and style of mineralisation, providing the necessary heat from the underlying magmas required for the hydrothermal activity. Although, these deposits are commonly found proximal to the volcanic settings, some exceptions of distal volcanic settings for these deposits (Wirralie and Yandan, Australia) have also been reported (White and Hedenquist, 1990).

The variable epithermal environments can be defined on the basis of different hydrological regimes which strongly control the recharge and discharge of the hydrothermal system, the distribution and types of alteration products and the localisation of mineralisation. Also, hydrothermal activity can be applied to classify epithermal deposits into silicic depressions, andesitic stratovolcanoes, cordilleran volcanism and oceanic islands (White and Hedenquist, 1990). In Korea, approximately one third of the gold resources are developed in the Cretaceous pull-apart basins, volcano-tectonic depressions and calderas. The Mugeug province in the central part and the Haenam-Jindo province in the south-western part of the Korean peninsula host major Au-Ag epithermal deposits (Yang et al., 2012).

The Mule Canyon deposits of Nevada are another example of low sulphidation deposits formed in the extensional regimes. The deposit lies near the west edge of the middle Miocene Northern Nevada rift and was formed during mafic magmatism and extensional faulting related to formation of the rift (John and Wallace, 2000). This deposit also shares its geologic settings with the other low sulphidation deposits in the area such as Sleeper, Midas, and Buckhorn (John et al., 2003).

2.2.2.1.2. Structural controls on mineralisation

Regional and local structural settings can significantly control the localisation and style of mineralisation in epithermal deposits. The regional fault structures can enhance the hydrothermal activity by acting as conduits and supplying the heat from underlying magmas (Hedenquist, 1986). Secondary faults, fractures, joints and even bedding planes are known to affect the migration of fluids.

Corbett (2002) noted that structure and host rock competency can control the mineralisation in low sulphidation epithermal environments, especially in adularia-sericite vein systems where brittle rocks fracture easily and are known to host mineralised veins. The fracture controlled permeability provided by small scale fracture networks facilitates the flow of hydrothermal fluids through the host rocks and the silicification caused by previous flows can promote further fracturing. The best example of this can be seen in the Coromandel Peninsula where fissure veins are well developed in Coromandel Group andesites and not in the overlying rhyolitic pyroclastics which are poorly mineralized (Brathwaite et al., 1989). Similar structural settings are present in the Philippines geothermal systems such as Acupan and Antamok deposits where mineralisation is highly localised in the fractures within the metamorphic rocks and as basement intrusions. The Hishikari and Konami deposits in Japan also share the same characteristics where mineralisation in the form of fissure vein gold deposits is contained within the basement shales (Corbett, 1998). Apart from this, impermeable barriers in a system can restrict the fluid flow which can enhance the pressure build up resulting in the boiling, hydrofracturing and metal deposition (Figure 2.2) (Cox, 2005). Hydrology is an important aspect governing the fluid flow in epithermal environments controlled by local topography, permeability and tectonic settings. The circulation of hot fluids depends upon hydraulic gradient and permeability which can enhance the free flow of fluids in the hydrothermal system and also governs the fluid upflow and outflow.

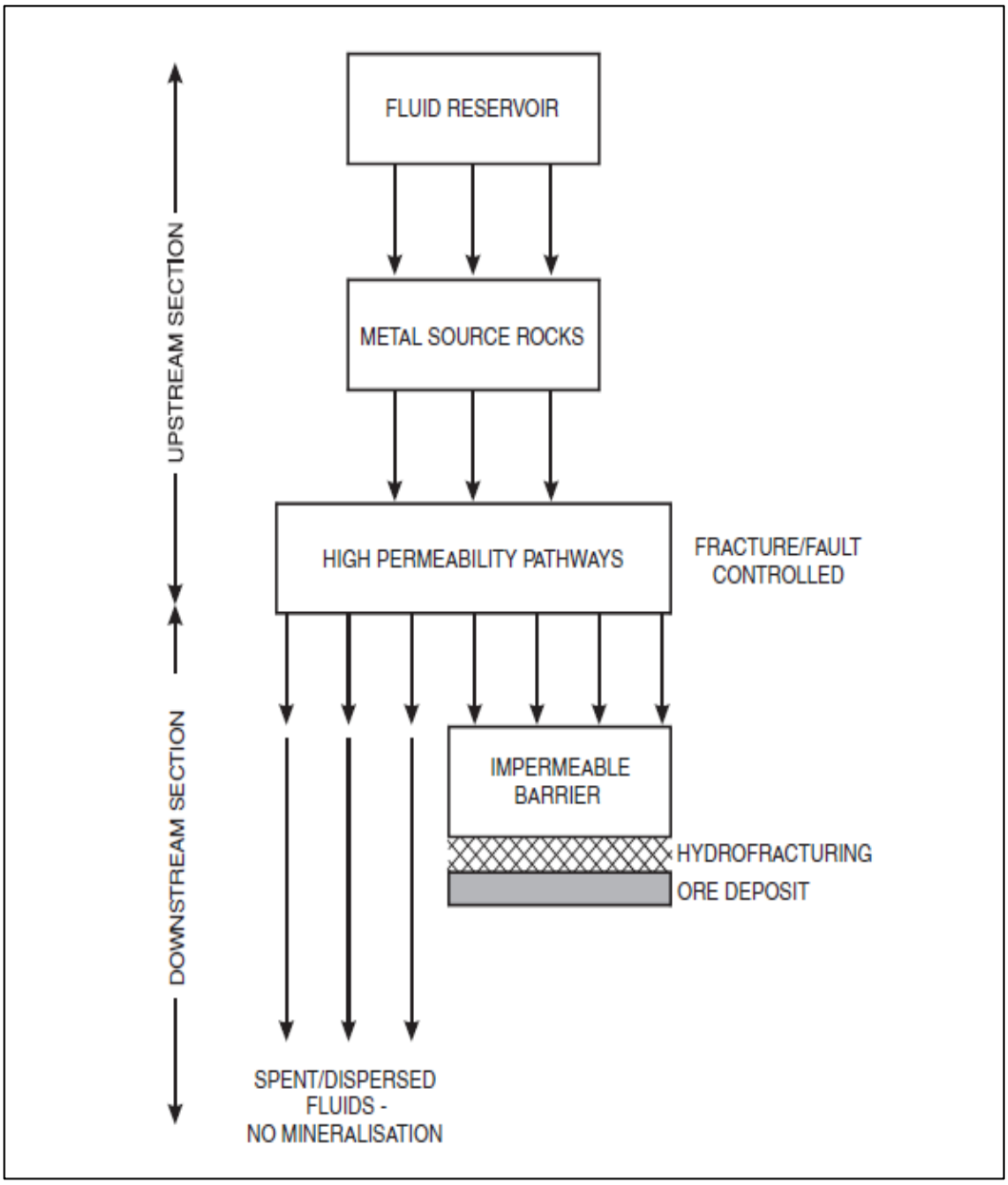

Figure 2.2. The conceptual fluid flow model in a fracture controlled hydrothermal system shows the movement of fluids within a system. The upstream section consists of a fluid source from which the fluids are channelled along progressively smaller pathways to interact with a metal source rocks and to a downstream section. The ore deposition can occur if fluids encounter an impermeable barrier which can cease the free movement of fluid resulting in a pressure build-up followed by effervescence or boiling, hydrofracturing and metal deposition. The lack of barrier could end in the dispersion of the fluids and no mineralisation is produced (From Cox, 2005; Pirajno, 2009)

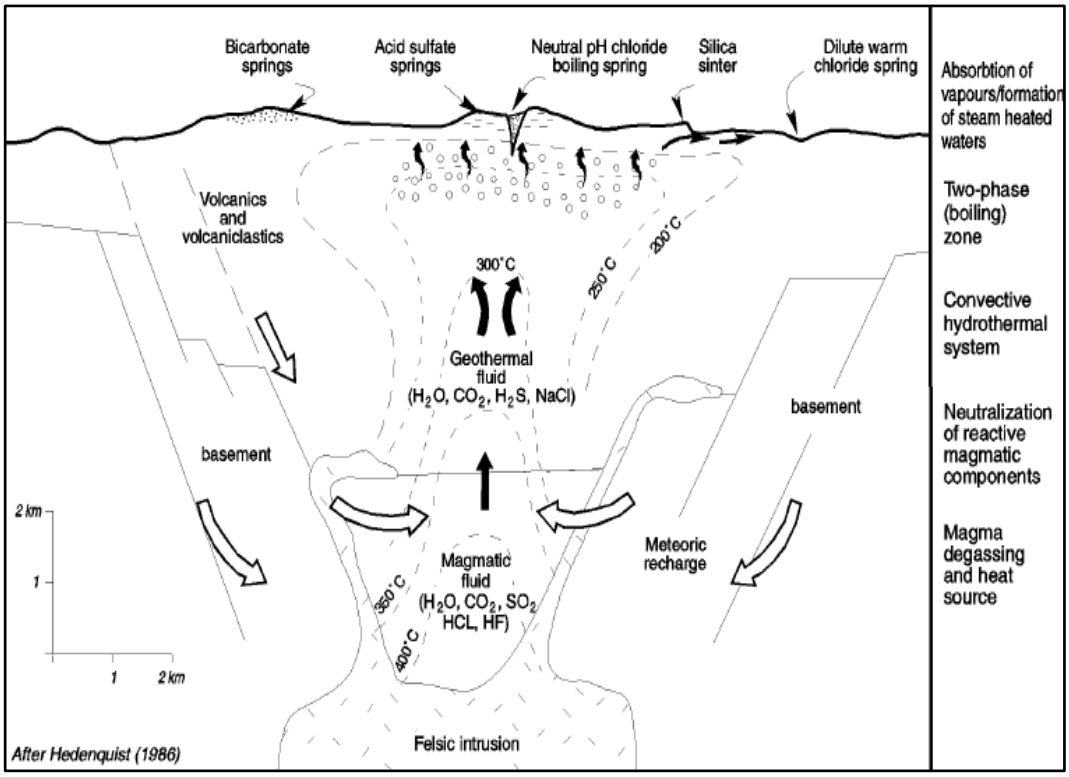

Figure 2.3. Conceptual model for the silicic back-arc hydrothermal systems. The generalised fluid flow model and the associated processes involved are shown alongside depositional characteristics (From Hedenquist, 1986; in Corbett and Leach, 1998).

2.3. Hydrothermal Alteration

Hydrothermal alteration is a complex process involving mineralogical, chemical and textural changes, resulting from the interaction of hot aqueous fluids with the rocks through which they circulate, under evolving physico-chemical conditions (Pirajno, 2009). Fenner (1934, 1936) published the first detailed accounts of subsurface hydrothermal alteration in an active geothermal system. Fenner studied the 124-m drillcore from Upper Geyser Basin of Yellowstone National Park and noted that thermal fluids can react with the rocks, resulting in mineralogical and chemical changes in their composition (Browne, 1978). Hydrothermal alteration is of great importance as far as mineral exploration is concerned as the alteration halos extend well beyond the limits of the mineralisation. The study of the alteration mineralogy and geochemistry can help in significantly narrowing the area of prospective mineralisation and can therefore considerably reduce the exploration cost by informing the explorer where to focus exploration efforts and drilling. The geothermal systems responsible for the formation of hydrothermal ore deposits are located in a

number of geological settings. Adularia-quartz epithermal systems (eg. Waihi) tend to show a distinct geological settings associated with crustal rifting within a continental crust in back arc rift zones (Corbett and Leach, 1998). The magmatic heat source in silicic continental rift environments is deep seated >5 km which constitutes melted continental crust of mainly granitic composition (Hendenquist, 1986; Henley, 1985). The meteoric water interacting with the heat source at depths (Figure 3.3) becomes chemically active with the addition of gases and other elements and results in the formation of chloride rich hydrothermal fluids. The intrusion of these hot fluids in the host rocks through primary and secondary permeabilities create a chemical disequilibrium between the fluid and host rocks and cause chemical and mineralogical changes. The chemical and mineralogical changes in the wall rock result in the alteration of the original minerals to new mineral assemblages that tend to be in equilibrium with the new changes. It is also possible that fluids themselves can change their chemistry after interacting with the host rocks (Browne, 1978). Also, with the migration of fluid to the surface, precipitation of the constituents in the fluids can occur as the result of the temperature and pressure variations, boiling and chemical changes due to the mixing of hot fluids with the surface groundwater (Skinner, 1979).

2.3.1. Factors Controlling the Hydrothermal Alteration

Browne (1978) in his paper on hydrothermal alteration in geothermal fields discussed specific factors which can affect and control the formation of hydrothermal minerals. He noted that temperature, permeability, pressure, rock type, fluid composition, and duration of activity can strongly influence the formation and distribution of hydrothermal alteration minerals. In addition, hydrothermal alteration in epithermal systems can be considered in terms of interaction of acidic fluids, near neutral chloride fluids, and alkaline fluids. Sillitoe (1994) described the mineralogy and zonation of hydrothermal alteration

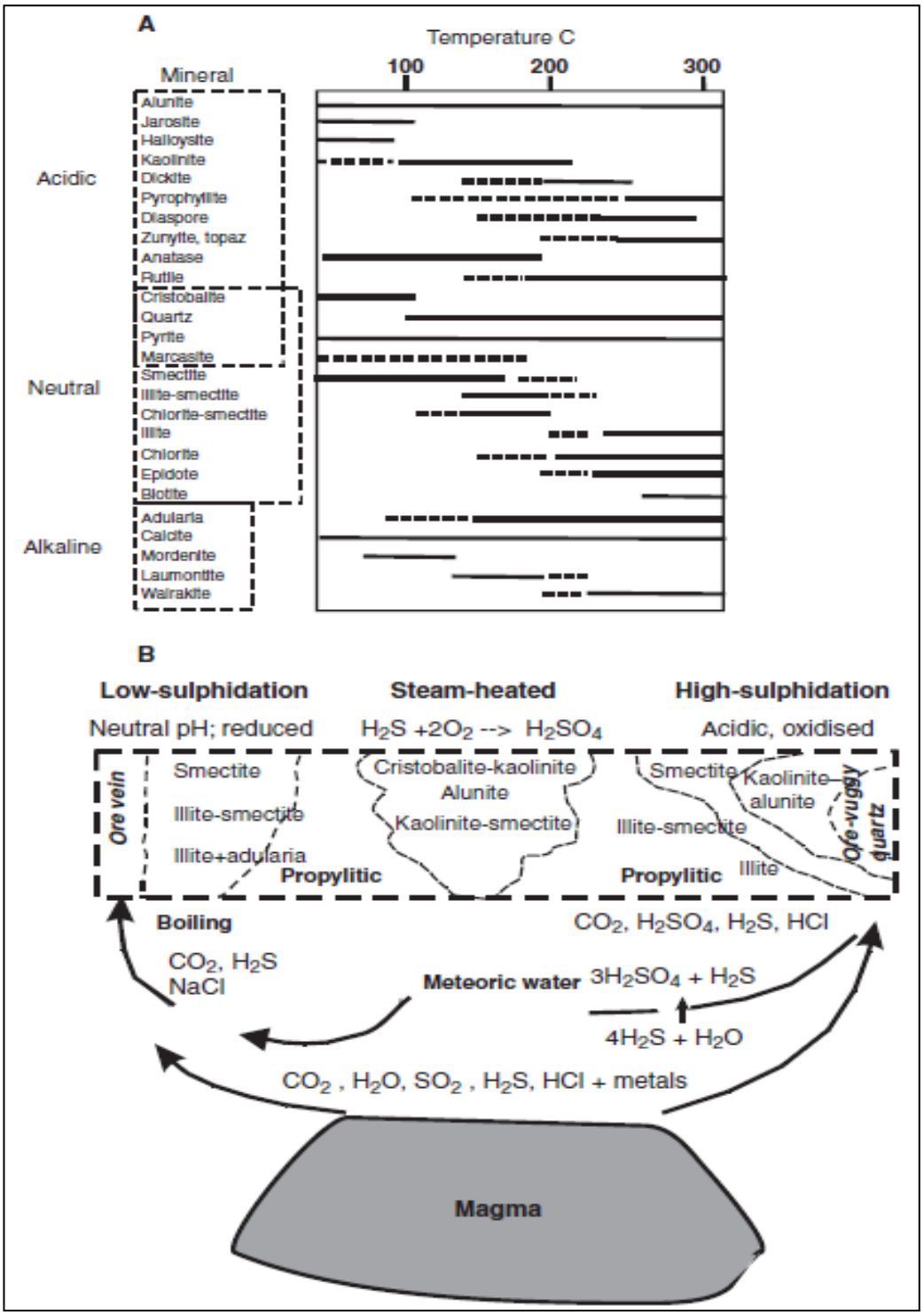

Figure 2.4. **(A**) Temperature and pH range of hydrothermal mineral phases in epithermal systems; **(B)** Simplified scheme of the distribution of hydrothermal minerals in high and low-sulphidation epithermal systems (Hedenquist et al. (1996); in Pirajno, 2009).

assemblages in detail and concluded that many alteration minerals are stable over limited temperatures and pH ranges and these characteristics could be used to reconstruct the thermal and geochemical structure of the hydrothermal system. The recognition of mineral assemblages is important in distinguishing low sulphidation, high sulphidation and alkali types of epithermal systems. Also, the hydrothermal alteration is found to occur through phase transformation, growth of new minerals, mineral dissolution and precipitation, and ion exchange reactions (Henley & Ellis, 1983).

2.3.1.1. Temperature and Pressure

The range of temperatures responsible for the formation of certain minerals varies from field to field. In the lower temperature range (< 180°C) the chief mineral phases related to acid-sulphate geothermal fluids are kaolinite, alunite, cristobalite, gypsum, opal, native sulphur, quartz and sulphides (Figure 2.4A). Epidote, occurs in geothermal systems above 220 ^{o}C. Other ortho, ring and chain sillicate minerals are uncommon in active geothermal systems, and occur only at high temperatures. Hydrothermal garnet, tremolite, pyrophyllite, and talc were also known to occur at high temperatures (Muffler & White, 1969). Browne & Ellis (1970) in their study on clay minerals in New Zealand geothermal fields noted that clay minerals formed at variable temperatures ranging from 60°C to 220°C. Also, surface kaolinite, which forms at low pH, only formed at temperatures below 60°C whereas dickite is known to occur between 150°-260°C at low pH conditions (Figure 2.4A). Montmorillonite is found to be dominant with increasing temperature and depth and found to be interstratified with illite and at temperatures above 220°C, thus illite plus chlorite is the most common clay-mineral found in these fields.

The presence and absence of clay minerals gives an idea about the depth and temperature ranges of the hydrothermal field as well as the mineralisation zonation (Pirajno, 2009). The variation in the basal spacing of clay minerals in low sulphidation epithermal deposits proves to be a good indicator of paleo-temperature. Progression in thermal stability results in a clear upward and outward zonation of minerals in these deposits (Reyes, 1990). Also, in low

sulphidation epithermal deposits, the ore associated alteration is produced by near-neutral pH waters with temperature increasing with depth and with increasing distance from the conduit of fluid flow. The alteration mineralogy and temperatures are directly related which can be crucial to indicate the range of thermal stability of temperature dependent minerals (Henley and Ellis, 1983). This information can be important for exploration purposes as it allows paleo-isotherms to be deduced from the distribution of alteration minerals, which in turn helps to locate conduits of paleo-flow, and to determine the level of erosion. The former is important as major ore accumulations occur in conduit zones. The latter is significant as most epithermal ore is deposited over the range of 180°-280°C (Hedenquist & Henley, 1985). Changes in the fluid pressure is another criterion which can affect the fluid composition in geothermal areas. The pressures though have little effect on hydrothermal alteration; they can substantially influence the induration and lithification of sediments (Browne & Ellis, 1970).

3.3.2.3. Host Rock Composition

Another factor which can influence the hydrothermal alteration is the parent rock characteristics. The texture, porosity, permeability and chemistry can control the alteration style and the nature of mineralisation (Honda & Muffler, 1970). Although, the initial mineralogy of the host rock have minute effect on equilibrium alteration assemblages above 280° C, however at lower temperatures , the nature of the parent material influences the alteration product. For example, high-silica zeolites are common in rhyolitic fields at Yellowstone and New Zealand, whereas low-silica zeolites are more common in basaltic fields of Iceland and andesitic fields of Kamchatka (Browne & Ellis, 1970).

2.3.1.3. Fluid geochemistry

The fluid composition is a well-known factor controlling the alteration mineralogy. The development of applicable thermodynamic techniques in the 1960's for high temperature multi-component equilibrium led to better understanding of the large-scale rock-water equilibrium controlling fluid compositions and alteration assemblages in geothermal systems. The work done

by Browne & Ellis (1970) on Broadlands and Wairekei, New Zealand also emphasised the importance of fluid chemistry affecting the alteration mineralogy and geochemistry. The mineral stability diagrams constructed by Browne & Ellis (1970) show that Broadlands water at 260°C, in the presence of excess silica, is in near equilibrium with albite, K-mica (illite), K-feldspar (adularia), calcite, wairakite and chlorite but andesine was found to be unstable under these conditions. They also demonstrated that due to steam loss through boiling in a homogeneous aquifer of slowly rising hot water, the important effects produced were rise in pH, loss of CO_2 and slight cooling. The fluid chemistry of the hydrothermal fluids is also variable with different geological settings. Reyes (1995) noted that the chemical composition of the fluids in magmatic arc geothermal systems in Philippines contain nearly 50 percent of the magmatic component and are more saline as opposed to New Zealand geothermal systems which contain less than 3-4 percent of magmatic component. Hedenquist and Henley (1985) also found New Zealand geothermal systems to show <1 wt percent NaCl the fluid inclusion data on banded quartz-adularia veins from the Waihi epithermal deposits showing neutral to near-neutral fluid composition.

2.3.1.4. Redox Reactions

The understanding of pH and redox state, along with temperature, fluid salinity, etc. in low sulphidation epithermal deposits is also crucial to determine the mineralisation zonation and fluid transportation and deposition processes. Boiling and solubility result in the separation of constituents from the fluids and are therefore major components controlling the mineralisation in hydrothermal regimes. In low-sulphidation deposits the ore is commonly associated with the least acidic alteration (adularia and calcite or illite). For example, in a low-salinity reduced fluid, gold is likely to be transported as a bisulfide complex. However, boiling operating at epithermal depths will cause CO_2 to be lost from the liquid, resulting in an increase in pH. This initially increases the solubility of gold, but eventually the loss of H_2S from the liquid causing the solubility to decrease, thus leading to the precipitation of gold (Henley et al., 1984).

2.3.2. Styles of Hydrothermal Alteration

Hydrothermal alteration has been classified further into different types on the basis of variable mineral assemblages which form at certain conditions and thus can provide crucial information about the alteration environments. Gifkins et al. (2005) divided the mineral assemblages on the basis of dominant mineralogy and chemical changes produced as the result of fluid-host rock interaction. The alteration intensity and type of mineral assemblage is a function of temperature and pressure and can change from one type to another with changing pressure and temperature conditions. The main alteration assemblages are described in brief as follows.

Argillic

The argillic (meaning clay in Latin) alteration assemblages consist of minerals formed at relatively low temperatures (>200-250°C) and moderately low fluid pH (4-5). This type of alteration is characterised by the formation of clay minerals because of intense H+ metasomatism and acid leaching (Pirajno, 2009). The typical alteration mineral assemblages consist of kaolinite and smectite being dominant and other low temperature clay minerals like illite, illite-smectite, halloysite, and can also contain chlorite group minerals in low quantities (Rose and Bart, 1979). This type of alteration inwardly grades into phyllic outwardly into propylitic zones. The extreme acid leaching in epithermal environments can result in silica enrichment with plagioclase and mafic silicates being replaced by clay minerals such as smectite, chlorite and illite or combination of clays (Pirajno, 2009).

Advanced Argillic

The advanced argillic style is characterized by kaolinite, pyrophyllite, or dickite (depending on the temperature) and alunite together with lesser quartz, topaz, and tourmaline. Some sulphides and amorphous clays may also present with variable concentrations. Temperature conditions are usually >250°C and pH <4.

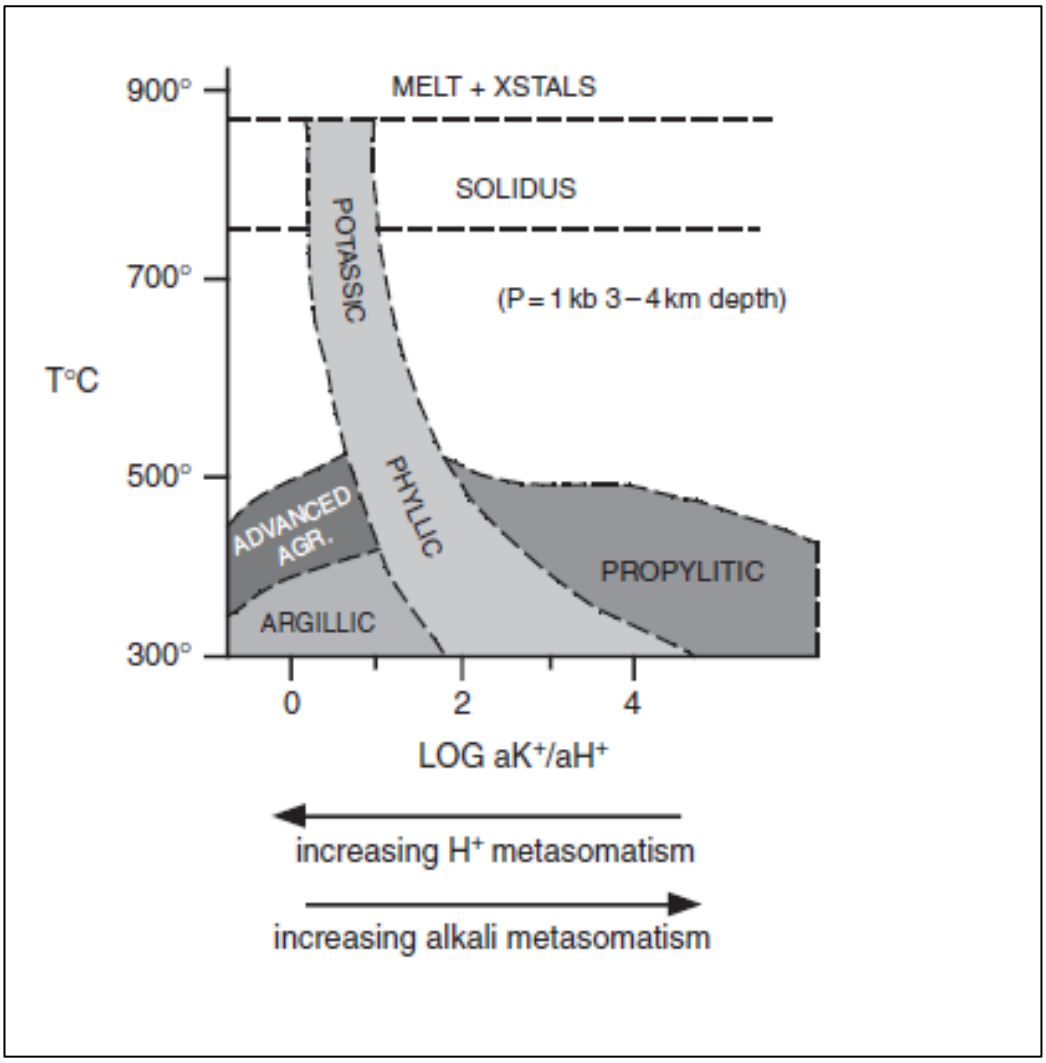

Figure 2.5. Conceptual evolutionary alteration model. Types of alteration as a function of temperature, K+ and H+ activities (After Guilbert and Park 1985; Burnham and Ohmoto, 1980; Pirajno, 2009).

Phyllic

Phyllic alteration is common in hydrothermally altered sequences and is formed at low to intermediate temperature ranging >200-350°C and usually characterizing the margins of the epithermal deposits. Common alteration minerals present are sericite being dominant and high temperature kaolinite and chlorite group minerals (Corbett and Leach, 1998). Mineral assemblages consists of quartz-sericite-pyrite and accessory amounts of chlorite, quartz, and pyrite. Trace amounts of calcite, zoisite and albite can also be present. Also, associated mineral phases such as K-feldspar, kaolinite, calcite, biotite, rutile, anhydrite and apatite can also be present. Phyllic alteration can grade into high temperature

potassic type by increasing amounts of K-feldspar and into the low temperature argillic type by increasing amounts of clay minerals (Figure 2.5) (Pirajno, 2009).

Propylitic

Propylitic alteration is typical of low temperature conditions usually <200-250°C and near neutral to alkaline conditions (Figure 2.5). The dominant minerals present are epidote, chlorite, albite, K-feldspar and pyrite. Low temperature propylitic alteration consists of zeolites in place of epidote. As zeolites are stable at certain pressure and temperature conditions, they can act as depth and temperature indicators (Meyer and Hemley, 1967).

Potassic

Potassic alteration is formed in the deeper parts of the epithermal system and are characteristic of high temperature and pressure conditions than other alteration types (Figure 2.5). The alteration type is characteristic of neutral to alkaline conditions with common minerals present as K-feldspar, adularia, quartz, magnetite, and sulphide minerals such as pyrite, chalcopyrite, and galena and iron sulphides. Sericite, albite, apatite, and anhydrite are also present with varying compositions (Corbett and Leach, 1998; Pirajno, 2009).

3. Geological Setting, Tectonic History and Stratigraphy

3.1. Introduction

This chapter deals with the regional and local geological settings of the deposit and host stratigraphy. The tectonic history, geologic age and occurrences of epithermal deposits in the region together with the structure and vein geometry is also described in brief.

3.2. Regional Geology

The Waihi area is a late Miocene volcanic-hosted area also known as Coromandel Volcanic Zone (CVZ) and is part of Hauraki Volcanic Region (HVR) (Christie et al., 2007). The Hauraki Volcanic Region extends from the Poor Knights Islands in the north to the Kaimai Ranges in the south. HVR is the largest and longest lived area of andesite-dacite volcanism in New Zealand and cover a land area approximately 4500 km² by volcanic rocks of Miocene to mid Pleistocene age (Skinner, 1986). The HVR also extends offshore with an area approximately 6000 km² submerged along the continental shelf north of Bay of Plenty consisting predominantly of igneous basement and is thus aerially larger than the nearby Taupo Volcanic Zone (TVZ) to the south (Thrasher, 1986).

The HVR is subdivided into three major volcanic zones on the basis of distinct morphological and tectonic features as Kiwitahi Volcanic Zone (KVZ) in the west (Cole, 1978a), the central Hauraki Rift (Hochstein and Nixon, 1979) and the Coromandel Volcanic Zone (CVZ) in the east (Skinner, 1986). Healy et al. (1964) defined the KVZ as a series of remnant andesitic lava flows and residual-mountain dissected andesitic volcanoes to the west of the Hauraki Rift. They range in age from mid-Miocene at the northern end and lower Pliocene at the southern end.

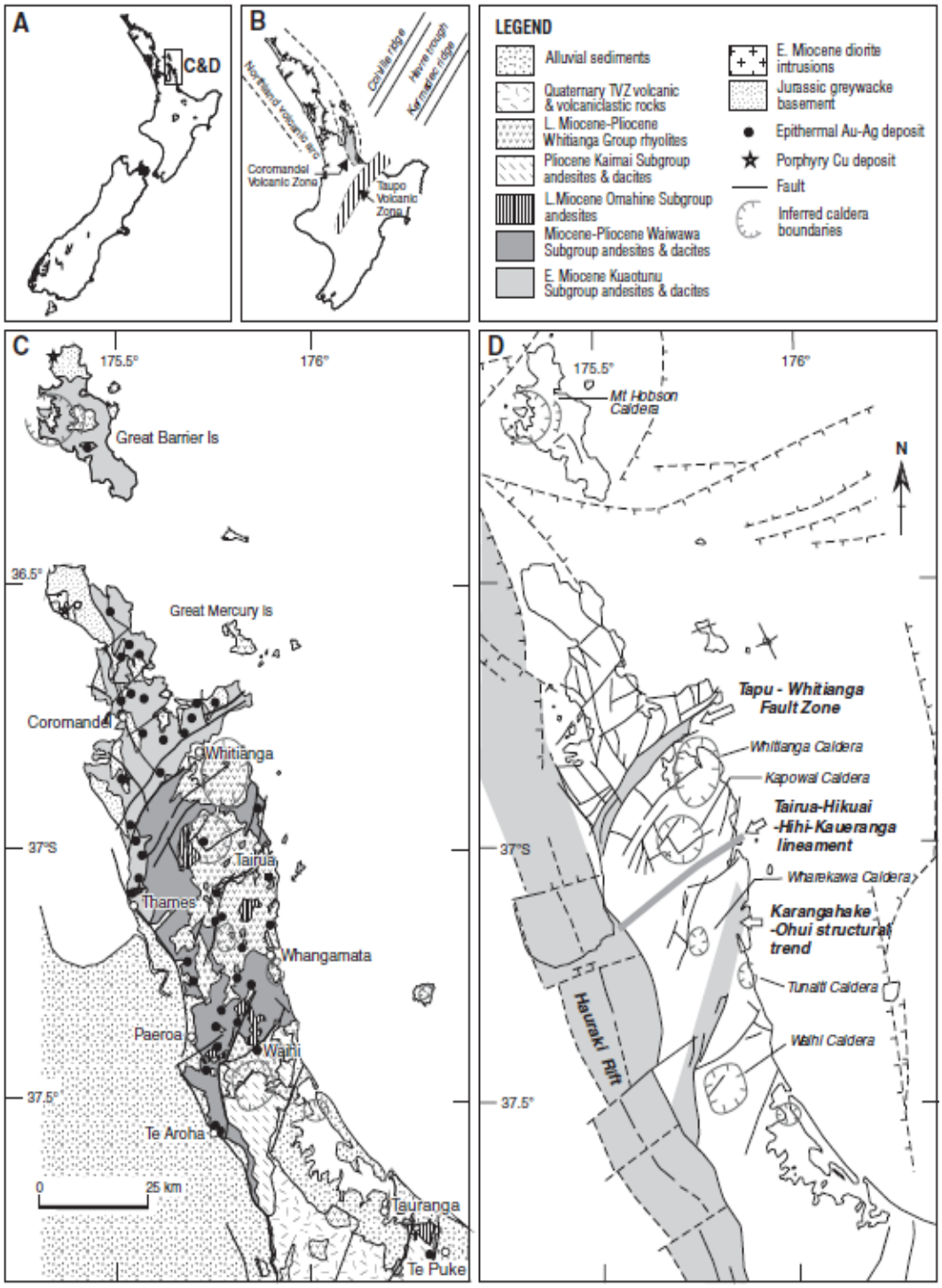

Figure 3.1. **(A & B)** Location of the Hauraki Goldfield and Coromandel Volcanic Zone. **(C)** Regional geology and location of mineral deposits in the region. **(D)** Structural features of the CVZ and Hauraki Goldfield (adapted from Skinner, 1986; Thrasher, 1986; Braithwaite and Christie, 1996).

The Hauraki Rift on the other hand is a young continental rift extending for over 300 km from Whangarei in the north to the TVZ in the south. The detailed geophysical surveys done by Hochstein and Nixon (1979) show set of fault angle grabens bounded by possibly active north northwest trending faults, dislocated into blocks by north easterly to east north-easterly cross faults. The depressions are filled with unconsolidated Quaternary sediments up to 0.7 km in depth and approximately 2 to 3 km of Pliocene and older volcanic and sedimentary rocks in the central parts of the rift (Hochstein et al., 1986).

The CVZ covers an area stretching from the Coromandel and Kaimai Ranges in the south to the Great Barrier and Little Barrier Islands in the north and includes a wide range of igneous rock with compositions ranging from basalt to rhyolite, as well as sub-volcanic and hypabyssal and plutonic rock complexes (Skinner, 1986). Hydrothermal alteration in this region has considerably altered the mineralogy and geochemistry of the host rocks. The CVZ was epicentre of volcanism in the North Island from the late early Miocene to late Pliocene and is known as the precursor to the Quaternary and Recent Taupo Volcanic Zone (Adams et al., 1994; Briggs & Krippner, 2006).

The regional fault pattern at the Hauraki Volcanic Region consists of NNW and NNE trends which is also similar to the offshore fracture trends (Skinner, 1986) and this trend resembles with the most of the Auckland region's fault pattern (Schofield, 1967). The analysis of faults and vein patterns by Skinner (1967, 1976, and 1979) show that these trends are controlled by pre-existing faults formed in the Jurassic basement rocks during the early Cretaceous Rangitata Orogeny. This implies that the Great Barrier Island and the Coromandel Peninsula is the result of Neogene arc volcanism over the greywacke graben and horst structures on which both the volcanism and Neogene tectonics have been superimposed rather than CVZ being in itself a NNE trending volcanic arc (Skinner, 1986). Normal faults trending north-northwest and northeast largely dominate the regional structure of the CVZ and are controlled by faults in the basement rock, with most of the northeast-striking faults downthrown on their southern blocks

(Figure 3.1) (Christie et al., 2007). The CVZ also consist of major caldera structures of which Kapowai Caldera is the largest.

3.2.1. Tectonic History and Age of Coromandel Peninsula

The tectonic history of Coromandel Peninsula started with the formation of greywacke basement rocks as the result of the accretion of sediments onto the margin of Gondwana during Early Cretaceous. The extensional tectonics dominated the area during Late Cretaceous and the basement rocks were subjected to erosion and covered unconformably by Early Tertiary sediments (Sporli, 1987; King, 2000). With the onset of modern plate boundary during Early Neogene, emplacement of Northern Allochthon took place followed by the establishment of the NW-trending Miocene Northland Volcanic Arc which propagated into the Coromandel Peninsula around 18 Ma, forming a convergent margin (Brathwaite & Skinner, 1997). This volcanic arc consisted of a western belt of basalt and basaltic andesite volcanic rocks and an eastern belt (CVZ) of predominantly andesite and dacite volcanic sequences. The andesitic volcanism began in the CVZ in the early Miocene and was active from 18 to 9 Ma. With the migration of plate boundary and cessation of volcanism in Northland around 14-12 Ma, there was an onset of extension in the CVZ followed by major rhyolitic and minor basaltic volcanism. From 6 to 4 Ma there was a transition to basaltic eruptions and abandonment of these volcanic centres which occurred in the Late Neogene (King, 2000). Volcanism ceased in the CVZ in the late Pliocene (1.9-1.5 Ma) with the shifting of volcanic centres to the Taupo Volcanic Zone (TVZ) (Carter et al., 2003; Briggs et al., 2005). The epithermal deposits of the Hauraki Goldfield are chiefly hosted in Coromandel Group andesitic volcanic rocks of the CVZ (Skinner, 1986; Brathwaite & Skinner, 1997). Some deposits also occur in the top of the underlying Mesozoic greywacke basement, early Tertiary rocks and the Whitianga Group rhyolitic volcanic rocks (Sporli et al., 2006).

Ages for the vein and wall rock adularia were obtained using $^{40}Ar/^{39}Ar$ method by Ward et al. (2005) for seven epithermal deposits and one porphyry copper prospect at the Coromandel Peninsula. The age of veins and host rocks in the Hauraki Goldfield young to the south. This is also evident from the ages of

mineralisation following the same trend, which also young to the south (Adams et al., 1974; Skinner, 1986; Adams et al., 1994; Mauk and Hall, 2003, 2004; Ward et al., 2005). The oldest $^{40}Ar/^{39}Ar$ age for vein adularia from the Paritu region date back to 16.315 ± 0.066 Ma. The vein adularia at the Opitonui deposit yield an age of 13.149 ± 0.016 Ma and samples of vein adularia from the Night Reef at the Broken Hills give an age of 7.121 ± 0.010 Ma. The samples at the Wharekirauponga deposit date back to 6.318 ± 0.061 Ma and the vein samples at the Maratoto deposit provide an age of 6.411 ± 0.022 Ma. Also, the ages at the Karangahake deposit range from 6.116 ± 0.116 to 6.901 ± 0.101 Ma and the Tui deposit yield an age of 5.714 ± 0.017 Ma.

3.2.2. Regional Volcanic Stratigraphy

The CVZ consists of andesite and dacite flows together with breccias and tuffs, forming a series of stratovolcanoes ranging in age from 18 to 3.8 Ma. These rocks interfinger with rhyolite tuffs and flows related to several caldera complexes which range in age from 12 to 1.95 Ma (Booden et al., 2012; Simpson and Chambefort, 2014). The andesite rocks predominate in the western side of the CVZ and rhyolites in the east (Skinner, 1986). The regional stratigraphy of CVZ consists of Late Jurassic marine sedimentary greywacke and argillite of the Manaia Hill Group forming the basement rocks. These rocks are exposed primarily in the northern end of the Coromandel peninsula (Figure 3.1). The basement rocks are overlain by very restricted non volcanogenic Oligocene coal measures and marine calcareous rocks of Torehina Formation (Te Kuiti Group). Also, minor volcanogenic marine conglomerate, sandstone and siltstone of Colville Formation of lower early Miocene age (Waitemata Group) are primarily deposited in the northern part of the CVZ (Skinner, 1969, 1979). These rocks are overlain by Miocene to Pliocene andesitic and dacitic volcanic rocks of the Coromandel Group and late Miocene to Pliocene rhyolites and pyroclastic rocks of the Whitianga Group (Skinner, 1986; Adams et al, 1994; Christie et al., 2007; in Simpson et al., 2007).

Table 3.1. Summary of regional stratigraphy of main Hauraki Volcanic Region (HVR) (Adapted from Skinner 1986).

Group	Sub Group	Formations	Age
Whakamarama		Waitearíki Ignimbrite Aongatete Ignimbrite	mid Pleistocene
	"Waitawheta Dacite"	Informal	Plio-Pleistocene
Kerikeri Volcanic	Mercury Basalts	Mercury Islands Woody Hill Colville Ridge	late Upper Miocene and/or younger
Whitianga	Minden Rhyolite	Ahu Ahu Rhyolite Whenuakite Rhyolite Ohena Rhyolite Purangi Rhyolite Ruahine Rhyolite Rangihau Rhyolite	Late Miocene to Pliocene
	Coroglen (Ignimbrite)	Ahu Ahu Ash Pumpkin Rock Ignimbrite Wharepapa Ignimbrite Carina Rock Ignimbrite	Late Miocene to Early Pleistocene
Coromandel	Omahine	Taurauikau Andesite	Late Miocene-Pliocene
	Kaimai	Pukepanga Uretara Waipupu	Late Miocene-Pliocene
	Kiwitahi	Several centres	Mid to Late Miocene
	Waiwawa	Tapuawtahi Andesite Taurahuehue Andesite Maumaupaki	Early late Miocene
	Kuaotunu	Cook Intrusives Huruhi Andesite Maunganui Basaltic Andesite Mahinapua Andesite Waitaia Sinter Rauporoa Basaltic Andesite Te Tutu Andesite Parakete Materangi Andesite Whangapoua Andesite Beesons Island Volcanics Tuateawa Andesite Te Karaka Andesite Kai-iti Porphyrites Kokumata Dacite Omoho Formation Port Charles Andesite Paritu Plutonics Cuvier Plutonics	Early to mid Miocene Late early Miocene
Waitemata	Kawau and Warksworth	Colville	Early lower Miocene
Te Kuiti		Torehina	Mid to upper Oligocene
Manaia Hill		Several formal units	Late Jurassic

3.2.2.1. Coromandel Group

The Coromandel Group rocks are further divided geographically into three major subgroups Kuaotunu, Waiwawa and Kaimai subgroups with an overlap of Omahine Subgroup. The Omahine Subgroup is similar in age and compostion with Kaimai Subgroup. The Subgroups are subsequently divided into more than 25 formations (Table 3.1) with regional unconformities separating the subgroups and local unconformities separating formations (Skinner, 1986). The rocks range in composition from andesites to rhyolites and dacites. The major subdivisions of Coromandel Group are described briefly as follows.

3.2.2.1.1. Kuaotunu Subgroup

Kuaotunu Subgroup rocks are predominantly deposited in the eastern part of the Peninsula and consist mainly of alternating pyroxene andesite and hornblende-pyroxene andesite to dacite sequences (Christie at al., 2007). The Subgroup consists of 17 formations and includes Cuvier and Paritu Plutonics of Late early Miocene (Skinner, 1986).

The other major unit is the andesitic Beesons Island Volcanics which lies in the western side of the Coromandel peninsula and extending from Colville south to Thames. This unit consists of subaerial/subaqueous pyroclastic and epiclastic breccias and conglomerates, flows and plugs and intensively hydrothermally altered to propylitic, argillic, and siliceous assemblages (Skinner, 1993).

3.2.2.1.2. Waiwawa Subgroup

The Waiwawa Subgroup rocks are subdivided into Taurahuehue Andesite and Tapuaetahi Andesite Formations and are cropped out in the southern and eastern part of the Coromandel Peninsula, chiefly to the west and north of the Mongakino and Waihi area (Adams, 1994). The Taurahuehue Formation overlies Maumaupaki Formation and lies southwest of Coroglento east of Thames and consist of sheet like flows, pyroclastics, and minor intrusives of phyric to glassy andesite rocks. These rocks mark the outer northern and western rim of the Kapowai Caldera. The Tapuaetahi Andesite rocks on the other hand cover an area of coastal hills from south of Hot Water Beach to Tairua and southwest to

Whenuakite consisting mainly of coarsely phyric andesite flows, pyroclastics, and intrusives that define the eastern rim of the Kapowai Caldera (Skinner, 1986, 1993; Adams, 1994).

3.2.2.1.3. Kaimai and Omahine Subgroup

The Kaimai and Omahine subgroup share almost the same age and composition with both subgroups dating back to late Miocene and Pliocene (Skinner, 1986). The Omahine Subgroup consists of Taurauikau Andesites which are chiefly composed of glassy, silicic andesite-dacite flows, minor intrusives forming a high plateau between the Waiwawa, upper Rangihau and Kaueranga Valleys (Adams, 1994). The Kaimai Subgroup consists of Pukepanga, Uretara and Waipupu Formations of which Waipupu Formation hosts most of the epithermal deposits of the Waihi area including Correnso deposit. The Waipupu Formation is subjected to extensive hydrothermal alteration and date back to Late Miocene to Pliocene (Adams, 1994).

3.2.2.2. Kerikeri Volcanic Group

The Kerikeri Group of rocks contain Mercury Basalt Subgroup which range compositionally from olivine and olivine-augite basalt to pyroxene basalt and basaltic andesite and age approximately to late Upper Miocene and/or younger (skinner, 1977, 1979). The Mercury Basalts are restricted to the north-eastern part of the Coromandel peninsula and offshore islands. Mercury Basalts of the Mercury Islands lie on a submarine plateau 15 km long by 5-10 km wide trending ENE. The plateau continues further towards the southern end of the Colville Ridge which indicate the basalt flows being the extension of the ridge into the New Zealand landmass (Skinner, 1977). The Mercury Island basalts consist of individual flows, separated by basaltic scoria, spatter, lapilli and tuff, and rhyolitic ash. These rocks also intrude and overlie Mahinapua Andesite on the eastern Kuaotunu Peninsula and form swarm of dikes intruding Ruahine Rhyolite at Woody Hill (Skinner, 1986).

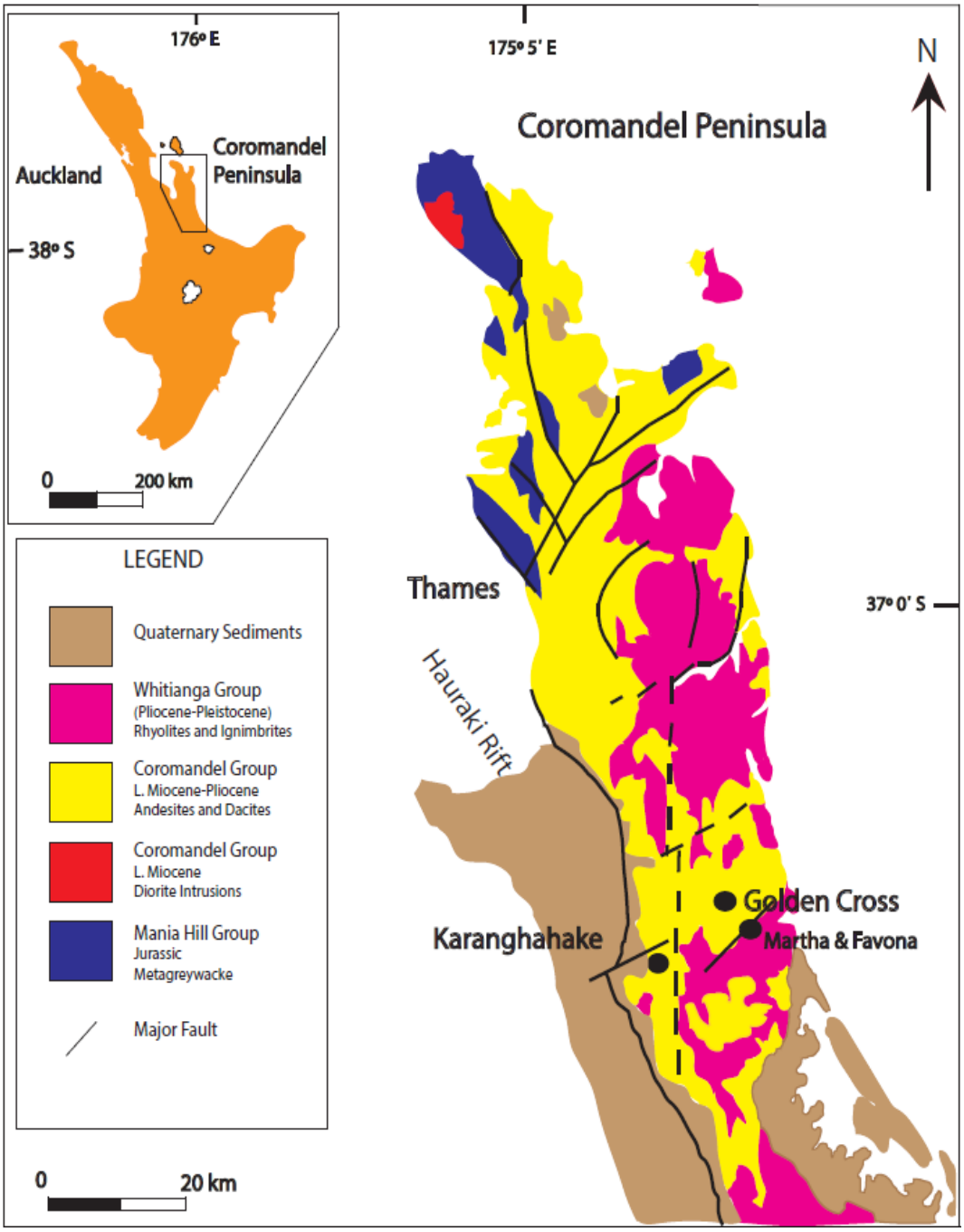

Figure 3.2. Geologic map of the Coromandel Peninsula, showing the location of major epithermal Au-Ag deposits, major faults and stratigraphic units (Adapted from Skinner, 1986; Mauk & Simpson, 2007).

3.2.2.3. Whitianga Group

The Whitianga Group rocks consist of late Miocene to Pliocene rocks which are restricted predominantly to the eastern coast and central part of the Coromandel Peninsula. The Group is further subdivided into two subgroups on the basis of the composition of rocks as Minden Rhyolite Subgroup and Coroglen Subgroup.

3.2.2.3.1. Minden Rhyolite Subgroup

The Minden Rhyolite Subgroup rocks are composed chiefly of flow-dome and caldera complexes which consist of calc-alkaline to alkaline felsic lavas of late Miocene to Pliocene age. Rhyolitic eruption centres dominate the east and west of the Waihi area. The Ruahne Rhyolite of Minden Subgroup occurs in Whitianga and Kapowai and consist of phyric, glassy and perlitic crystal-rich rhyolite intrusives, domes (Adams, 1994).

3.2.2.3.2. Coroglen Subgroup

The Coroglen Subgroup units consist of pyroclastic-volcaniclastic formations of Late Miocene to early Pleistocene and found in the central and southern parts of the Coromandel peninsula (Adams, 1994). The main formations of this subgroup are Carina Rock Ignimbrite, Wharepapa Ignimbrite and Pumpkin Rock Ignimbrite.

3.3. Local Geology

The Waihi region is a late Miocene volcanic-hosted area which is a part of 200 km long by 40 km wide metallogenic province and consists of 50 epithermal Au-Ag deposits along with several porphyry Cu-Au occurrences. The area is located within the Coromandel Volcanic Zone (CVZ), part of Hauraki Volcanic Region (HVR) (Christie et al., 2007). The Late Jurassic greywacke and argillite of the Manaia Hill Group form the basement rocks and are exposed primarily in the northern end of the Coromandel peninsula (Figure 3.2). These are directly overlain by Miocene to Pliocene andesitic and dacitic volcanic rocks of the Coromandel Group and late Miocene to Pliocene rhyolites and pyroclastic rocks

of the Whitianga Group (Skinner, 1986; Adams et al, 1994; Christie et al., 2007; in Simpson and Mauk, 2007).

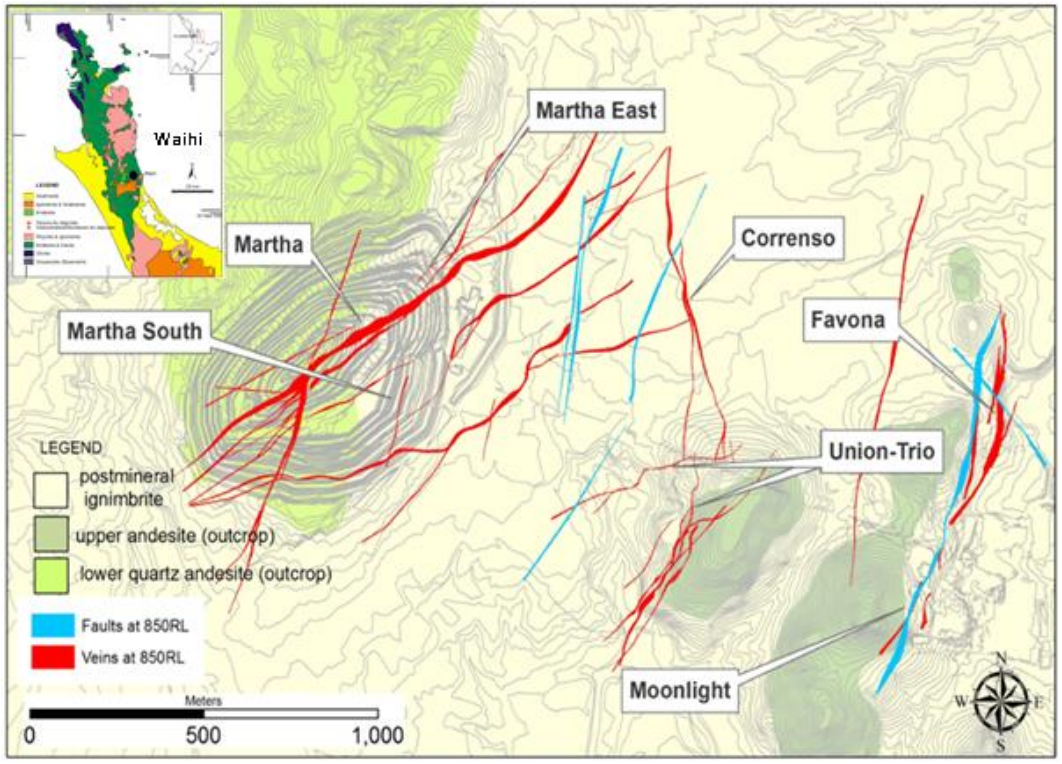

Figure 3.3. Location and extent of Correnso Vein with adjacent veins in the Waihi area with major faults (Adapted from Newmont Waihi Gold, 2014).

Epithermal deposits of the Hauraki Goldfield are chiefly hosted in Coromandel Group andesitic volcanic rocks of the Coromandel Volcanic Zone (Skinner, 1986; Brathwaite and Skinner, 1997). Some deposits also occur in the top of the underlying Mesozoic greywacke basement, early Tertiary rocks and the Whitianga Group rhyolitic volcanic rocks (Sporli et al., 2006). The Correnso deposit is located within the Waihi epithermal system, striking NNW and extends over 800 meters strike length between the Union Hill-Trio deposit to the south and the eastern end of the Martha vein system to the north. The Miocene andesitic volcanic sequence of the Waipupu Formation is informally subdivided into Upper Andesite and Lower Andesite units (Hobbins et al., 2012) and the differences between the two is discussed in detail in the next section.

3.3.1. Host Stratigraphy

The Correnso deposit is located adjacent to other Au-Ag vein systems that collectively form a zone of highly mineralised deposits in the Waihi area. Apart from the world class Martha deposit, the other deposits in the area include Favona, Union-Trio, Amaranth, and Moonlight. The Correnso deposit contains highly mineralised Au-Ag quartz veins hosted in the Miocene andesite of the Waipupu Formation (Hobbins et al, 2012) and rock sequence outcrops at Martha Hill and Union Hill. The Waipupu Formation is informally subdivided into Upper Andesite and Lower Andesite units with a post-mineral ignimbrite unit on the top (Figure 3.4). The characteristic features of the units are given in the next page.

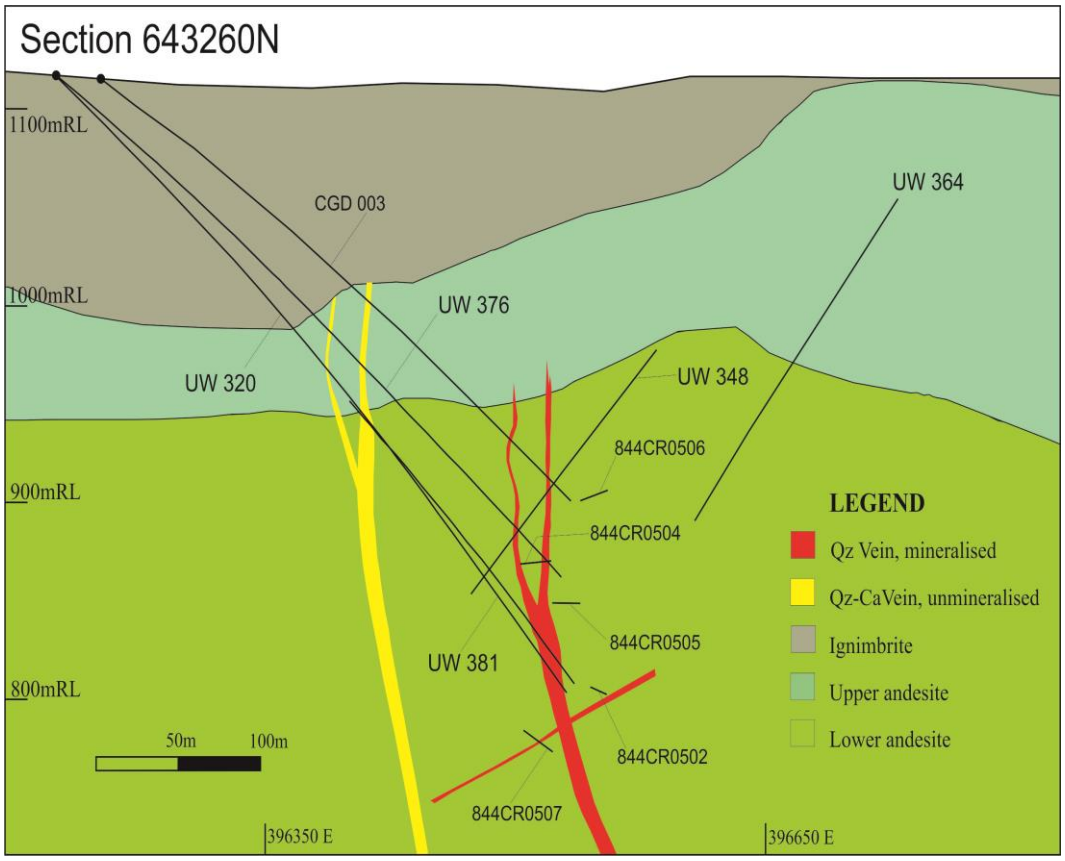

Figure 3.4. Location of the Correnso Au-Ag vein (In red) with drillcore locations studied for this study. The yellow vein is an unmineralised vein. The local stratigraphy of the area is also shown (Modified after Newmont Waihi Gold, 2013).

The Lower Andesite Unit is distinct from its upper unit because of the presence of quartz phenocrysts being more dominant. The lower quartz-phyric unit is also host to high grade Au-Ag mineralisation which gradually decreases in width and grade as it extends to the upper unit. The Upper Andesite Unit on the other

hand is marked with the presence of more volcaniclastic horizons consisting of porphyritic andesite, autoclastic or epiclastic breccias and tuffs. The two units are separated by a tuffaceous marker horizon which is more prevalent at the north end of the vein system and mostly absent further south with a thickness varying from a few centimetres to tens of metres (Hobbins et al., 2012).

3.3.2. Local structure and Vein Geometry

The Waihi area is home to highly mineralised Au-Ag veins hosted in the host rocks of the Waipupu Andesites. The mineralisation covers an area extending east of Waihi town and is restricted to the northwest by Waihi Fault and to the southwest by the margin of large depression also known as Waihi Basin (Smith et al., 2006; Hobbins et al., 2012). The major faults at Waihi exhibit a northeast to north-northeast strike which is roughly perpendicular to the east-directed subduction which formed the Coromandel Volcanic Arc and dip steeply toward the northwest or southeast. There are also other minor faults which are aligned north-south and northwest-southeast (Hobbins et al., 2012).

The Correnso vein lies east of Waihi town adjacent to Martha and Favona deposits with an overall strike of north-northwest, different to the strike of other veins identified in the area. Drillcore and other exploration data from Newmont Waihi Gold shows the structure and extent of the Correnso vein, suggesting a main single vein separating into two sub-parallel veins as Correnso East and Correnso West from the centre and protruding into the Upper and Lower Andesite units. The vein dips steeply or moderately steeply to the east. The northern mineralisation zone of the Correnso deposit exhibits more fault and fracture zones within the vein and vein margins compared to the central part where minor development of fault breccias is limited to the central part of the vein (Hobbins et al., 2012).

3.4. Mineralogy and Geochemistry of the Waihi area

The Coromandel Volcanic Zone (CVZ) comprises about 50 low-sulphidation (adularia-sericite) epithermal Au-Ag vein deposits and porphyry Cu deposits. The epithermal deposits of the Hauraki field have produced 320, 000 kg of Au and 1.5

million kg of Ag since 1862 (Christie et al. 2007). Apart from the world class Martha Hill, other economically important epithermal systems in the Hauraki field include Ohui, Broken Hills, Onemana, Neavesville, Golden Cross, Karangahake and Favona. The adularia-sericite epithermal systems of the Hauraki Goldfield are of the quartz vein type, the majority of which are hosted in andesite and pyroclastics and to a lesser extent in rhyolitic rocks. The veins are widest in massive andesites, whereas in rhyolitic rocks thin quartz veinlets and silicified breccia zones are more common. The quartz veins of the Hauraki epithermal systems are open-space fissure fillings, commonly displaying crustiform banding. Vein minerals apart from quartz include calcite, manganiferous carbonates, adularia, siderite, barite and anhydrite. Pyrite is a common sulphide mineral; electrum and native Au constitute the chief economic ore minerals (Christie et al., 2006). Though the whole area is composed of good mineralization of gold and silver, this literature review is focussed on deposits close to Waihi (Martha, Favona and Golden Cross) because of their close proximity to the Correnso Vein with the same general geological setting.

This thesis is focussed on studying the alteration mineralogy, geochemistry around the vein system and lateral variations in the lithogeochemistry and mineralogy. These have been assessed through a series of holes which intersect and surround the Correnso vein using a series of oriented drill holes which together defined a cross section (Figure 3.4). The brief description of the hydrothermal alteration, mineralogy and geochemistry of the area with Correnso deposit with respect to the published literature is described as follows.

Hydrothermal Alteration, Mineralogy and Geochemistry

The hydrothermal alteration is prominent in Waihi area and the host rocks dacites and andesites have been intensively hydrothermally altered. Christie et al. (2007) described the hydrothermal alteration in their paper on epithermal Au-Ag and related deposits of the Hauraki Goldfield. Hydrothermal alteration is widespread in the area and alteration halos envelope an area ranging from ~5-120 km² with most of the alteration halos extending less than 50 km². The

hydrothermal alteration halos are found to overlap multiple deposits and episodes of geothermal systems (Braithwaite and Christie, 1996). Most common alteration type is propylitic characterized by the presence of quartz, chlorite, illite, albite, calcite, and pyrite and the alteration is weak distal to the mineralization with the pyroxenes and hornblende phenocrysts replaced with chlorite calcite and pyrite (Simpson et al., 2001). Argillic alteration is also found in and around Golden Cross, Martha and Favona deposits characterised by the interstratified illite-smectite present in the distal host rocks grading to illite proximal to the veins (Simpson et al., 2001; Simpson and Mauk., 2007; Christie et al., 2007).

The Martha Hill deposit exhibits three main alteration types: potassic, argillic and propylitic. The potassic type is represented by the assemblage quartz + adularia + illite + pyrite; the argillic type has illite + smectite + chlorite + pyrite; and the propylitic type has quartz + calcite + chlorite +illite + pyrite (Pirajno, 2009). Simpson and Mauk (2001) described alteration mineralogy of the Gladstone Hill deposit, adjacent to Martha Hill, area in detail. Late Miocene andesitic rocks of the Waipupu Formation were found to be extensively altered with all igneous minerals except quartz replaced by alteration minerals. The main alteration minerals occuring in the Gladstone Hill are quartz, illite, interstratified illite-smectite, pyrite, chlorite, adularia, albite, smectite, calcite, epidote, and kaolinite. Simpson and Mauk (2001) summarised that the formation of alteration minerals at Gladstone Hill prospect are similar to the pattern in geothermal systems where clay mineralogy commonly co-relates with temperature. Hollinger & Mauk (2001) also discussed about vein mineralogy and fluid inclusion studies on Gladstone Hill deposit. They described different veins, vein structures, and textures in detail and found pyrite and quartz veins to be common with pyrite veins being formed first. The fluid inclusion studies undertaken on inclusions hosted in quartz, calcite and amethyst veins identified two types of fluid inclusions; a two phase (liquid + vapour) liquid-rich inclusions and vapour-rich inclusions that contained greater than 95% vapour. They concluded that dominant primary texture in the Gladstone Hill and Martha areas are crustiform

banded veins and massive veins. The occurrence of platy texture replaced by quartz suggested this texture to be formed under the conditions of boiling.

Simpson et al. (2000) also described the alteration mineralogy of hydrothermal alteration at Golden Cross, Waihi somewhat similar to Martha Hill deposit. Main alteration minerals present are quartz, adularia, chlorite, illite, interstratified illite-smectite, pyrite, calcite, and kaolinite, together with minor smectite, siderite, marcasite, titanite, leucoxene, and alunite. The hydrothermal alteration varies greatly and in some places and rocks are altered over large distances. Simpson et al. (2000) suggested a paragenetic sequence of hydrothermal minerals in the Empire zone with quartz and pyrite to be formed first and followed by the partial alteration of adularia to illite or illite smectite followed by kaolinite, minor pyrite, marcasite and rare alunite over-printed the above minerals. The study also confirmed the alteration mineral assemblages formed from a near-neutral to weakly alkaline pH chloride water known to be originating from deeply circulating meteoric waters heated and then ascending from several kilometres depths (Henley and Ellis, 1983). They also noted that the abundance of calcite and the absence of calcium zeolites indicated that these chloride-rich waters contain considerable concentrations of dissolved CO_2, and boiling led to the direct deposition of platy calcite and adularia in veins.

Mauk et al. (2006) also studied the Favona epithermal deposit for mineralogy and geochemisty. The hydrothermal alteration was found to be intense with all igneous minerals except for quartz to be replaced by hydrothermal alteration minerals. The hydrothermal minerals show distinct zonation around the deposit and the alteration assemblage of quartz, adularia, illite, chlorite, and pyrite are suggested to be formed from upwelling alkali chloride fluids. The geochemistry of altered rocks indicate that hydrothermally altered andesites in most of the samples are enriched in Si, K, Rb, Ba, S, Au, As, Sb and depleted of Na, Sr and Ca.

Correnso being the most recent discovery also shares the alteration mineralogy, geochemistry and hydrothermal alteration zonation with its proximal deposits. Hobbins et al. (2012) described the hydrothermal alteration of Correnso deposit

to be complex which includes horizons of extensively altered host rocks alternating with the less altered and massive porphyritic andesites known as “hard bars”. The deposit is informally divided into upper and lower andesite units showing variable alteration zonation with the upper andesite unit being intensely altered than the lower unit. Detailed alteration zonation, primary and secondary mineralogies, and geochemistry is studied for this project and is described in the following chapters.

4. Petrography and XRD Analysis

4.1. Introduction

This chapter focuses on the results obtained by studying primary and alteration mineralogy under petrographic microscope to identify potential vectors towards epithermal veins. X-ray diffraction (XRD) analysis was also done for 68 samples and results are presented in this chapter. Petrographic analysis of the samples collected from the host rock and main Correnso vein show alteration mineralogy similar to the adjacent Martha deposit. The hydrothermal alteration has significantly altered the host rocks which is clearly visible in hand specimens and thin sections. Alteration intensities range from intensely altered samples to fresh or less altered and number of samples exhibit their original volcaniclastic textures still intact. The methodology for the preparation of samples is also described in brief.

4.2. Methodology

The preparation of slides for petrographic analysis was done at University of Waikato petrology lab. Sixty four samples were selected and made into thin sections for petrographic analysis on the basis of alteration intensity and distinct visible features like alteration halos, quartz and calcite veins, samples containing breccia and clays etc. and eleven slides were further polished to study opaque mineralogy and other sulphide minerals. Core samples were first cut into small blocks (3.5x2.5x2.5 cm) using a saw and then grounded to remove uneven surfaces on a glass plate using aluminium oxide powder. The ground surface of the blocks were then washed and put on a hot plate with ground surface sitting upwards to avoid any contamination and left for complete drying on hot plate at 60 degrees. Since the majority of the samples were hydrothermally altered and the veinlets and vesicles were common, the samples were surface impregnated using Aradlite K39 solution with a 2:1 ratio of resin and hardener and put on hot

plate at 60 degrees for 6 hours. Glass slides were then frosted on one side using Struers Discoplan-TS and then washed and put on hot plate for 2 hours at 60 degrees to dry. Hillquest resin was then mixed with hardener using a ratio of 2:1 and heated on glass plate to make it less viscous and mixed cautiously to not form any air bubbles. The blocks were then mounted against frostered part of glass slide and carefully moved along the block to remove any visible bubbles. Mounted slides were left on the hot plate to dry overnight.

The mounted blocks were cleaned from any leftover resin using a blade to avoid any unevenness and then cut down to ~1 mm thickness using a saw fitted on Struers Discoplan-TS. The rest of the sample was then grounded to ~30 microns with frequent checking of glass slide under microscope for interference colours to determine the right thickness required for petrographic analysis. The samples were then labelled with the required information. Eleven slides were also selected for studying opaque minerals. These slides were further ground using a Buehler-Metaserv grinder-polisher and frequently analysed under reflected light to check for the correct thickness where opaque minerals can be identified clearly.

4.3. Primary Mineralogy

Primary mineralogical features for sixty four samples was studied using a petrographic microscope at the University of Waikato. Optical properties of the minerals were applied to identify the minerals in the samples. Hydrothermal alteration products and its effect on the primary mineralogy was also studied. The major primary minerals identified, in order of abundance are quartz, plagioclase, clinopyroxenes, and orthopyroxenes with minor amounts of zircon and amphiboles. Very few samples have the primary andesite texture preserved as hydrothermal alteration has partially or completely altered the original minerals. Petrographic analysis suggest an alteration pattern with respect to the mineralisation where certain mineral assemblages were found at certain levels and depths of the vein system. The detailed alteration mineralogical features are presented in the alteration mineralogy chapter and the primary minerals identified are given in the following pages.

Plagioclase

Plagioclase is ubiquitous in samples and is variably replaced by calcite in majority of the samples. The phenocrysts have experienced differential levels of hydrothermal alteration but most of the samples are partially or wholly replaced by calcite. Some samples show inclusions as pyroxenes and opaque minerals (Fe-Ti oxides) within a plagioclase crystal. The size and shape of the phenocrysts vary from sample to sample. Most of the phenocrysts are found as crystal clots showing a glomeroporphyritic texture but are also present as single isolated crystals. They range from medium to large sized (0.4 - 3 mm) phenocrysts to lathes and fine crystallites in the groundmass. The shape of the crystals appear to be well defined in fresh and some partially altered samples where it ranges from euhedral to anhedral and subhedral. Samples which have undergone intense hydrothermal alteration display relic textures of the original phenocrysts but quite a number of samples are so altered that the textures are hard to recognize. Also, some samples exhibit a rounded resorbed rim around the phenocrysts (Figure 4.1C) representing a sieve texture formed as the result of disequilibrium during the crystallisation phase. In some samples, crystals with sieve texture and normal plagioclase crystals lay side by side within the same slide. The magma mixing is evident from different textural appearances as crystals exhibiting a smooth and nice euhedral shape represent a fresh magma while other crystals show a blotchy and irregular shape representing an early crystallisation phase.

Oscillatory zoning is also present in fresh samples as concentric rings within a plagioclase crystal but it is not widespread and quite a number of samples exhibit patchy and reverse zoning as well. Also, some crystals display a primary polysynthetic twinning. Carlsbad twinning is also present but it is not common though. Most of the primary texture is found in the samples containing “hard bars” (areas of andesites with less alteration) where it is commonly preserved as large, intact crystals, presumably reflecting the low permeability of these hard bar units. It is also present in groundmass as lathes and fine matrix.

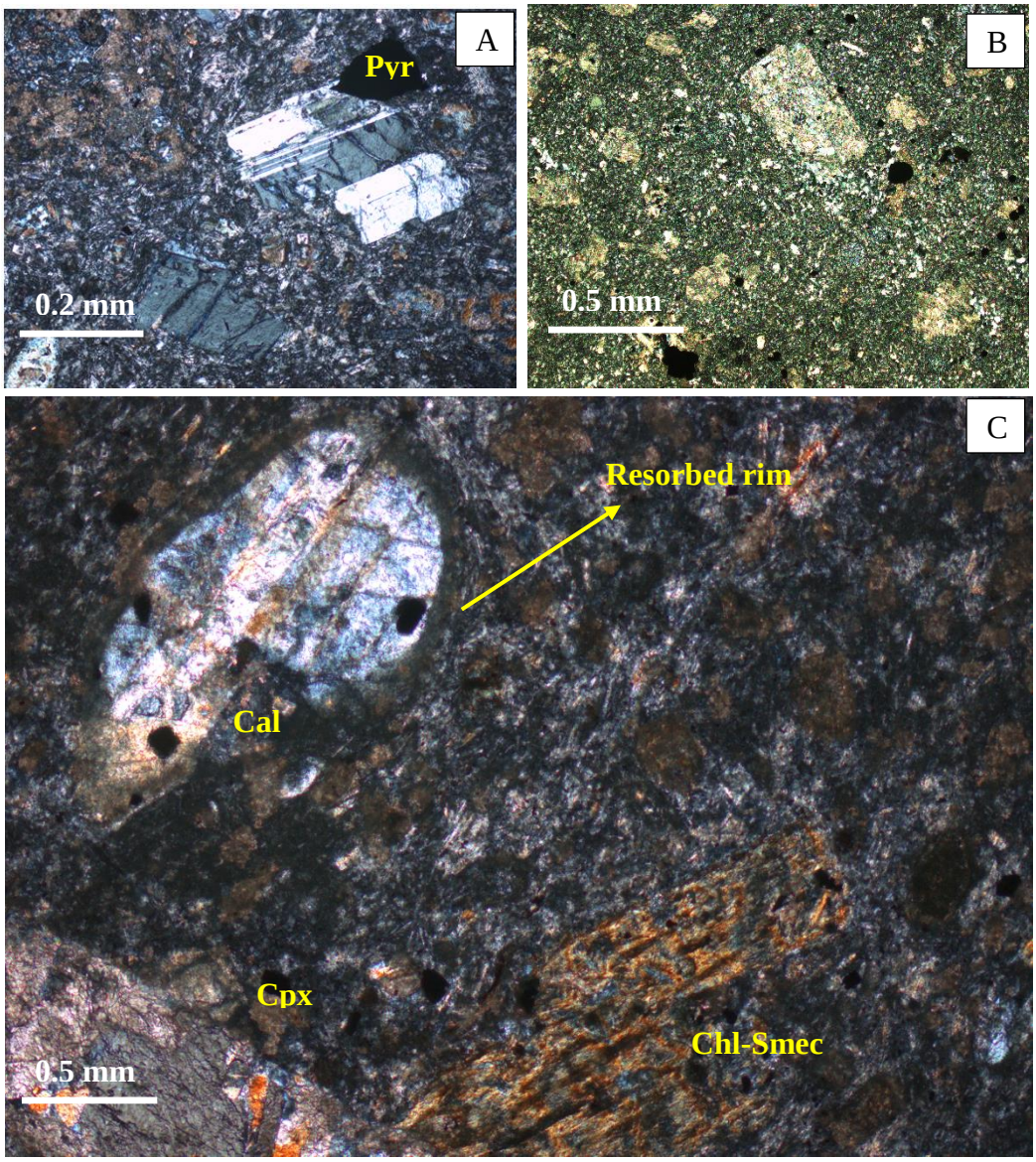

Figure 4.1. Pictomicrographs of Plagioclase phenocrysts. (A) Fresh plagioclase from drillcore UW320/481.20. The original igneous texture is still intact. (B) Partially altered plagioclase phenocryst replaced by sericite CRO507/334.10 (C) Plagioclase crystal partially altered and replaced with calcite from drillcore UW320/559.10. The rounded rim represents disequilibrium during the crystallization phase. Partially altered clinopyroxene crystal at the bottom left is also seen being replaced with chlorite and calcite. The one on the right is possibly replaced with chlorite-smectite. (Chl-Smec: Chlorite-Smectite, Cpx: Clinopyroxene, Cal-Calcite, Pl: Plagioclase).

Clinopyroxenes

Clinopyroxenes are the second most abundant minerals present after plagioclase in the Correnso deposit. Hydrothermal alteration has resulted in the replacement of original igneous texture with secondary minerals. In most of the samples, the primary andesitic texture is hardly preserved and majority of the phenocrysts are partially or wholly replaced by chlorite, pyrite, and quartz. The only clinopyroxene identifiable is augite (Figure 4.2 A) which is also restricted to fresh or least altered samples, especially collected from the samples containing “hard bars”. The phenocrysts display, light orange, purple and yellow colours under cross polarised light (Figure 4.2 A). Some of the samples contain clinopyroxenes exhibiting oscillatory and sector zoning.

Orthopyroxenes

Orthopyroxenes are also present as residual or relic textures in number of slides which are partially or intensely hydrothermally altered and replaced by secondary minerals like chlorite, calcite, and other clay minerals such as illite and smectite. Hypersthene is the only orthopyroxene found in its original form and again restricted to fresh or least altered samples (Figure 4.2 C).

Amphiboles

Primary amphiboles were rarely encountered in the thin sections as they are the first to disappear with the onset of hydrothermal alteration. Only one slide contained a hornblende phenocryst with its original igneous texture partially intact (Figure 4.2 B). Other slides exhibit partially altered or relic texture of the original amphibole crystals replaced with chlorite, quartz or other clay minerals. The relic texture is usually prismatic or diamond shaped cross sections. The colour ranges from light green to dark brown.

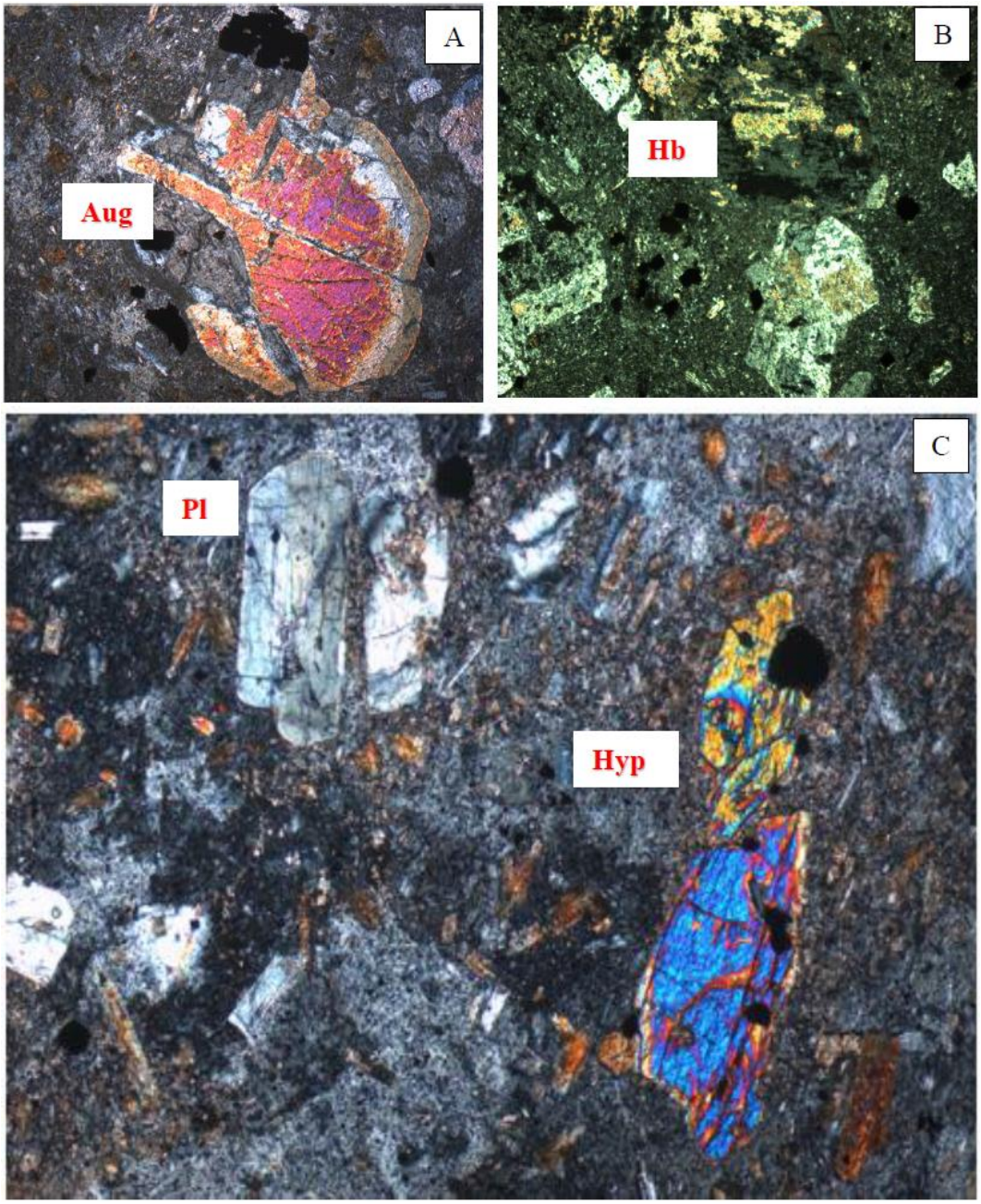

Figure 4.2. Pictomicrographs of pyroxene and amphibole phenocrysts. (A) Fresh pyroxene phenocryst from drillcore UW320/481.90m. The original igneous texture is still intact. (B) Partially altered amphibole phenocryst possibly hornblende replaced with chlorite at the outer edges from UW364/360.70m. (C) Hypersthene phenocryst from fresh andesite in drillcore UW348-116.45m with intact plagioclase and quartz-plagiocalse groundmass. (Hyp: Hypersthene, Aug: Augite, Pl: Plagioclase, Hb: Hornblende).

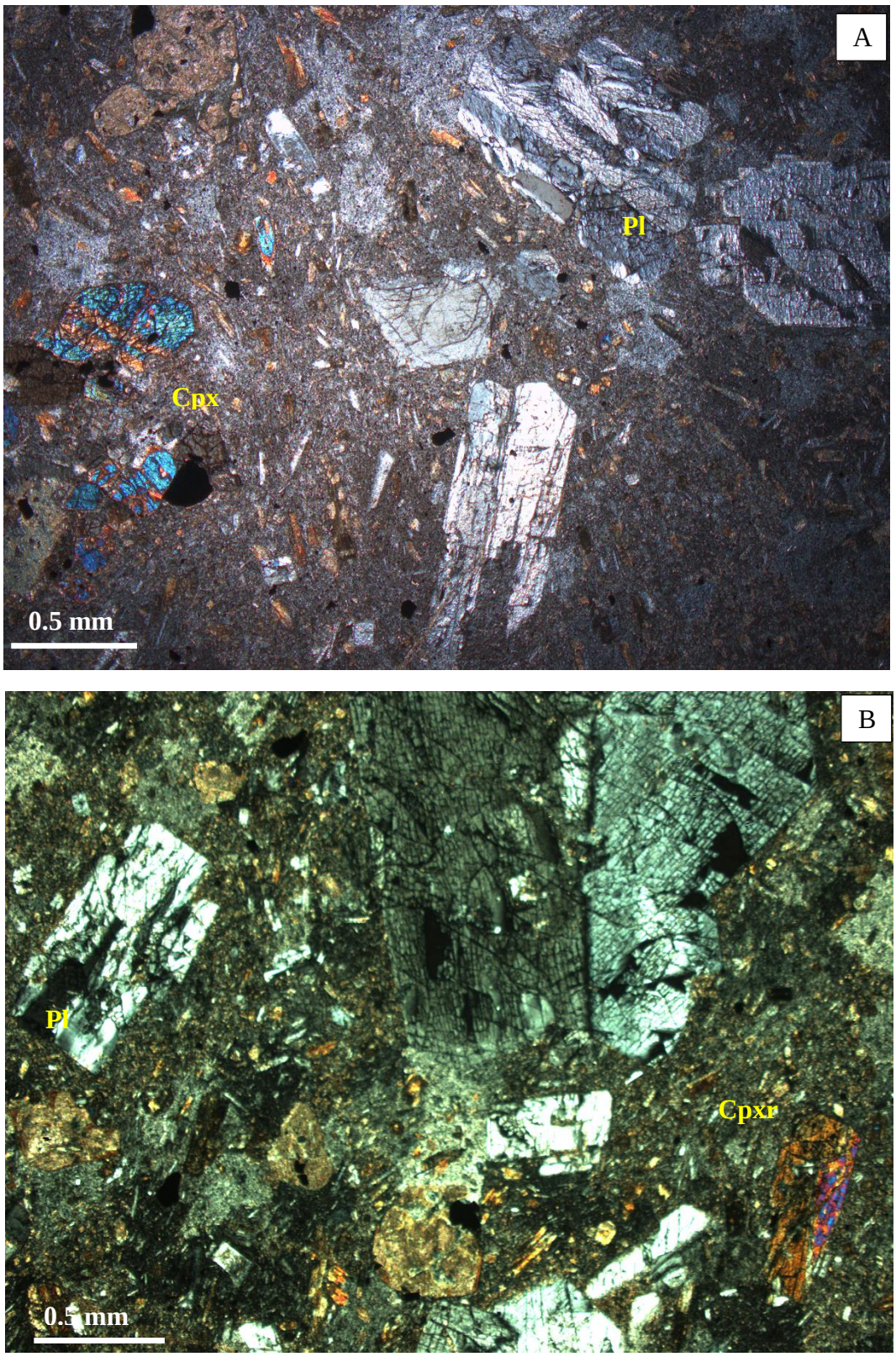

Figure 4.3. Variable alteration intensities undergone by pyroxene phenocrysts. (A) Fresh andesite with plagioclase and pyroxenes from UW348/122.50m. (B) UW348/128.60m. Less altered slide with plagioclase still intact but pyroxene has undergone partial alteration and has been replaced with chlorite.

Quartz

Quartz is also a ubiquitous mineral present both in host andesite and in veins. Although large veins run through the samples close to the main ore body, some tiny veinlets are also present in a number of samples, in association with calcite. Primary quartz occurs as single discrete crystals spread across the slide. Large quartz phenocrysts (Fig. 4.4A & B) of magmatic origin (inferred from the embayment structure) are more abundant in the lower andesite unit, inferring a different rock type than the overlying upper andesite unit. It is also present as fine grained groundmass in most of the core samples along with plagioclase, pyrite, and chlorite. The detailed overview of the secondary quartz is present in the alteration mineralogy chapter.

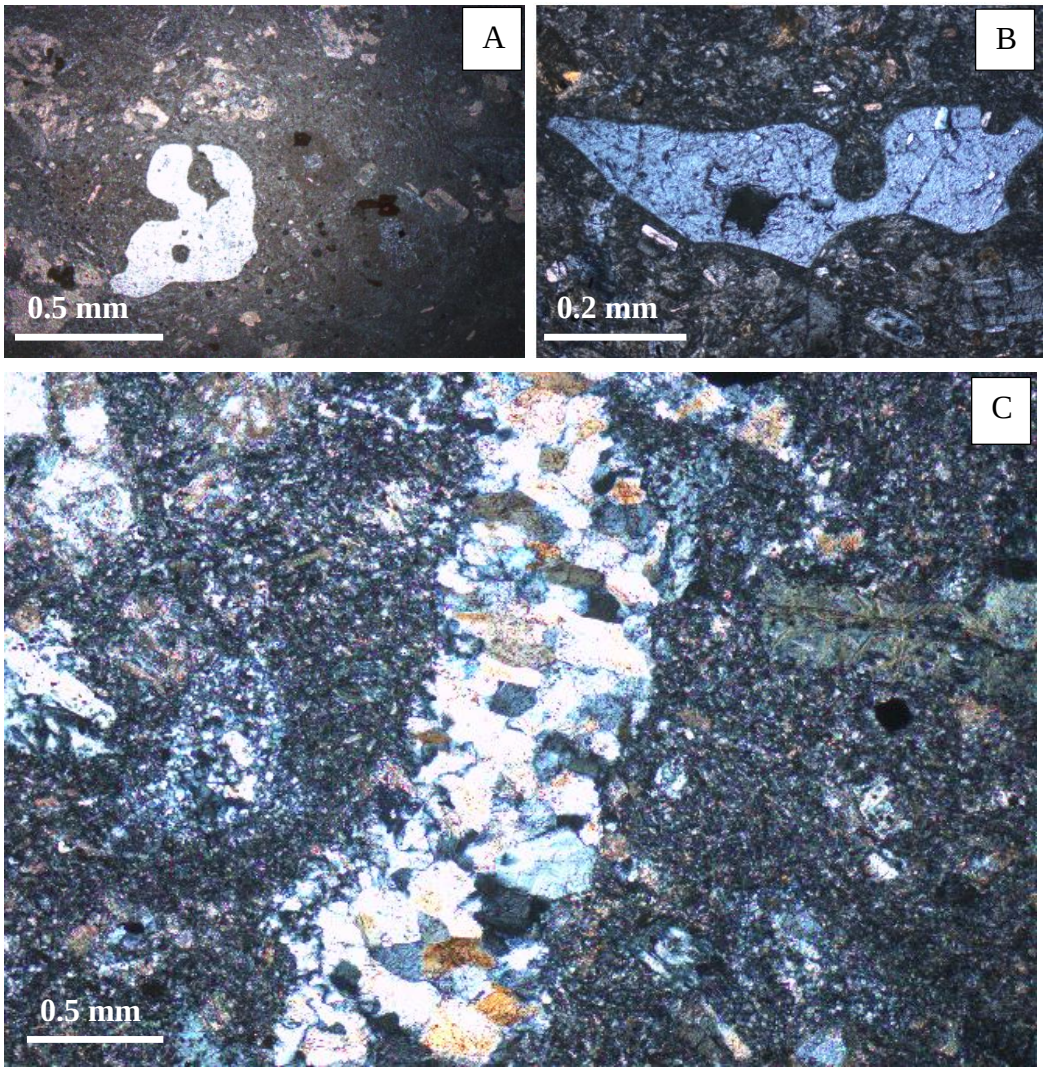

Figure 4.4. Pictomicrographs of quartz phenocrysts. (A) & (B) embayment structure of the quartz crystals representing original igneous texture. (C) Quartz present in the veins and also as groundmass in the sample UW320/.

Zircon

Zircon is present in couple of samples characterized by easily identifiable tetragonal crystals besides its straight extinction. The crystals range in colours appearing as blue to reddish brown colour. The drillcore sample CRO507/334.10 contains zircon crystals still intact (Figure 4.5 E) suggesting hydrothermal alteration has no effect on zircon.

Limonite

Limonite is found in few samples in the form of channels usually filling the voids and open spaces within the grains or following the veins and veinlets across the slide (Figure 4.5 A). The slides containing limonite exhibit rusty brownish or reddish flakes formed as the result of the weathering and often staining nearby minerals.

Opaque Minerals

Opaque minerals are also present both in host rock and in veins. They are present mostly in the altered samples as cubic shaped crystals (Figure 4.5 B) and also as fine grained or disseminated in the groundmass (Figure 4.5 D). The cubic shaped crystals are identified in polished slides as pyrite. They display variety of shapes ranging from cubic to sub-hedral crystals found as discrete single crystals spread across the slide in host rocks or as clots mainly in veins. In some samples, they are present as flows within the veins identified as other iron sulphide minerals besides pyrite (Figure 4.5 C).

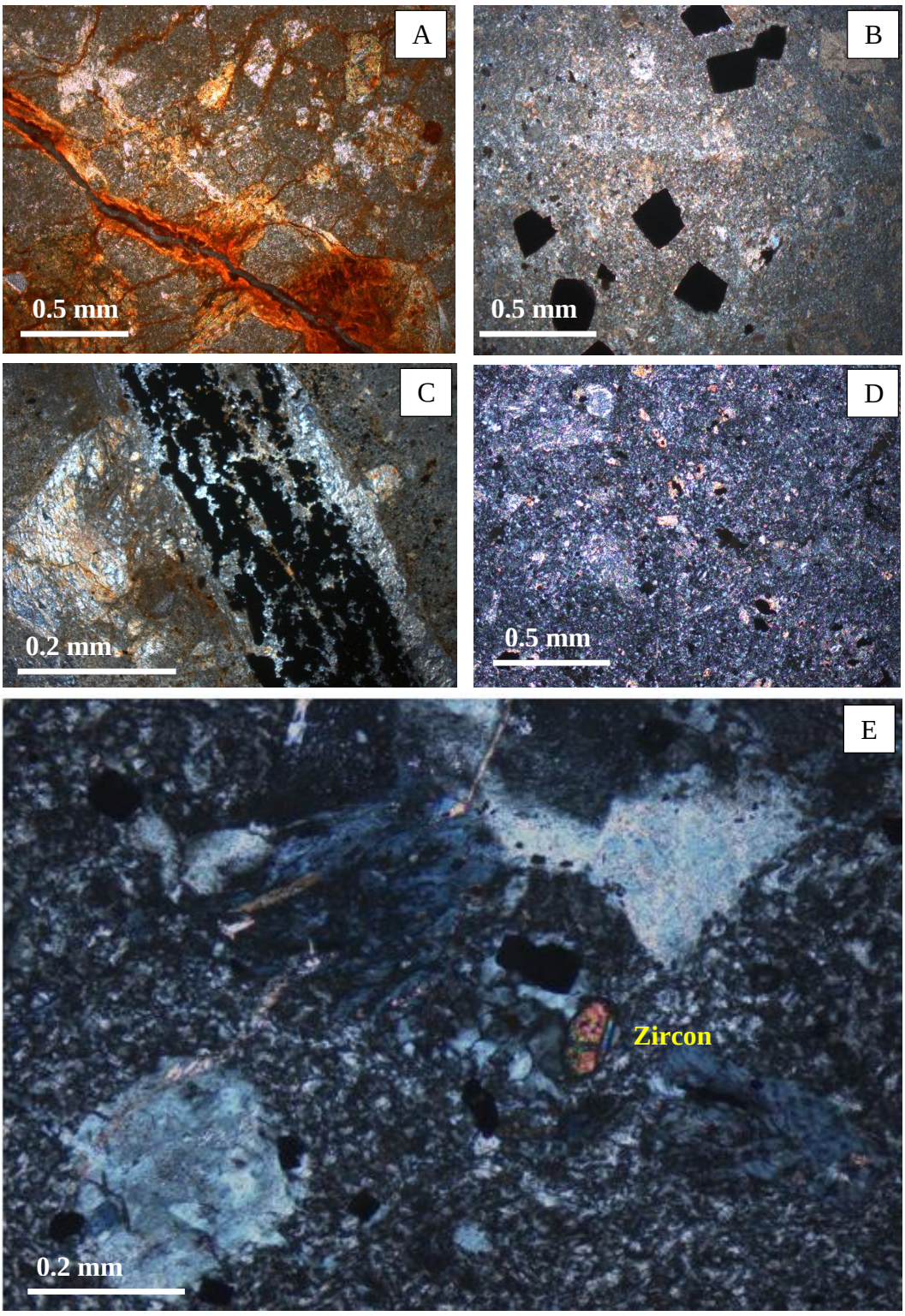

Figure 4.5. (A) Limonite channels filling gaps and voids in sample in UW348/192.8m. (B) Cubic shaped crystals of opaque mineral possibly pyrite. (C) Vein of opaque minerals proximal to the mineralization zone. (D) Fine, disseminated opaques in the groundmass. (E) Zircon crystal in the feldspar, quartz groundmass.

Groundmass

The groundmass consists of quartz, plagioclase, calcite, chlorite and other clay minerals. In fresh and least altered samples it primarily consists of feldspar as plagioclase laths and quartz. These are variably replaced with calcite, chlorite and clay minerals with opaque minerals replacing primary igneous minerals. The texture of the groundmass ranges from granular quartz and pyroxenes to plagioclase laths. In some samples it shows trachytic texture (Figure 4.6C) representing flow banding of the lava. Devitrified glassy texture is also present in some samples representing original feature (Figure 4.6D).

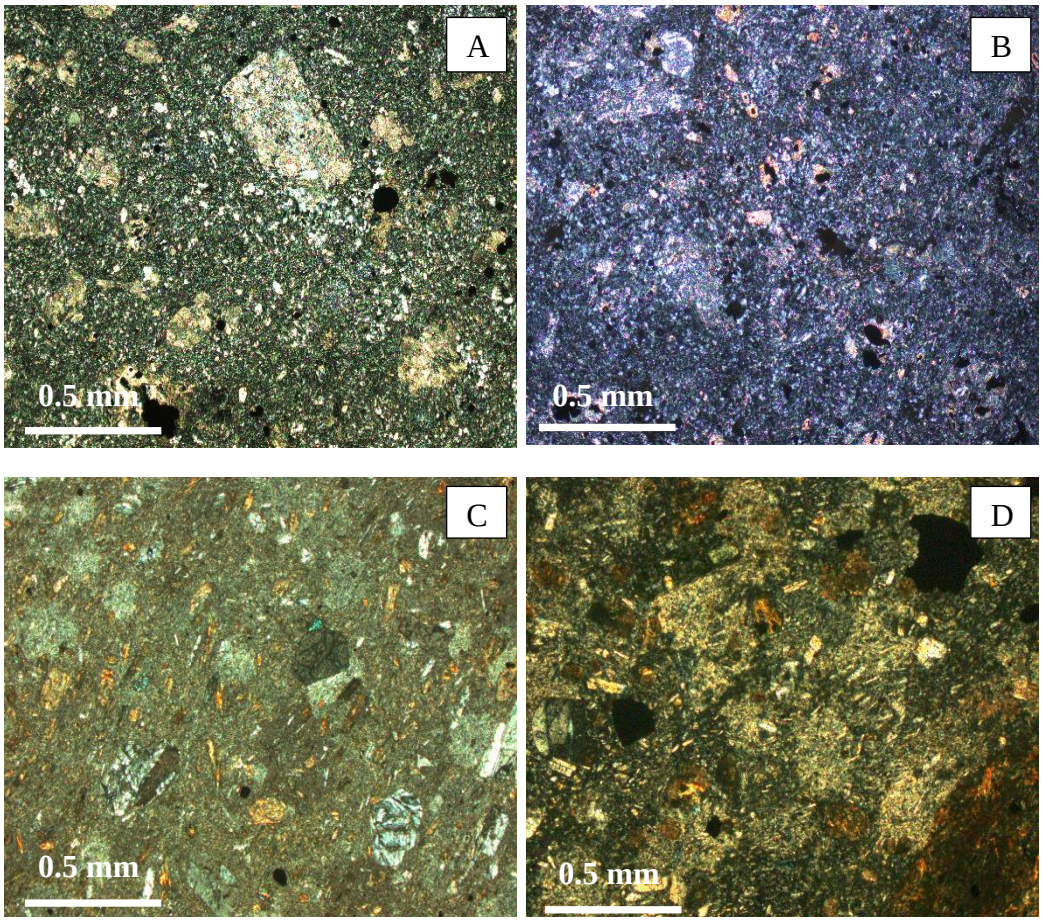

Figure 4.6. Groundmass textures and mineralogical features. (A) Groundmass with calcite, Fe-Ti oxides and quartz from the sample UW320/415.60 (B) Another example of groundmass containing quartz, calcite and chlorite in UW 348/181.85. No original minerals present. (C) Trachytic groundmass texture in the sample CGD003/177m (D) Devitrified glassy groundmass texture representing original texture in the sample UW320/481.90m.

Breccia

Hydrothermal breccia zones can be used as effective vectors to the mineralization in epithermal deposits. Phreatic breccias were also identified at Correnso deposit which is texturally similar to the breccia types identified by Corbett and Leach (1998) in the phillipines geothermal fields. These breccias form as the result of vapour driven explosions at shallow crustal levels (Hedenquist and Henley, 1985; Corbett and Leach, 1998). These type of breccias are commonly associated with adularia-sericite low sulphidation epithermal deposits (Corbett and Leach, 1998).

In Correnso vein system, pebble dykes and dike-like breccias are cross cut by all vein phases and thought to be formed prior to the epithermal veins (Sporli and Cargill, 2011; Hobbins et al., 2012) with cavities filled with post-brecciation hydrothermal fluids. Hydrothermal breccia clasts were found in a number of samples and were visibly identified in hand specimens as well as in thin sections. Most of the samples identified with breccia include angular to sub-rounded clasts (Figure 4.7A & B) of host andesite enclosed within a fine grained matrix. The matrix range in colour from light green to dark green but in samples proximal to the mineralization, the colour of the matrix is brown to dark brown. In hand specimens, the breccia displays variable textural features such as jigsaw shaped pattern which signifies minimal transport of original rock type with the voids and cavities filled with hydrothermal fluids (Figure 4.7C).

Breccia mineralogy

Breccia mineralogy is similar to the host rocks and consists of host andesite clasts enclosed in a mush of fine grained matrix. The clasts consist of pyroxenes and feldspars that have undergone variable alteration intensities being replaced with chlorite and calcite and other clay minerals and the groundmass consists of chlorite, quartz, calcite and clay minerals. In Some samples, chlorite crystals display a wavy texture such as the highly brecciated slide UW 348/181.85 (Figure 4.7A). This wavy texture signifies the breccia shear zones where the breccia has slided against each other and through which hydrothermal fluids have passed affecting the primary mineralogies.

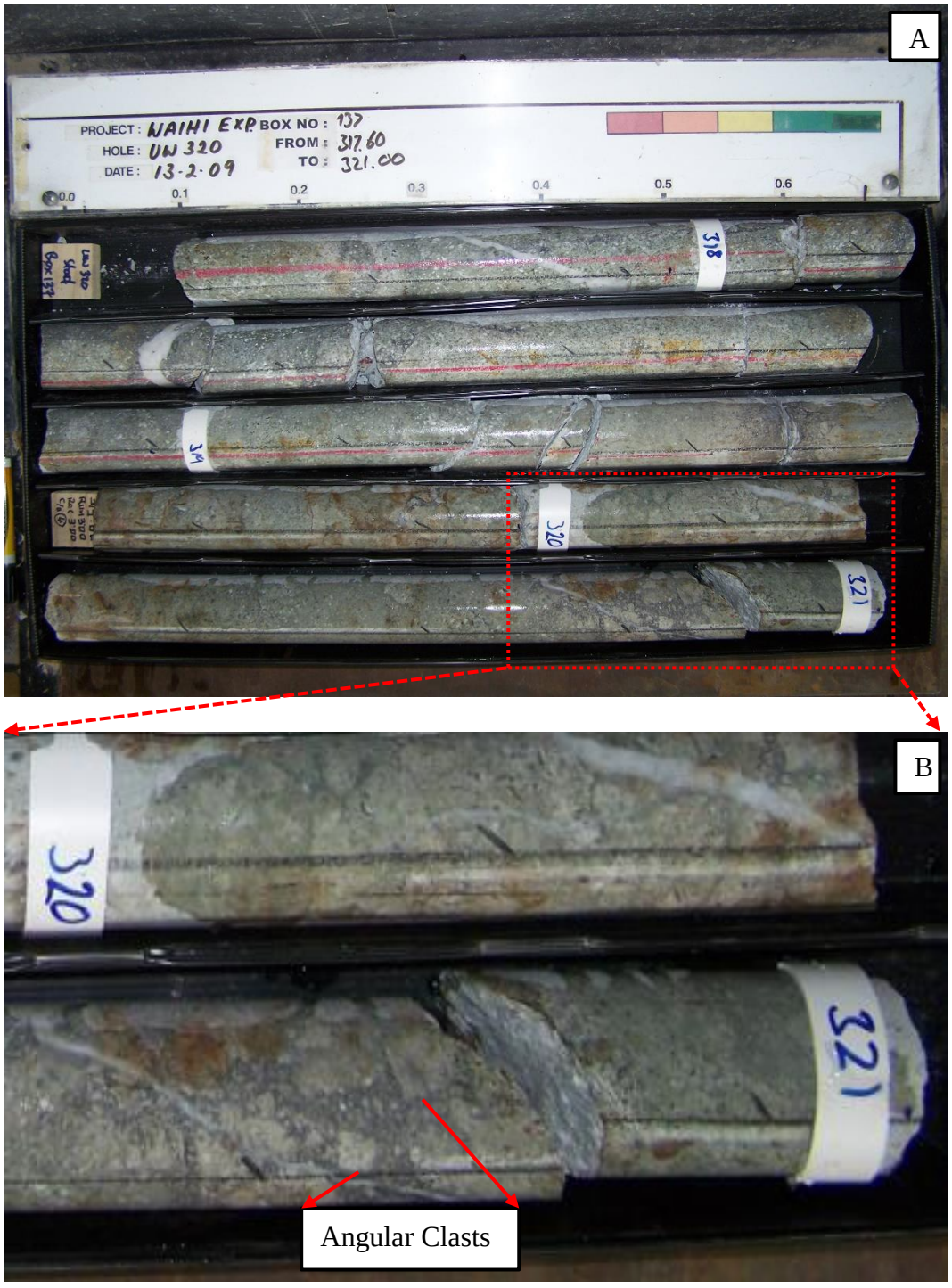

Figure 4.7. (A) Drillcore sample UW320/317.60-321.0m contains breccia visible very clearly from 320m onwards. (B) Enlarged view of the above core with texture of breccia easily identifiable with angular to sub-rounded breccia clasts enclosed in rock matrix.

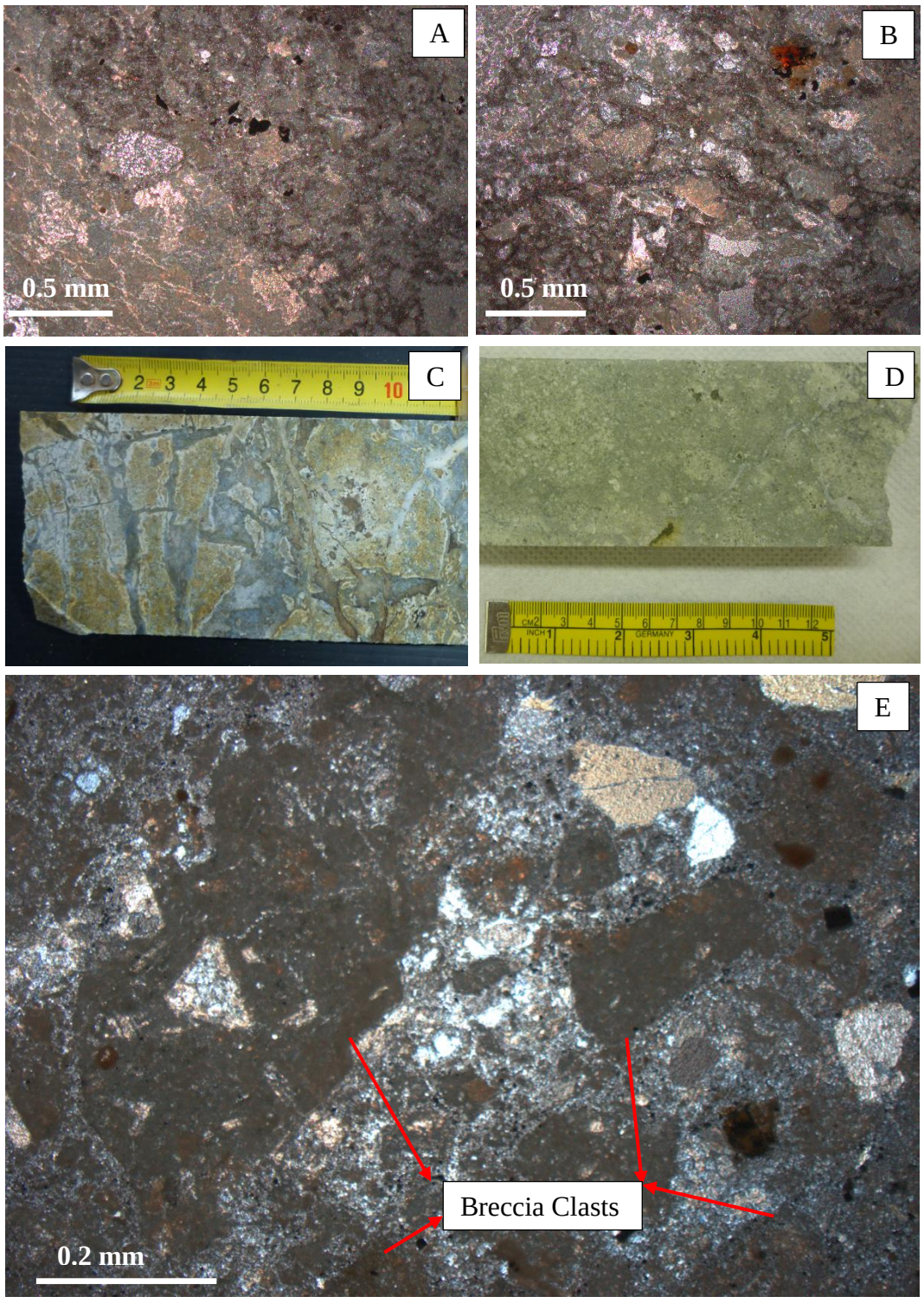

Figure 4.8. Various forms and textures of breccia (A) Sample UW348/181.85m showing wavy texture of chlorite crystals (B) Relic texture of angular breccia clasts altered to calcite and chlorite. (C) Jigsaw shaped breccia. (D & E) Breccia shape and texture in sample UW320/321.50m. Figure D is the core sample and Figure E is the thin section of the same sample.

4.4. Alteration Mineralogy

Low sulphidation epithermal deposits are characterised by variable entrainment of metals which are formed as the result of circulating near neutral hydrothermal fluids of meteoric origin (Corbett and Leach, 1998). The zonation pattern of alteration minerals can form distinct patterns which can be identified by studying mineral assemblages which form at certain depths and conditions and the sequence of alteration and mineralisation associated with these deposits can illustrate the progressive evolution of the hydrothermal system.

Though the presence or absence of certain mineral assemblages in low sulphidation epithermal regimes depend heavily on temperature, pressure, pH and host rock geochemistry, the other factors which can significantly control their formation are regional geological, tectonic and structural settings (Pirajno, 2009).

The alteration mineral assemblages can thus be characterised into different types and can be effectively used to determine the permeability, temperature and pH conditions (Figure 4.9). For example, certain clay minerals like kaolinite and dickite form under high temperature and acidic conditions whereas illite and chlorite form from near neutral chloride waters and at temperatures >150 °C. Some mineral species can also be used as temperature, permeability and boiling indicators. The presence of platy calcite suggests the boiling zone in the system whereas cristobalite, a silica mineral, is indicative of low temperature settings. The temperature sensitive alteration assemblages can thus help in determining the areas of thermal stability where certain minerals prefer to precipitate (Henley & Ellis, 1983; Reyes, 1990). In addition, the presence of adularia can indicate the high temperature and alkaline conditions and is used as a permeability indicator. It infers a high permeability if occurs alone or with quartz, medium to low if mixed with albite (Browne, 1970). The identification of alteration assemblages can thus help in determining the paleo-temperatures, paleo-flow paths, paleo-depth conditions and can considerably help focus mineral exploration efforts.

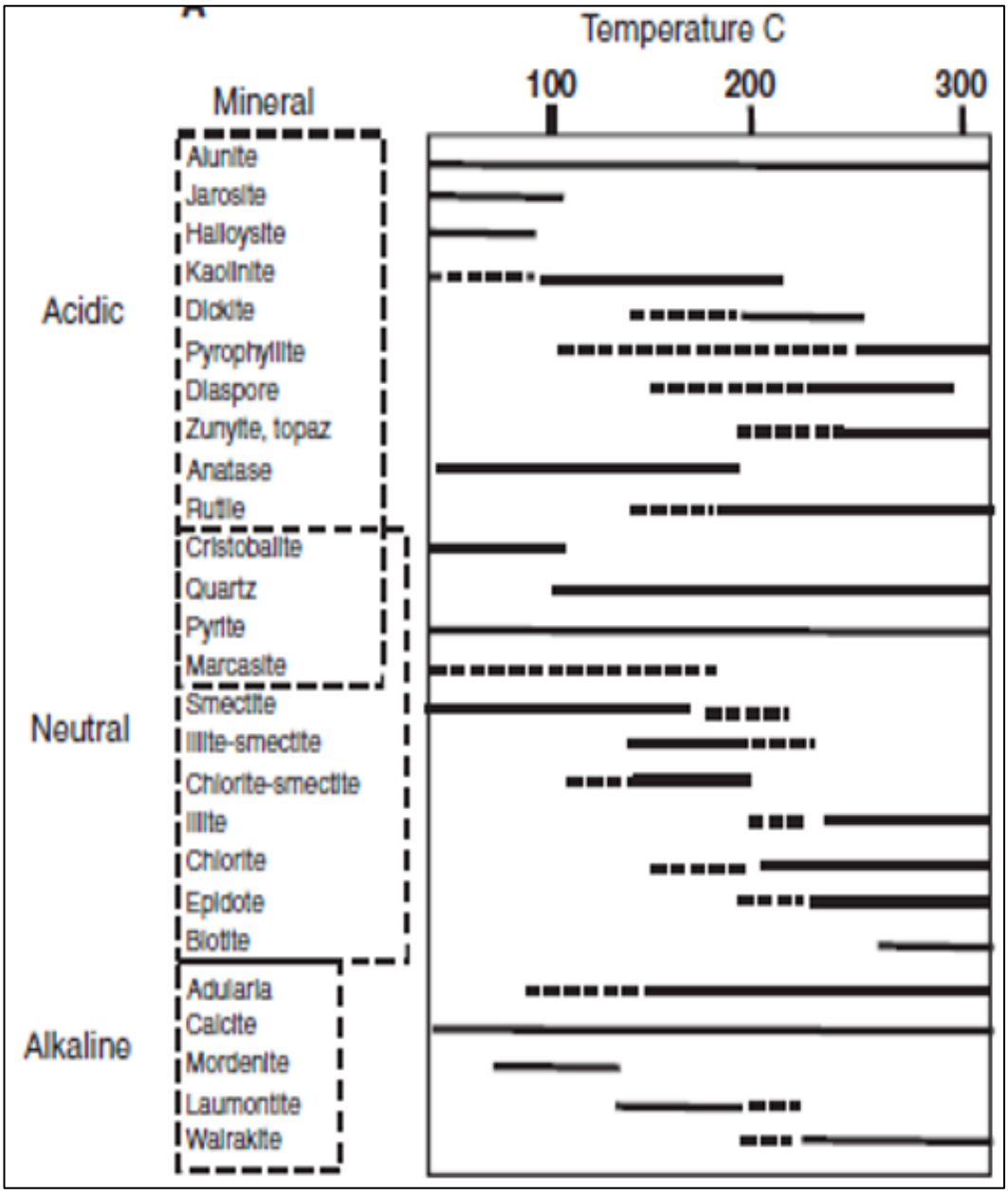

Figure 4.9. Temperature and pH range of hydrothermal mineral phases in epithermal systems (Hedenquist et al. (1996); in Pirajno, 2009).

Table 4.1. Alteration intensity observed in the thin sections at Correnso deposit. Major minerals identified in the order of their absence or presence with respect to the hydrothermal alteration.

Alteration Intensity				
Fresh	Less Altered	Partially Altered	Highly Altered	Intensely Altered
Original Andesite texture present. Feldspars and Pyroxenes easily identifiable.	Plagioclase intact. Pyroxenes partially altering to chlorite. Original igneous texture still present	Plagioclase partially altered to calcite. Pyroxenes completely altered. Original igneous texture still identifiable.	Feldspars and pyroxenes completely altered. Original igneous texture absent and replaced by relic texture.	No relic texture. Intense alteration
Plagioclase	- - -	- - -		
Pyroxenes	- - -			
Quartz	- - -	- - -	- - -	- - -
Calcite		- - -	- - -	- - -
Pyrite	- - -	- - -	- - -	- - -
Chlorite	- - -	- - -	- - -	- - -

The alteration mineralogy for this project was studied by thin section petrography and XRD analysis. The methodology of the preparation of powdered samples for the XRD and further analysis is described in brief in this chapter. Alteration intensity was also observed in the samples along with mineralogy and divided into five main alteration types on the basis of the presence or absence of primary and secondary minerals (Table 4.1). This is very helpful in determining the areas of high or low alteration zones and is discussed in detail in the hydrothermal alteration and geochemistry chapter. Also, the alteration minerals were further categorised into different mineralogical assemblages and their characteristic features and mineralogical associations are described as follows.

4.4.1. XRD analysis

A total of sixty eight samples were selected for the XRD analysis for clay and alteration mineralogy. The samples were cut into small blocks by the saw and cleaned off any dirt or foreign materials present on the surface. The dry blocks or chips were then put into agate ring mill and crushed into fine powder using the Ring mill at Earth Science lab. The air dried powdered samples were then mounted on discs and put in the sample holder which can hold fifteen samples at a time. These holders were then run on a PANalytical Empyrean X-ray diffractometer at 45 kV and 40 mA using Cu $K\alpha_1$ radiationfor the analysis at the University of Waikato XRD laboratory.

Raw data was obtained using the Panalytical High score plus software and then processed using the same software. The minerals were identified by searching the peaks and then matching these peaks with the ICDD PDF-4 Minerals database by identifying the baseline and peaks, and then identifying minerals utilizing the semi-automated “search and match” function. XRD results obtained from the samples show a very clear alteration zonation pattern at the Correnso deposit which is described in detail in the following pages.

4.4.2. Alteration Assemblages and Mineralogy

The alteration mineralogy identified at the Correnso deposit is divided into different mineral assemblages on the basis of their alteration styles, alteration type and their association with the respective hydrothermal environments. Four major alteration assemblages were found in the Correnso system from the results obtained through thin section petrography and XRD analysis. The detailed description of the alteration styles and their characteristics is already defined in the chapter two and therefore much emphasis is given on mineralogical description here. The minerals, their characteristic features and alteration type found at Correnso deposit are described herein.

4.4.2.1. Argillic alteration

Agillic alteration or clay alteration is characterized by the presence of clay minerals and is further divided into advance argillic or intermediate argillic on the basis of intensity of the host mineral breakdown. It is formed commonly at temperatures below 250 °C by H+ metasomatism. The main clay minerals associated with this type of alteration are smectite and kaolinite group of minerals. The advanced argillic style is characterized by kaolinite, pyrophyllite, or dickite (depending on the temperature) and alunite together with lesser quartz, topaz, and tourmaline. Mineralogical assemblages of argillic alteration found at Correnso deposit are described as follows.

Smectite

Smectite usually occurs at low temperatures (<100-150 °C) and pH conditions similar to illite (Corbett & Leach, 1998). Smectite has been identified both in thin sections and XRD analysis. It is the third major alteration mineral found in host andesite after quartz and chlorite. The main types of smectite group minerals identified in XRD analysis were nontronite (iron-rich member of the smectite group), montmorillonite giving a basal spacing of with 14 Å, and in lesser amounts as saponite. It was also found interlayered as chlorite-smectite (Figure 4.11B) with tosudite and corrensite as main minerals, and also as illite-smectite in the form of rectorite. In thin sections, smectite replaces pyroxenes and is identified by their higher refractive indices and lamellar structure.

Illite

Illite is very hard to identify in thin sections because of its fine grained particles and was identified only in two thin sections (Figure 4.10A). The presence of illite group minerals suggest fluids with pH range of 4-6 and temperatures ranging from 200-250 °C and can co-exist with kaolin group minerals at fluid pH range of 4-5 depending on the fluid salinity and temperature (Hemley et al., 1980; Reyes 1990b; Corbett & Leach, 1998).The XRD shows the presence of illite in most of the samples in all of the drillcores analysed with its lattice spacing at 10 Ångstorm of 001. Samples from drillcore UW320 and CGD003 show the presence

of illite proximal to the main Correnso vein with gradually decreasing away from the vein.

Intersratified illite-smectite

Illite-smectite zone in a hydrothermal regime suggests temperatures ranging from 100-200°C and pH of 4-6. The smectite content within the interlayered illite-smectite clays progressively decreases with increasing temperature over the 100-200 °C range (Harvey and Browne, 1991; Corbett & Leach, 1998). Illite-smectite was identified in thin section (Figure 4.10) as well as XRD analysis, where it show a basal spacing of 17 Å.

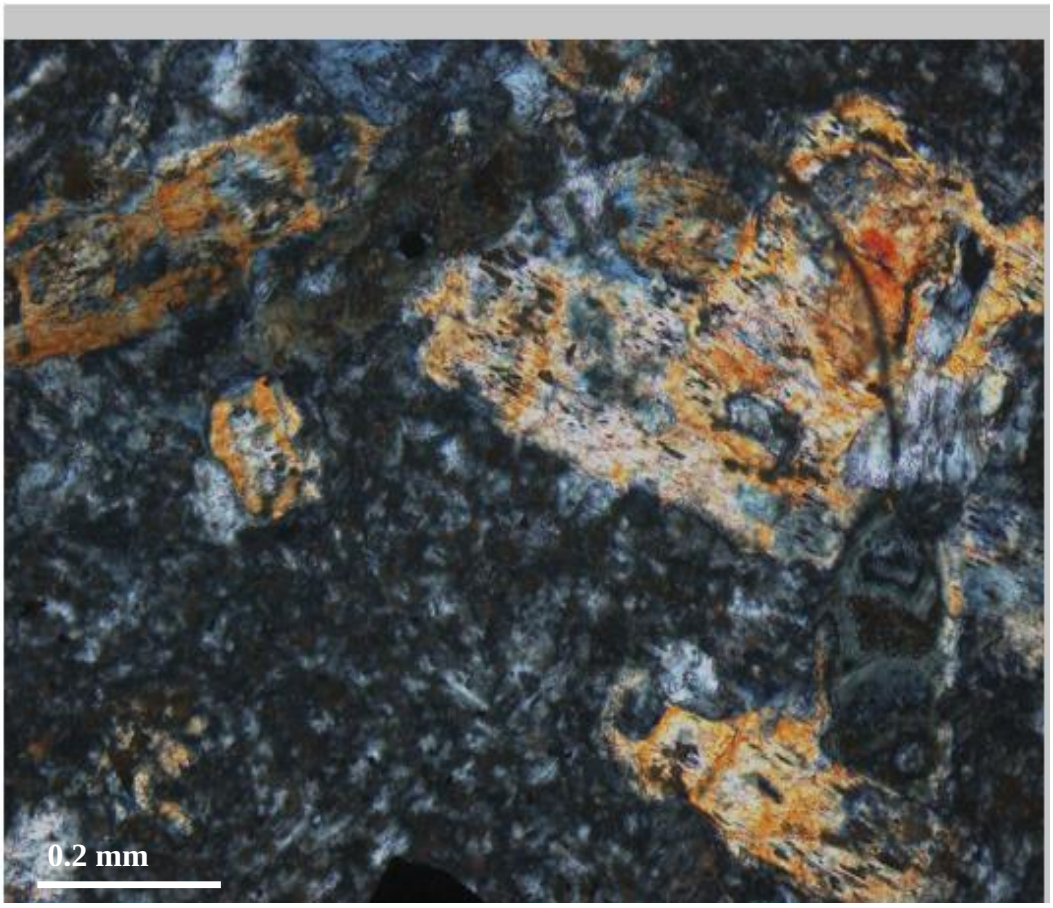

Figure 4.10. Illite-smectite replacing the primary pyroxenes in the sample UW 348/285.50. The high order colours suggest the illite presence and greyish yellow part is probably smectite.

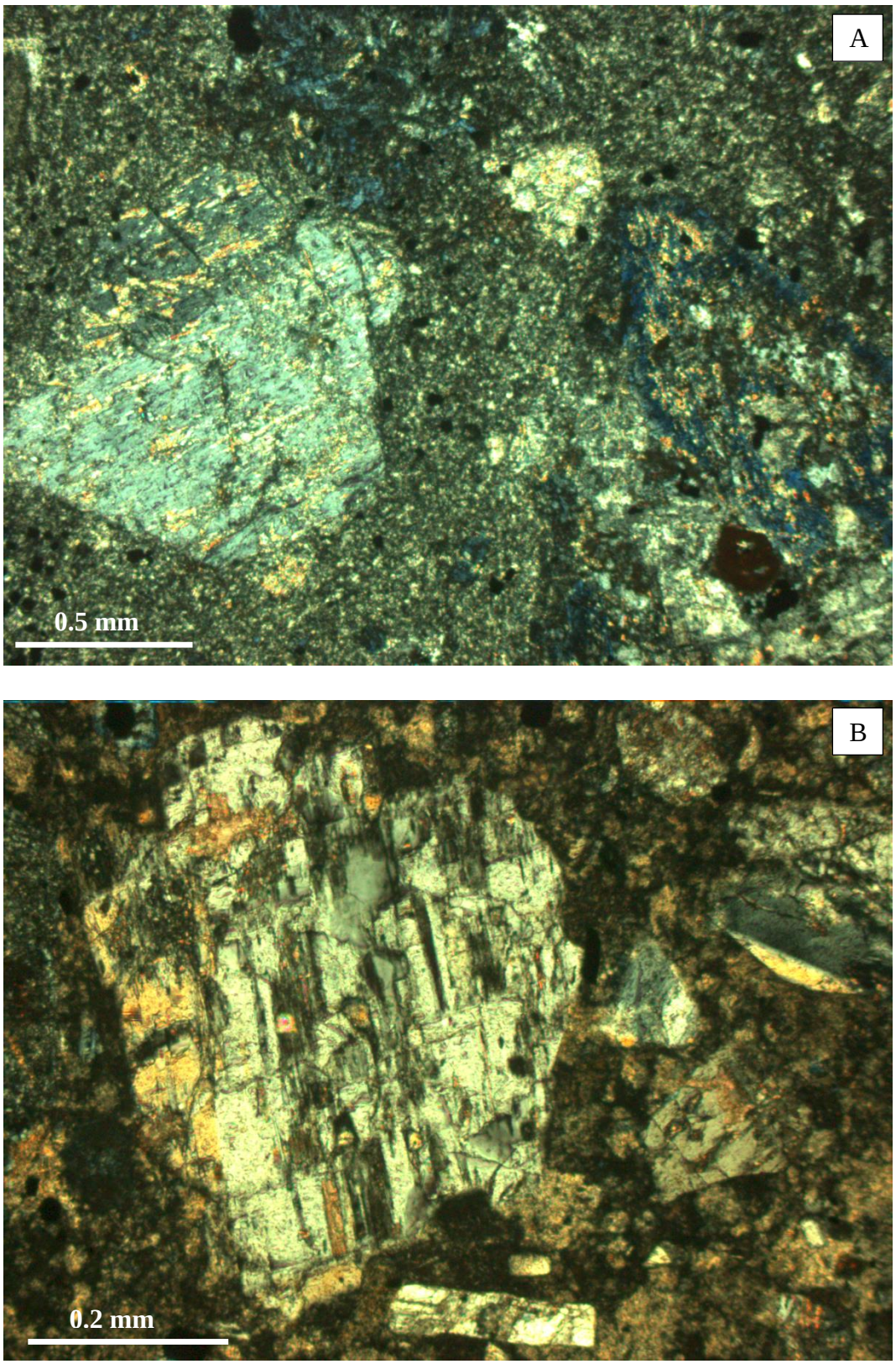

Figure 4.11. (A) Illite replacing the pyroxenes and feldspars. Also present on the far right is the Prussian blue chlorite replacing a pyroxene crystal. (B) Another example of pyroxene being replaced by chlorite-smectite in the sample UW320/425.80.

Interstratified chlorite-smectite

Chlorite-smectite occurs at low-temperatures which can grade to chlorite at higher temperatures and under slightly acid to near neutral pH conditions (Kristmannsdotter, 1984; Corbett & Leach, 1998). Chlorite-smectite was also identified in couple of thin sections and XRD analysis. In XRD, tosudite, corrensite, and rectorite were identified which are chlorite-smectite group minerals in the samples from drillcore UW348.

Vermiculite

Vermiculite is a clay mineral and is similar to tri-octahedral micas and smectites. It is an alteration product of phlogopite, chlorite, pyroxene and also form as the result of weathering of biotite. It was identified by XRD analysis with a basal spacing of 10.7 Å in a number of samples from drillcores UW348, UW320, and UW364. In these samples vermiculite was found only distal from the main Correnso vein, usually in the upper part of the system.

4.4.2.2. Advanced argillic

The advanced argillic assemblage consist minerals mainly of kaolin group which are derived from moderately low pH fluids of approximately pH 4 whereas alunite group of minerals are formed fluid pH range of 3-4. Dickite forms at temperatures ranging between 150-250 °C and same pH range as kaolinite (Reyes, 1990; Corbett & Leach, 1998). No minerals of this group were identified in the thin sections and only showed their presence in the XRD analysis. These were identified as dickite, alunite, and kaolinite. These were found only in the samples distal to the mineralization and at upper levels of the system, present particularly in the drillcores UW320 and UW CGD003.

4.4.2.3. Potassic alteration

Potassic alteration is a high temperature alteration type (500–600 °C) and commonly formed in the core of the system and characterized by the formation of new K-feldspar and/or biotite usually together with minor sericite, chlorite, and quartz. Magnetite/hematite and anhydrite may also occur as accessory

minerals. The main mineral assemblages found at the Correnso deposit which have undergone potassic alteration are as follows.

K-feldspar (Adularia)

Adularia is a high temperature K- feldspar, which is generally distinguinshed from plagioclase by its K-content (<5-10%). It is found as a replacement product for plagioclase, either alone or together with albite (Pirajno, 2009). Adularia, albite and quartz have traditionally been used in geothermal exploration as an indicator for permeability which can be classified as high if adularia occurs alone or with quartz and medium to low if mixed with albite (Browne, 1970; Anderson, 2011).

Adularia was identified in only one thin section and it was not identified by the XRD analysis. However, other alkali feldspars were identified in the XRD including microcline, orthoclase and sanidine in large number of samples. Considering the typical mineralogical composition of andesites which consist predominantly of plagioclase with minor amounts (or absence) of alkali feldspars, the alkali feldspars identified here in large amounts are inferred to be adularia. Further work is needed to determine this.

Magnetite and Ilmenite

Magnetite is present in samples associated with lead and pyrite. It was not identified in thin sections (as only a relatively few polished sections were made) but XRD analysis identified magnetite in a number of samples in drillcore UW320 and CGD003. It is commonly found as an accessory mineral and in minor amounts. Ilmenite was also found in samples proximal to the mineralisation, particularly in the veins. It was only identified in one thin section and is present associated with sulphide minerals. XRD analysis also identified magnetite in quite a number of samples proximal to the mineralisation.

4.4.2.4. Phyllic (Sericitic) Alteration

Phyllic alteration style is commonly associated with the low to intermediate temperatures (200–350 °C) and is formed in a variety of hydrothermal deposits, usually characterizing the margins of the epithermal deposits. Major mineral assemblages found at Correnso deposit are as follows.

Quartz

Quartz is ubiquitous mineral present both in host andesite and in veins. Primary quartz and its properties have already been discussed in the primary mineralogy chapter, emphasis is given here on hydrothermal quartz which is predominantly concentrated in the form of massive veins. It is also present as small veinlets often crosscutting each other. In thin sections, it was easily identified but other silica minerals like crsitobalite and tridymite were identified in two samples by XRD as they are quite hard to differentiate because of their close resemblance with quartz and were thus identified using XRD. Cristobalite and tridymite are low temperature alteration quartz minerals, formed under progressively slower cooling environments (Corbett & Leach, 1998). These were found in samples distal to the mineralisation.

The texture of silica ranges from fine grained crystalline quartz found as thin colloform and crustiform banding which forms under rapid cooling (Corbett & Leach, 1998). It is also found in the form of groundmass infilling gaps and voids in primary minerals. The colour of the crystals range from pale grey to light yellow to white.

Sericite

Sericite is a fine grained muscovite which may contain some illite, and is encountered at levels which are transitional between illite and well crystalline muscovite. The presence of sericite infers fluid pH near-neutral to slightly acid and temperature above about 220°C. (Britten, 1981). It is often called white mica and its crystallinity increases with increasing temperature which can be monitored by XRD analyses of its peak patterns (Corbett & leach, 1998).

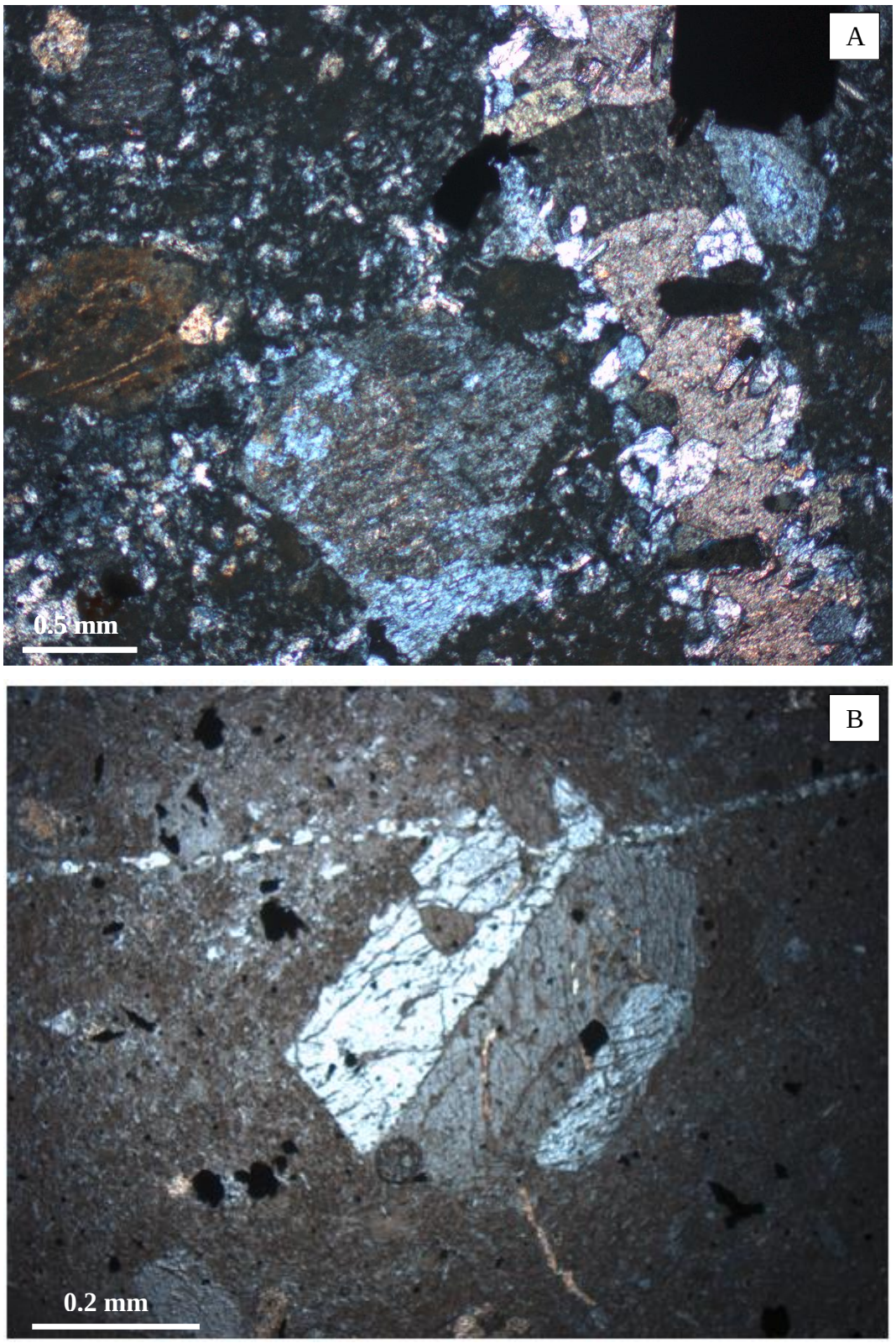

Figure 4.12. (A) Adularia replacing plagioclase phenocryst on the lower left side. (B) Possible sericite (Muscovite) crystal present in the sample CRO507/334.10.

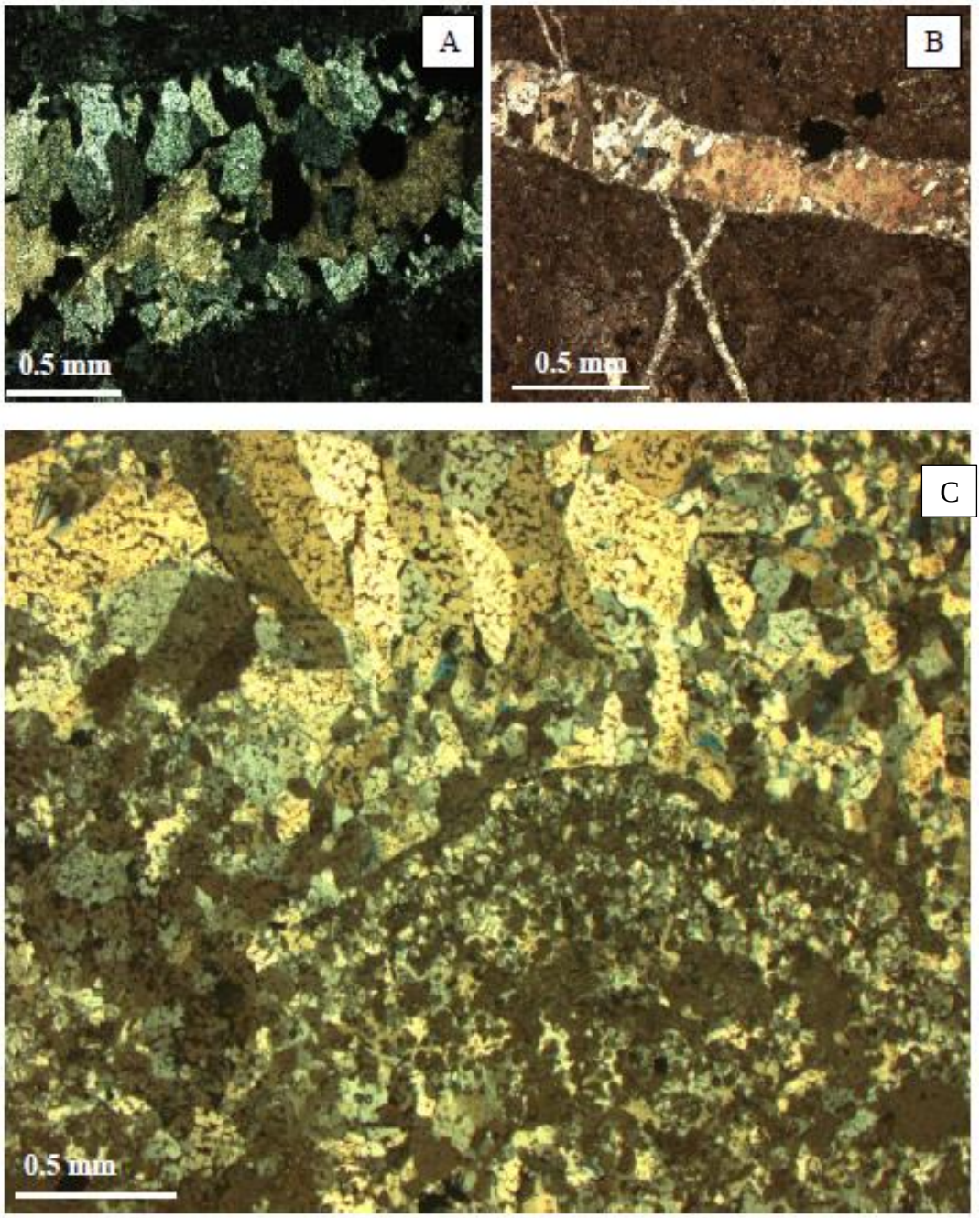

Figure 4.13. Secondary quartz present in the veins. Quartz is the major vein mineral with calcite and sulphides present in the mineralised veins. (A) Quartz present alongside calcite in the sample UW364/255.90. (B) Sample CGD003/333.90. Quartz and calcite veins cross-cutting each other. The big calcite-quartz vein overprints the small quartz veinlets suggesting quartz-calcite vein formed at the late stage of the hydrothermal alteration. (C) Sample UW320/445.90. Massive quartz present in the mineralised zone. The groundmass is also fine disseminated quartz.

Sericite at Corenso deposit is found commonly proximal to the mineralisation in the form of muscovite. It forms a blanket of phyllic or sericitic alteration zonation around the vein system. Quartz is commonly associated with the sericite with minor amounts of chlorite, calcite and albite.

4.4.2.5. Propylitic Alteration

Propylitic alteration is typical of low temperature conditions usually <200-250°C and near neutral to alkaline conditions with low temperature propylitic alteration consisting of zeolites in place of epidote. Chlorite as the ubiquitous mineral with secondary albite is commonly encountered in this type of alteration type (Corbett & Leach, 1998). The major mineral assemblages identified in this study consist of following minerals.

Albite

Though albite was not identified in the thin sections, it is present in most of the samples as identified from the XRD analysis. The replacement of alkali and plagioclase feldspars on large scale can result into albitization, a sub-type of propylitic alteration. Albitization is most common where chloritized biotite is rare or absent, thereby restricting the formation of epidote and mica (Andersen, 2011).

Chlorite

Chlorite is a common alteration mineral which can occur in a range of different alteration zones and deposit types. It is the second most abundant mineral in the Correnso deposit and replaces pyroxenes (augite and hypersthene) and hornblende. It also occurs as major groundmass constituent along with quartz and sulphide minerals. Partially altered samples of pyroxenes were observed in many slides (Fig. 4c) replaced to chlorite. The samples from the lower andesite unit contain more chlorite than the upper unit where it is found commonly associated with quartz and calcite. Also, it tends to exist in shallow as well as deep parts of the system and forms a zonation pattern which is laterally and vertically spread across the considerable distances. In thin sections, it is identified by its typical green colour and exhibit strong pleochroism. Some

samples also show a distinct blue Prussian colour. XRD analysis show clinochlore (Mg-rich) as the most common chlorite mineral which is present in almost all of the samples.

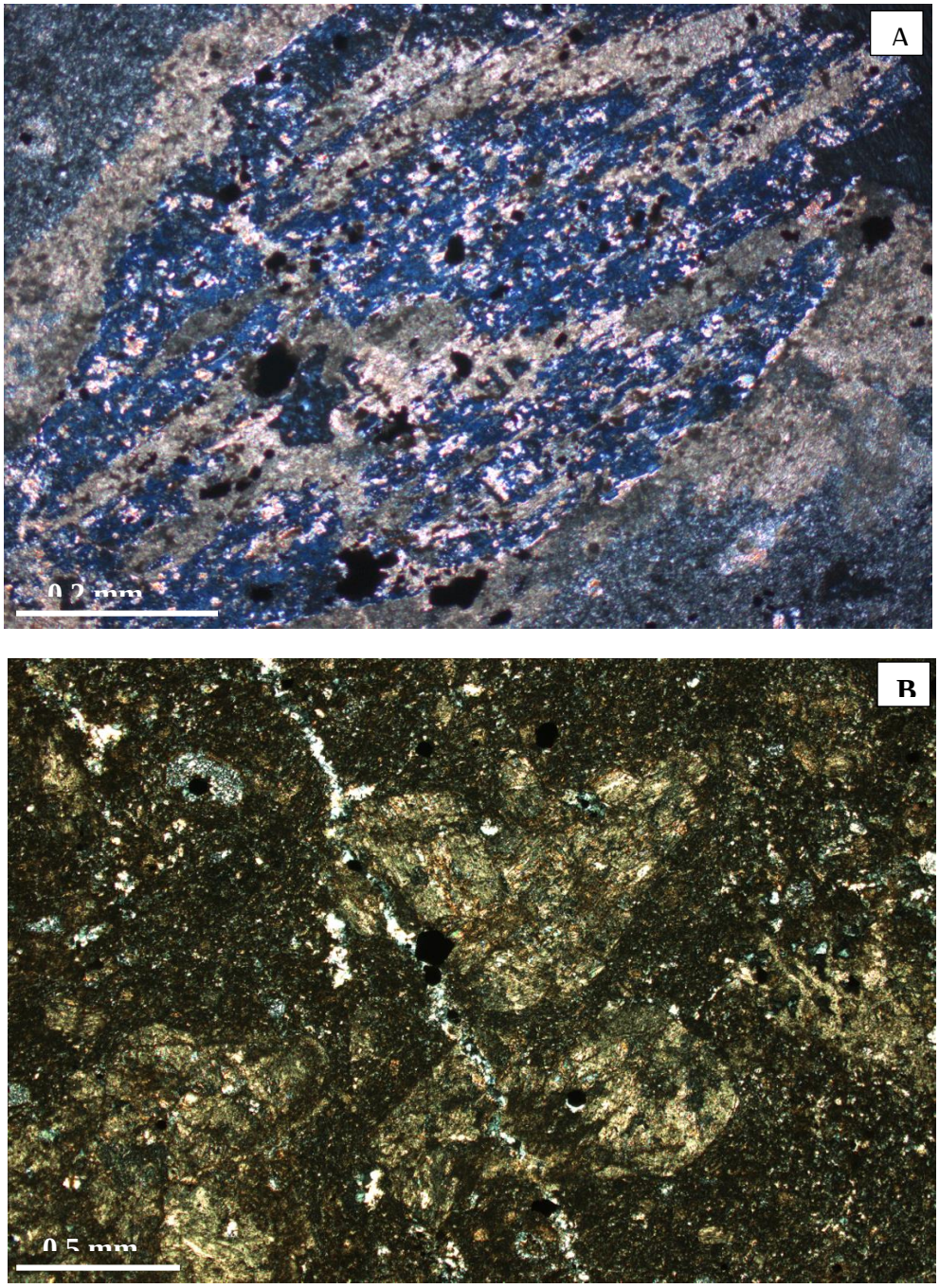

Figure 4.14. (A) Prussian blue chlorite present in the sample CRO507/334.10m. (B) Greenish chlorite replacing primary pyroxenes in the sample UW320/415.60

Calcite

In hydrothermal deposits, the exsolution of CO_2 from the boiling fluids leads to a pH increase in the solution and results in the precipitation of the calcite. Though other factors also control the precipitation of calcite such as pH, temperature, and aqueous calcium ion activity, the role of CO_2 is ubiquitous (Browne and Ellis, 1970; Browne, 1978; Henley and Hedenquist, 1986; Keith and Muffler, 1978; Simmons and Christenson, 1994). The presence or absence of calcite can thus be used in identifying the zones of boiling and subsequent precipitation.

At Correnso deposit, calcite is one of the major minerals present in most of the samples and is found in both in host rock and veins. Two types of calcite was identified in thin sections and XRD analysis: (1) vein hosted and (2) as groundmass. The latter is one of the main alteration products replacing plagioclase phenocrysts in the host andesite and ferromagnesian minerals in the groundmass where it is found in association with quartz and plagioclase laths. The shape of the crystals range from massive or compact to bladed, the latter found proximal to the mineralisation and in the veins. The colour exhibited under the polarised light range from light pink to light yellow and golden white. The hydrothermal calcite on the other hand is present in the form of platy or blade shaped crystals representing boiling and alkaline conditions and is restricted to the veins and veinlets where it is found inter-grown with quartz, corrensite, and chlorite. In thin sections, it exhibits a twinkling texture when the stage is rotated whereas the platy calcite shows lamellar twin bands exhibiting high order interference colours.

Zeolites

Zeolites are common alteration minerals in active and fossil geothermal fields with steep geothermal gradients. They occur as low-temperature, low-pressure alteration products usually filling vugs and cavities and are used as geothermometers (Utadu, 2001). XRD results show zeolites present in quite a number of samples and were found at shallow levels of the system, usually distal to the ore body.

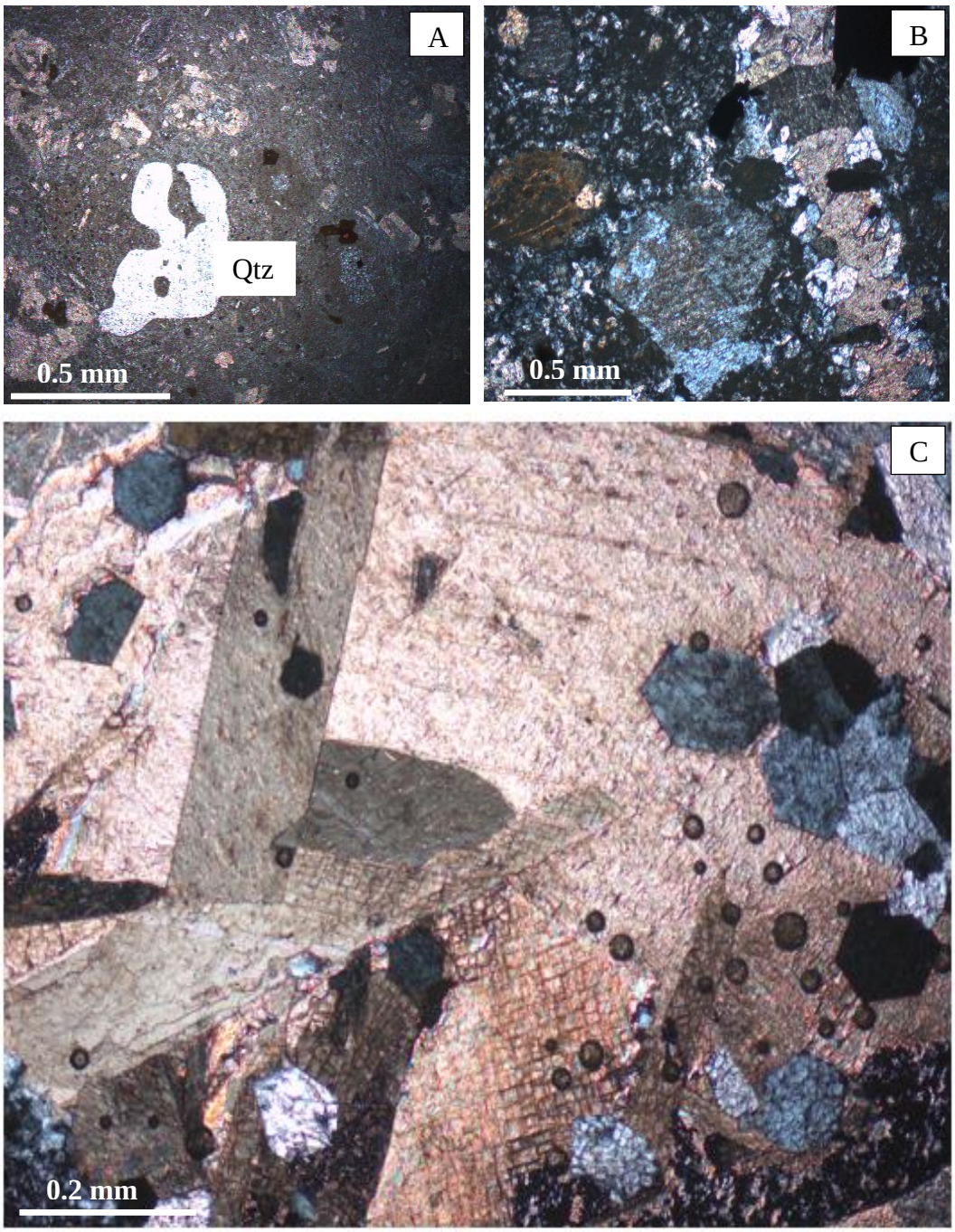

Figure 4.15. Various types of calcite textures. (A) Calcite present as groundmass and replacing plagioclase crystals in the sample UW348/138.65. (B) Calcite vein with associated quartz present in the vein. Calcite is present as massive and compact. (C) Platy calcite in the vein suggesting the boiling conditions in the sample UW364/381.90.

4.4.3. Sulphide minerals

Correnso vein system shares common sulphide mineralogy with the adjacent Martha mine (Hobbins, 2012). Sulphide minerals are present in abundance proximal to the main Correnso vein and in the quartz and calcite veins in the deeper parts of the system although pyrite is found in both upper and lower andesite sequences in the form of groundmass as identified by visual and petrographical study . The major minerals present are pyrite, chalcopyrite, galena and sphalerite with trace amounts of magnetite where pyrite is the most abundant mineral followed by sphalerite. The brief description of the minerals and their characteristics found in the samples is given below.

Pyrite

Pyrite is the dominant sulphide mineral present in most of the samples as both disseminated and in clustered form. It is found in veins as well as in the host rock displaying variety of shapes with cubic shaped crystals being dominant. The colour of the crystals range from yellowish white to light yellow and some crystals display striations. Also, a number of slides show pits of void spaces within the pyrite crystals which are formed because of excessive polishing causing plucking of crystals from their crystallographic cleavage plains.

Chalcopyrite

Chalcopyrite occurs in two forms as fine disseminated grains and as isolated discrete crystals both associated with sphalerite and pyrite crystals and also with galena. Its association with sphalerite comes in the form of poorly shaped irregular crystals often intergrown and also as fine grained disseminated inclusions crystographically oriented within the sphalerite crystals also known as chalcopyrite disease. (Fig. It is identified by its distinct yellow colour which is more pronounced than that of pyrite and is found mostly in the veins proximal to the mineralization. It is also found sporadically in trace amounts across the host rocks.

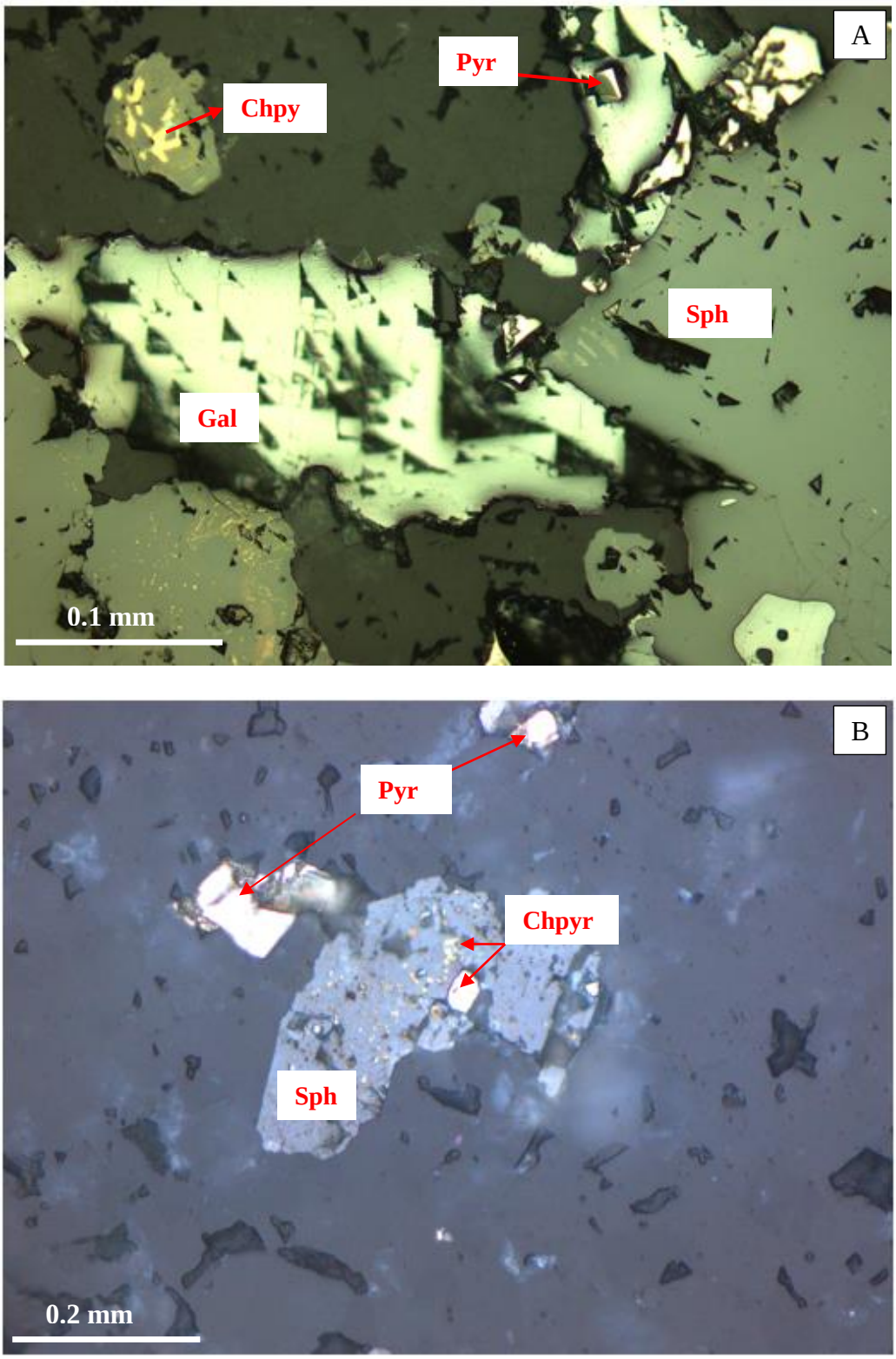

Figure 4.16. Sulphide minerals present in sample UW364/437.05m. (A) Pyrite with typical cubic shaped crystals. Chalcopyrite within a sphalerite. Galena with triangular pits. (B) Chalcopyrite crystal enclosed within shalerite and also in fine disseminated form. (Pyr: Pyrite,Gal: Galena, Sph: Sphalerite, Chpyr: Chalcopyrite)

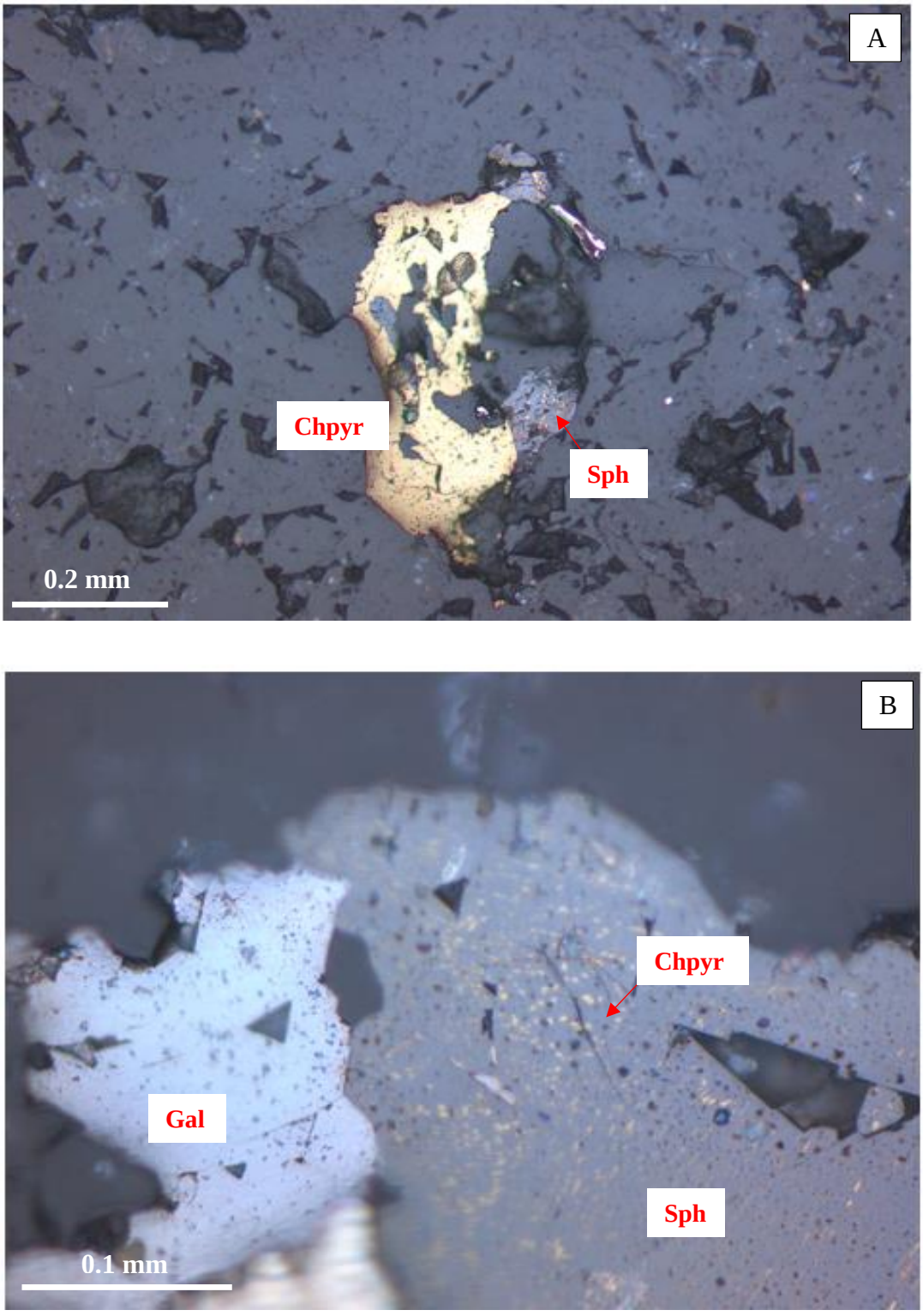

Figure 4.17. Major sulphide minerals in sample UW364/437.05. (A) Big chalcopyrite crystal with sphalerite filling the voids and empty spaces. Chalcopyrite is also present as fine grained and disseminated within the sphalerite. (B) Galena with typical triangular pits. (Gal: Galena, Sph: Sphalerite, Chpyr: Chalcopyrite).

Sphalerite

Sphalerite is another sulphide mineral present in the veins or the samples proximal to the mineralization. It is commonly found in association with galena and chalcopyrite with the latter disseminated or intergrown within the sphalerite crystals. The colour of the crystals ranges from dark grey to brownish grey in the polished slides and the crystals exhibit curved or irregular shape. The crystals display internal reflection which is helpful in identifying sphalerite in reflected light. Quartz is also found as inclusions within the sphalerite crystals.

Galena

Galena occurs in the samples proximal to the mineralization but mostly within the veins and is found in association with sphalerite and pyrite. It can be easily identified by perfect cubic cleavage exhibiting distinctive triangular pits. The colour in the samples range from greyish white to white.

Gold

Gold was not identified in any of the thin sections or in hand specimens. P-XRF did identify gold in many samples close to the mineralisation but it lacked in accuracy and effectiveness to pick gold in samples which contained gold as confirmed by assay data acquired from Newmont Gold Waihi. It is noted that the assay data from Newmont Gold Waihi is on a scale of 0.5 to 2 metres, whereas core samples on the order of 10-20 cm long, meaning that the scale of sampling is a potential issue. Hobbins et al (2012) in their paper on Correnso deposit have identified gold in thin sections in the form of electrum found as inclusions within sulphide minerals and quartz. They also noted that the economic gold mineralisation is confined to the veins and is not disseminated within wallrock.

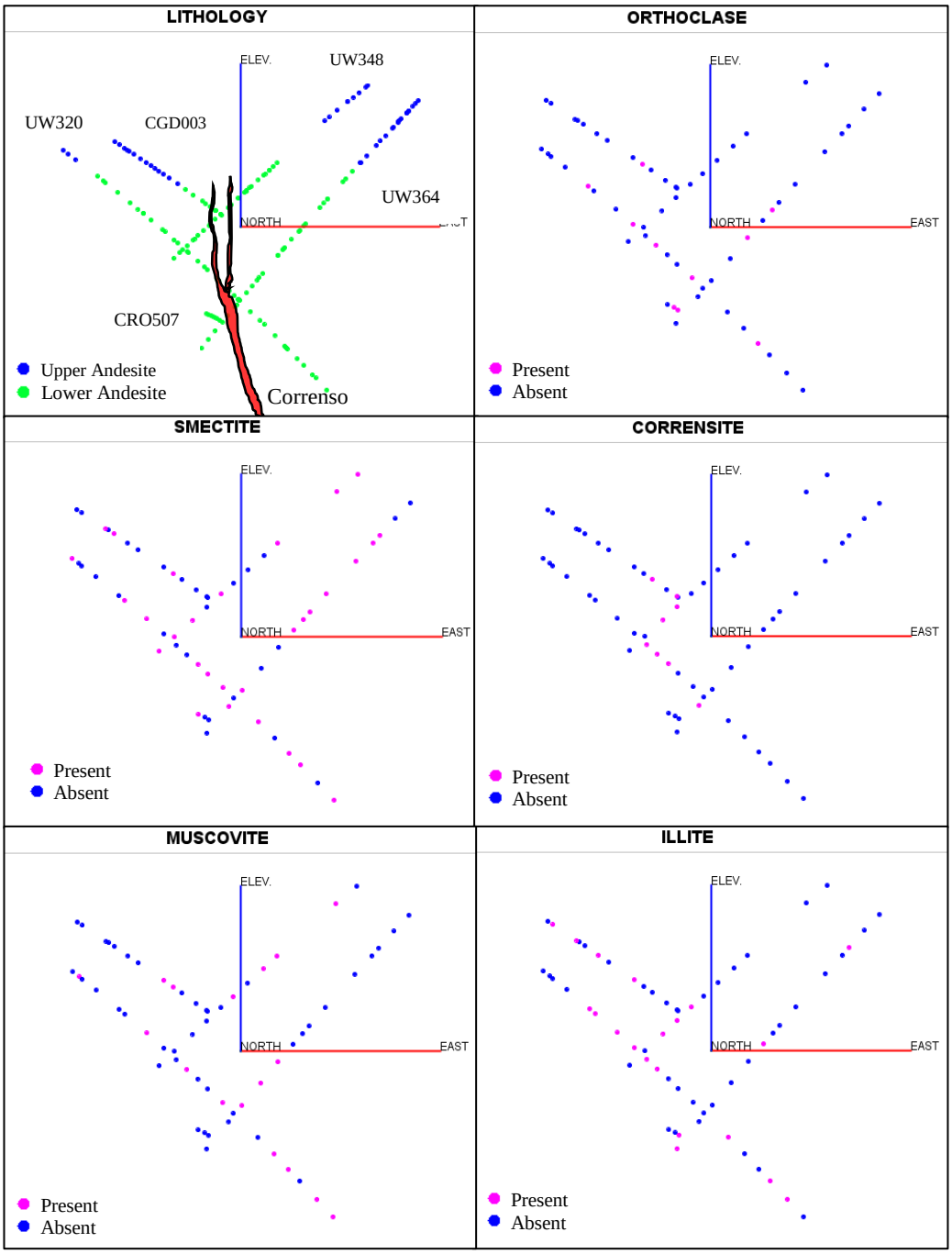

Figure 4.18. Cross section view of the Corenso Vein showing the distribution of lithology (upper and lower andesite), and various hydrothermal alteration minerals identified from XRD analysis. The abundance and depletion of these minerals associated with vertical and lateral variations with respect to the mineralisation suggest a pattern which can be used as vector to the mineralisation. The alteration zonation pattern inferred from the presence or absence of these alteration minerals is more or less common with the typical mineralogical assemblages found at the low sulphidation epithermal deposits.

4.5. Discussion and Summary

Carbonate-base metal epithermal deposits are characteristic of mineralogical assemblages commonly dominated by quartz and occur in association with adularia and/or late sericite/illitic clay. The mineralisation is associated with pyrite-sphalerite-galena and carbonate veins and contains magnetite and illmenite as accessory minerals (Corbett and Leach, 1998).The assemblages identified at the Correnso deposit are consistence with the above mentioned type of epithermal deposits and can thus be inferred as low sulphidation epithermal type associated with carbonate-base metal deposits. The primary and alteration minerals identified from the thin section and XRD analysis suggest quartz being the ubiquitous mineral and occurs throughout the whole life of the system. Chlorite is the second abundant mineral replacing the primary ferromagnesium minerals. The vein mineralogy consists essentially of pyrite, chalcopyrite, galena and sphalerite. Zeolites were also present as accessory minerals in many samples. Hydrothermal breccia zones were also identified and the breccia mineralogy is almost similar to the host rock mineralogy. The overall mineralogical pattern can be described as quartz ± adularia ± sericite assemblage which is typical of back arc low sulphidation epithermal deposits. These assemblages are very similar to those previously described from the other deposits found adjacent to the Corenso deposit such as Martha and Golden Cross, part of the Waihi epithermal system. The distribution of clay and other alteration minerals identified in the XRD analysis has been illustrated as graphs using IOGAS software (Figure 4.18).

Hydrothermal alteration has significantly altered the host rocks which was noted well in the thin sections. XRD analysis show three major types of alteration assemblages where the overall alteration pattern can be inferred as quartz-chlorite-adularia-sericite-calcite-pyrite alteration assemblage. The presence of these particular assemblages suggest the formation of these minerals from near neutral chloride waters. Potassic alteration is confined mainly around the vein system which is evident from the presence of K-feldspars found more commonly in the samples proximal to the mineralisation (Figure 4.18). This is in turn surrounded by the sericitic alteration with muscovite and quartz as the common

alteration minerals and is restricted proximal to the mineralisation. The argillic alteration consists of clay minerals such as illite, smectite and interstratified clays, and overprints both the alteration types. Propylitic alteration envelops the mineralisation and consists mainly of albite, chlorite and calcite as major minerals. Chlorite and albite were also found in almost every sample, proximal as well as distal to the mineralisation and extending laterally and vertically to considerable distances.

5. Hydrothermal Alteration and Geochemistry

5.1. Introduction

Visual logging was done for eight drill cores and samples were collected and pulverised for pXRF and XRD analysis. Sampling and analytical methods are presented along with a brief description about the pXRF unit and its applications and use. Results present in this chapter suggest hydrothermal alteration has significantly altered the rocks around the vein system and the deposit exhibits a clear mineralogical and geochemical alteration zonation. The upper and lower andesite units show variable degree of hydrothermal alteration with upper unit more altered than the lower unit. Quartz, chlorite, and calcite are the major alteration products. Quantitative analysis of rock samples using p-XRF shows that some potential pathfinder elements such as Rb, S, As, and K are elevated in the host rocks surrounding the vein, and may be used to indicate proximity to mineralization. The role impermeable barrier (Hard bars) with regards to fluid flow and alteration pattern are presented herein.

5.2. Sampling and Analytical Methods

Alteration intensity was studied for ten drill cores by drill core logging and studying various characteristics of core samples such as colour variation, host rock composition, texture, lithology, alteration style and intensity, presence or absence of veins and vein mineralogy. A scale of 1 to 5 (with an associated colour scheme) is assigned to classify the alteration intensity ranging from fresh/least altered to intensely altered rocks (Fig. 3). The logging data was incorporated with further exploration data provided by Newmont Waihi Gold and an alteration intensity map (Fig. 5.3) was produced which shows the scale and intensity of hydrothermal alteration. One hundred and sixty two samples were collected for geochemical analysis. The samples were first used for XRD and thin section preparation and leftover chips were crushed into fine powder to ensure the homogeneity of the material. The powders were then placed in small plastic cups

closed at one end with a very fine transparent plastic film for analyses and on the other side by a plastic lid. The samples were then run on bench top Olympus DeltaX pXRF spectrometer at the University of Waikato and analysed using 3-beam soil geochemistry mode with a beam time of 30 seconds for each beam at 50, 20 and 10 kV with a spectral resolution of ~ 140 eV for a total analysis time of 90 seconds. The results were then projected into graphs using IOGAS suite and studied for elemental addition and removal as well as their spatial distribution. As pXRF was widely used for this study, so a brief introduction and its application has been described in brief in this section.

5.3. Portable XRF (pXRF): Application and use

5.3.1. Introduction and Working Mechanism

The use of portable XRF has become widespread for the past few years in the mining industry for effective exploration purposes. Because of its portability and ease of use, it is rapidly becoming a “must have” tool in the arsenal of professional exploration geologists. Although conventional XRF analysis is still looked upon as a superior geochemical analysis tool (thanks to its ability to measure Na and Mg accurately), the time constraint and sample processing limitations of conventional XRF units have made pXRF very useful and cost-effective over its big counterpart. It is now used to obtain real time geochemical analyses in significantly less time and has thus promoted the collection of large multi-element geochemical data sets, coupled with the widespread availability of inexpensive ICP-MS multi-element data. Its multi-disciplinary use in the field of geology has become widespread ranging from grade control to lithogeochemistry and geometallurgy to soil sampling (Gazley and Fisher, 2014).

The working mechanism of the portable XRF is similar to the conventional XRF instrument. The p-XRF unit emits X-rays that excite atoms in the sample being analysed resulting in the displacement of inner shell electrons. The space left by these displaced electrons is filled by the outer shell electrons and this process initiates the release of electromagnetic radiation with an energy equivalent to the difference in energy between the two electron shells (Figure 5.1A).

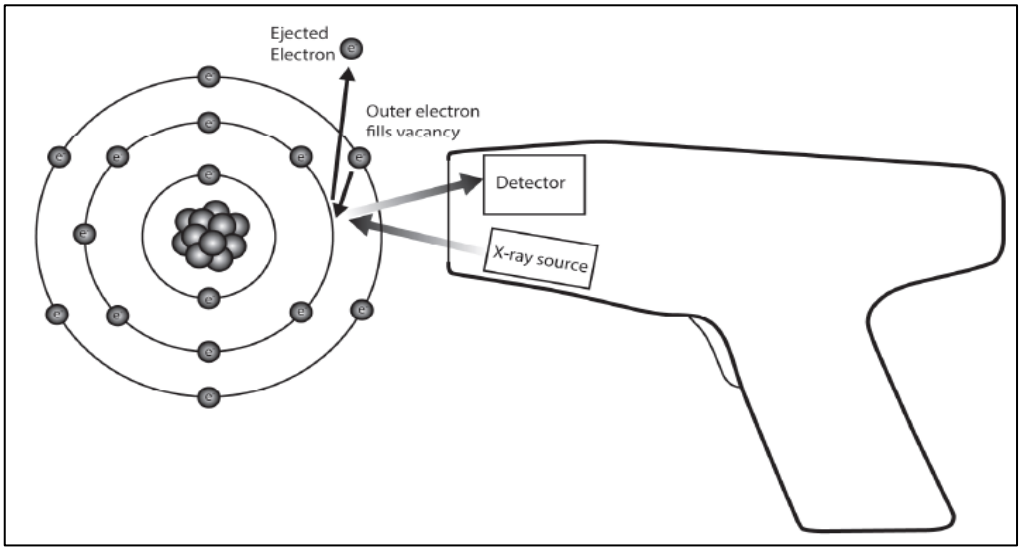

Figure 5.1. (A) Internal working mechanism of the portable XRF unit (From Gazley and Fisher, 2014). (B) Olympus Innova DeltaX p-XRF instrument used in this study (From instrument manual, University of Waikato (2014).

The wavelength of the energy emitted is characteristic of each element and the intensity of the energy is proportional to the concentration of the element in the sample (Gazley and Fisher, 2014).

5.3.2. Application and Use

Conventional geochemical methods are both cost and time consuming, and can often hamper the quick decision-making in the exploration environments. Also, the time lag between the sample collection, analysis and results can significantly delay the acquisition and the utilization of results in active exploration and development. But conventional geochemical techniques are also regarded highly for their accuracy and reliability for years now. P-XRF on the other hand though still in its infancy has proved to be reliable in providing robust geochemical results as reported by Gazley et al. (2011), Gazley and Fisher (2014). The accuracy and validity of the results obtained through p-XRF depend largely on the individual using it as well as the conditions of the analysis. The quality assurance and quality control (QA/QC) also depend on the user and therefore proper training and minimum industry standards are to be followed for effective results.

In order to present the data for public reporting, the JORC Code (2012) (Joint Ore Reserves Committee) has set the minimum industry standards in Australasia which require certain parameters such as make and model of the unit, reading times, calibrations, factors applied and their derivations to be supplied along with the analysis (Gazley and Fisher, 2014).

5.3.3. Reliability and Validity

The reliability and validity of the results obtained from the portable XRF has become a topic of debate and discussion in the recent past as its use is not only limited to mining industry but also in other fields such as archaeology, soil sciences, biology etc. Not much literature is published on the reviews and validity of the pXRF as well as verification and effectiveness of the analytical data obtained from the instrument which makes it hard to This has somewhat made it difficult for potential buyers to make choices on the basis of the current information available.

Many researchers have used this technology in a number of fields. Gazley and Fisher (2014) in their paper mentioned its use by Kalnicky and Singhvi (2001); Kilbride, Poole and Hutchings (2006); Carr et al. (2008); Markey et al. (2008); Hürkamp, Raab and Völkel (2009); Radu and Diamond (2009); Jang (2010) and Peinado et al. (2010) to determine the extent of environmental pollutants and other heavy metals in the soil samples. Also, its use in archaeology as a non-destructive method to analyse artefacts has been published in literature by Craig et al (2007); Phillips and Speakman (2009); Kato, Kakai and Shindo (2009); Jia et al (2010); Nazaroff, Prufer and Drake (2010) and Tykot (2010). Morris (2009) in his paper first presented the methods for the analyses of geological samples. Gazley (2011) and Gazley et al. (2011) expanded this further and presented case studies on its application. Piercy and Davis (2014) in their paper did evaluation of performance and potential applications of pXRF for exploration lithogeochemistry.

The validity and accuracy of the pXRF data as outlined above depend on number of factors. A due care and precision for collecting samples and pXRF handling is required for correct and accurate analysis. Gazley and Fisher (2014) on their paper of review of the reliability and validity of pXRF data put emphasis on following JORC Code (2012) and also discussed about the limitations of the pXRF. They suggested that sampling in the field to identify geochemical anomalies should also accompany the samples to be collected and considered for follow-up analysis to show reproducibility of the data. They also noted a number of key issues with regards to the instrument such as modern models of the pXRF have larger detectors and better detection limits than the older models. Also, different units are optimised for different purposes so utmost care should be taken to ensure that right unit is used for required purposes. Instrumental drift is another issue which may occur with time and can affect the calibration. This can be fixed by tracking analytical drift and servicing the unit with a new threshold set or calibration established. Another major issue with the instrumentation to be considered is analytical and sample interferences. They noted that though elements are identified by their respective energy peaks, there are certain pairs of elements that have peaks that overlap each other. This can be problematic for

elements such as W, As, Pb, Zn and Au, Ba and V, Fe and Co and rare-earth elements.

Also, sampling is another factor that should be taken into consideration. Sample heterogeneity is required for accuracy as the area covered by X-rays for analysis is very small and therefore it cannot represent the broad description of the sample. The fine powdered sample can thus do justice for correct analyses as grain size and inconsistent material can alter the results. Moisture in the samples are known to affect the analyses, therefore care should be taken while sampling. However this can be corrected by monitoring moisture contents in the field and applying a post processing correction to account for this (Parsons et al., 2012). Consideration of all the minimum standards and limitations are therefore required to avoid incorrect and inaccurate analyses. More literature and further reviews in the future will help in increasing reliability and data quality of p-XRF and can help in its establishment as mainstream analytical tool.

5.4. Hydrothermal Alteration and Metasomatism

Hydrothermal alteration apart from host rock lithology, regional and local structural settings can significantly control the localisation and style of mineralisation in epithermal deposits. The regional fault structures can enhance the hydrothermal activity by acting as conduits and supplying the heat from underlying magmas (Hedenquist, 1986). Secondary faults, fractures, joints and even bedding planes are known to affect the migration of fluids. These structural features also influence the primary and secondary permeabilities, hence affecting the distribution of mineralisation. Primary permeabilities are known to strongly affect the mineralisation where permeable and porous units allow the easy migration of fluids through them. These permeable units are prone to fracturing after the emplacement of intrusions, where silicification can cause brittleness. The subsequent fracturing is initiated at the cooled margins of the intrusion and extends into the host rocks, thereby creating secondary permeability. The primary permeabilities also occur along the formation contacts or brecciated zones, especially in the stratigraphic units with little lateral continuity such as andesitic stratovolcanos with discontinuous lava flows

(Corbett and Leach, 1998). The hot meteoric dominated circulating fluids can travel to considerable distances with the aid of the permeable zones resulting in the zoned alteration and mineralisation (Henley and McNabb, 1978).

The impermeable units on the other hand in a certain deposit act as a barrier for fluid flow and the migration of fluids is limited or controlled by joints, fractures or secondary faults. These impermeable barriers can restrict the fluid flow resulting in the pressure build up resulting in the boiling, hydrofracturing and metal deposition (Figure 3.2) (Cox, 2005). The intrusion by hot fluids in the impermeable units can significantly enhance the fracture permeability along intrusive margins which can then act as fluid channels. These low permeable rocks can hinder the equilibrium between rocks and the reservoir fluids and primary minerals or glass can persist to high temperatures. One of the examples of this control is common in dense welded tuffs at Broadlands in Wairakei. These tuffs have locally remained little unchanged, even at high temperatures, as the rocks are relatively impermeable to fluid infiltration (Browne & Ellis, 1970). In this study the “hard bars” have been identified which are found to be impermeable units controlling the fluid flow and its distribution across the Correnso system.

Rowland and Simmons (2012) studied hydrologic, magmatic and tectonic controls on fluid flow at Taupo Volcanic Zone. Fluid flow in the TVZ is largely controlled by magmatic source, but permeability and porosity is a major factor controlling the lateral and spatial distribution of fluid flow. Apart from hydrothermal alteration affecting the porosity and permeability of a fluid reservoir, intergranular host-rock porosity and secondary permeability induced by fault-fracture network permeability produced by tectonism, volcanism and/or dike emplacement control the fluid flow. Where intergranular porosity is low, fracture permeability largely controls the fluid flow. The sealing of these fractures by mineral deposition occurs rapidly in the active systems and active deformation is required for generating and maintaining permeability and sustain large scale fluid flow (Cox et al. 2001). Sibson (1996) also noted that different stress regimes and fluid overpressures in a hydrothermal system can self-

generate structural permeabilities by migrating fluids and can largely control the nature and distribution of mineralization.

5.5. Visual Alteration Mapping

For visual alteration mapping, a scale of 1 to 5 was assigned with associated colour scheme and further defined as fresh, weak, strong, high and intense depending on the host rock composition, texture, lithology, alteration style and intensity. Alteration intensity map was produced using this scheme which shows the spatial distribution of alteration and the mineralisation zones. The brief description of the alteration and other features in the drillcores recorded in this study by visual mapping is described herein and is visually represented in the alteration intensity map in the next few pages.

Drillcore UW320

The top of the drillcore UW320 consists of sandy ignimbrite and lapilli sized pumice clasts up to 178 meters where it first comes in contact with Upper Andesite. From 178m to 220m interstratified ignimbrite and andesite layers form most of the stratigraphic units and can be easily identified by their varying colours. Intense clay alteration has completely destroyed the original fabric of andesite and disseminated pyrite is visible. At 230m, massive quartz veins envelope the andesite unit followed by the propylitic alteration of andesite with green clays filling the gaps and cavities. Calcite veins also occur here, and quartz phenocrysts in andesite are visible along with pyrite and breccia clasts (Figure 5C). From 260m to 340m, green chlorite (chlorite + corrensite) along with occasional quartz and calcite veins dominate the andesite unit. The breccia zones are more prominent after 270 meters onwards and dominate the rock unit from 320m onwards (Figure 5D). At 360m the change in alteration style is noted

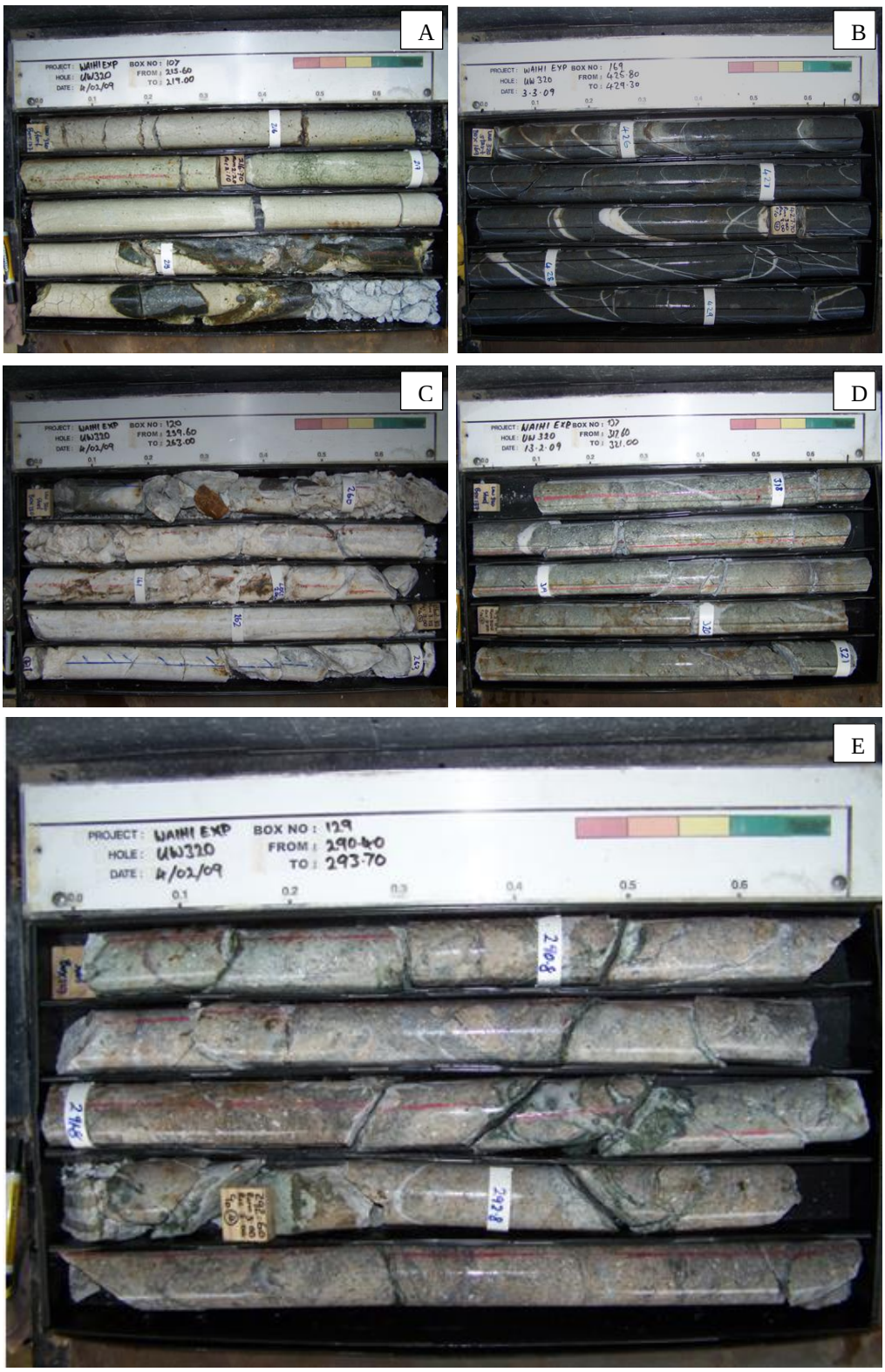

Figure 5.2. (A) Interlayered ignimbrite and andesite layers at UW320/215.60m. (B) Quartz veins present in the less altered andesite unit (hard bars). (C) Calcite and quartz dominated veins (D) Chlorite altered andesite at UW320/312m with breccia clasts. (E) Angular breccia clasts. Green clays filing the gaps and voids at UW320/290m.

from green chlorite to grey argillic (clay + carbonate). From 410m to 438m, the alteration style changes from argillic to quartz-phyric and calcite/quartz veins start to come in. Massive crustiform banded quartz veins form most of the stratigraphic unit from 438m to 462m where quartz replaces andesite with base metals and corrensite. This is followed by pale green clay altered andesite with vein breccia and calcite veins. The pyrite is also visible as veinlets and groundmass. From 468m to 483m dark grey and less altered rock (Figure 5.2B) unit (hard bars) are common with minor calcite and quartz veins. The lower part of the andesite consists mainly of pale greyish-green quartz-phyric flow mainly of chlorite/corrensite/illite altered sequences. The alteration intensity and hard bars location is shown in detail in the alteration intensity map.

Drillcore CGD003

The upper parts of the drillcore is the rhyolite unit which consists of coarse grained, porphyritic, pumiceous ignimbrite. The ignimbrite unit at upper parts is sandy, well welded and strong with highly to moderately weathered. The lower part of the ignimbrite unit contains large lithic and felsic fragments. The contact with andesite unit and ignimbrite in this drillcore is at 178m where strongly weathered and clay altered andesite is present. The colour of the lithology is yellow to yellow brown indicating the presence of yellow clays (possibly smectite?). At 192m, green coloured porphyritic andesite is present with minor pyrite which continues up to 220m (Figure 5B). Less to moderately argillic alteration is visible up to 222m which is followed downhole up to 261m with green grey propylitic altered andesite. Moderate to high silicification with carbonate alteration is widespread. A more clay altered unit follows downhole to 285m which consists of small quartz and calcite veins with pyrite crystals. The zone of brecciation is visible after this with quartz and calcite veins now more common. The interfingered units of less altered and moderately to highly altered andesite with quartz, amethyst and calcite veins with breccia (Figure5E) follow up to 335m where it comes in contact with dark green strongly clay altered andesite.

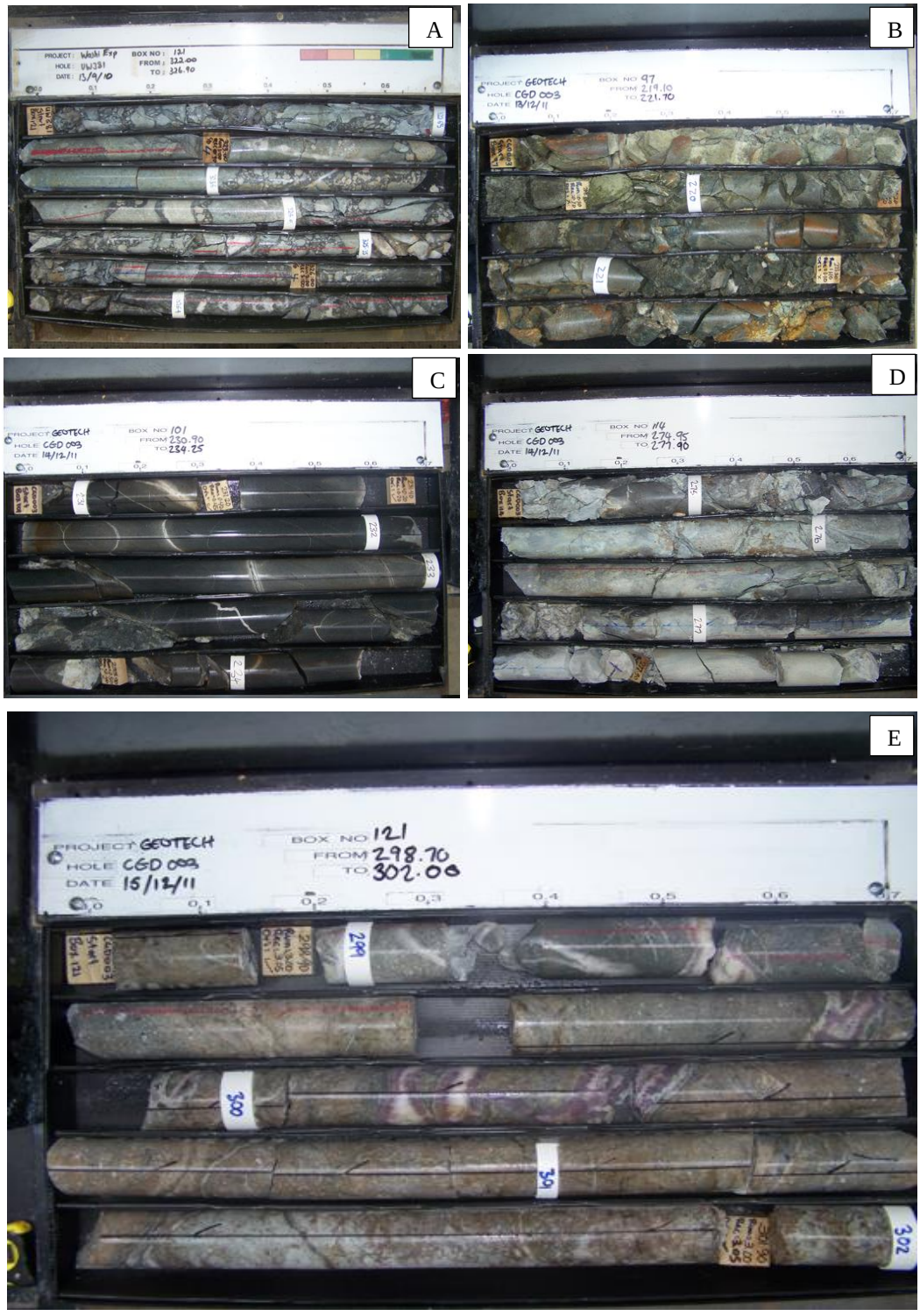

Figure 5.3. (A) Jigsaw shaped hydrothermal breccia at UW381/322m. (B) Propylitic alteration at CGD003/219m. (C) Quartz veins in the hard bar (D) argillic altered andesite at UWCGD003/274.95). (E) Amethyst and quartz veins with breccia clasts at CGD003/298.70.

Drillcore UW381

The alteration style at the drillcore UW381 is somewhat similar to the UW320. The contact with the andesite unit is at 190m. The upper part of Upper Andesite unit consists of paleosols and rhyolite unit. This is followed downhole by grey-greenish coloured andesite which is strongly crushed and fractured. The fractures and veins are filled with vuggy quartz and calcite with minor pyrite. From 200m to 220m blue-green coloured andesite unit is present which is mainly chlorite/quartz/pyrite altered with limonite and chlorite filling the gaps and voids. Massive to small alteration possibly illite/chlorite downhole is present from 280m onwards. Massive quartz veins are present after 320m which interlayer with intensely clay altered andesite from 320m to 400m. From 420m to 455m massive white vuggy quartz veins with calcite and pyrite are present with jigsaw shaped hydrothermal breccia (Figure 5.3A). The quartz veins are followed by crystalline quartz, pyrite and chlorite rich lithology.

Drillcore UW348

Upper parts of the drillhole consist of brown peaty soil followed by highly weathered ignimbrite which makes its contact with highly weathered andesite at 13m. Interlayered moderately to highly weathered andesite with colours ranging from yellow-brown to green-grey and grey-brown are present up to 52m (Figure 5.4A). A strongly altered brecciated porphyritic unit comes in contact with the upper lithology and is easily identified with brown-orange colour. This is followed downhole by poorly sorted grey to grey-brown lithologic unit which is strongly brecciated and contains limonite. The unit is variably clay altered with quartz, calcite and pyrite veins present and comes in contact with strongly fractured and sheared andesite at 92m.

The interlayered units of variable grades of alteration intensity follow downhole up to 175m where upper parts of these units are more clay altered and gradually change to propylitic alteration downhole and is more carbonate rich. This comes in contact with a green to grey moderately altered andesite-quartz unit which continues to 186m (Figure 5B). A weakly altered andesite unit follows with alternating units of variable colours and composition to 297m with quartz veins

present ranging from massive to tiny quartz, calcite and pyrite veinlets. The overall alteration style of this unit is clay altered at the upper parts and more silicic in the lower parts where it eventually comes in contact with a massive quartz vein with clay altered units (Figure 5C). The coarse platy calcite is common in and around the main vein and hydrothermal breccia is common. A green to grey green unit is present after the main quartz vein downhole which consists of more clay altered and silicic material. This unit is again followed by intervals of massive quartz veins and moderately to strongly altered andesite unit which continue till the end of the drillhole but less quartz veins at the end.

Drillcore UW364

The contact between with the Andesite unit and the top paleo-soil unit is at 7m and a blue-green to grey-green unit with moderate clay alteration follows up to 20m. A green-brown to green-grey propylitic altered unit is present from 20m-45m with occasional weakly to moderate layers of argillic alteration. This is followed by a grey coloured moderately to strongly brecciated clay/quartz altered andesite unit with minor quartz and pyrite veins. Intervals of clay altered/silicic and brecciated units are present up to 180m which consist of vuggy and coarse banded quartz veins with tiny calcite and pyrite veinlets. Pyrite is also present in disseminated form throughout the unit. The unit is weakly to moderately clay ad quartz altered.

A grey coloured tuff breccia unit is present from 181m-197m which is followed downhole by grey-green brecciated unit and moderately to highly clay altered andesite. Intervals of clay altered and variably altered andesite units with different colours and compositions are present which consist of breccia at regular intervals up to 455m where massive colloform banded quartz veins (Figure 5.4F) come in contact with the upper lithology. The Correnso vein consists of silicic material and other clay minerals (likely corensite?) together with pyrite and minor calcite. The lower end of the drillcore consists of more calcite veins and alteration style more silicic. The drillcores below were mapped for selected lengths and brief description of the visual mapping is given as under.

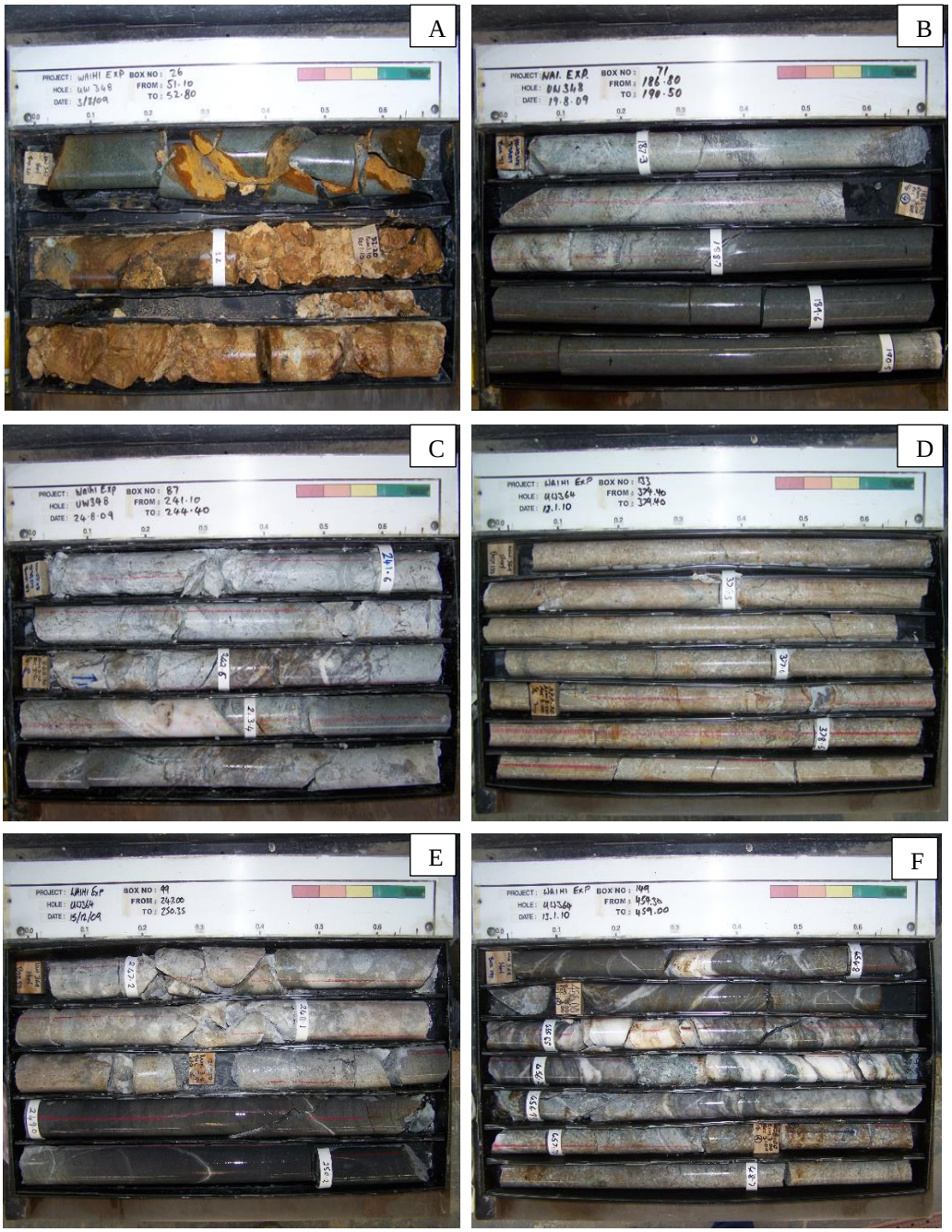

Figure 5.4. (A) Highly weathered green coloured andesite at UW348/51m. Green colour represents chlorite alteration. (B) Moderately altered grey andesite at UW348/186m. The alteration style changes from argillic to propylitic as visually identified by the colour change. The black colour is less altered andesite unit (hard bar). (C) Intensely altered andesite unit with massive quartz veins at UW348/241m. (D) Clay altered andesite at UW364/374m. (E) Clay altered andesite alongside less altered host alternating units of variable colours and composition to 297m with quartz veins present ranging from massive to tiny quartz, calcite and pyrite veinlets. The overall alteration style of this unit is clay altered at the upper parts and more silicic in the lower parts where it eventually comes in contact with a massive rock with quartz veins at UW364/247m. Angular breccia clasts can be seen easily in the grey andesite. (F) Massive colloform quartz veins at UW364/454m quartz vein with clay altered units (Figure 5C).

Drillcore CRO505

The drillcore CRO505 was mapped from 320m to 340m. The upper part of the hole above 320m consists of massive colloform quartz vein (Figure 5.5A) which is moderately to strongly brecciated with silicic material. From 320m onwards it is grey-green and weakly fractured with vuggy and banded quartz veins present (Figure 5B). Clay alteration is prominent downhole than the upper part.

Drillcore CRO506

This drillcore was mapped from 330m to 360m. At 330m the unit is dark grey and contains silicic material with pyrite disseminated and in the form of small veinlets. Breccia along with quartz veins is also common (Figure 5C). From 335m onwards the unit is light grey green and moderately to strongly argillic altered and consists of pyrite and quartz veinlets. The lower parts of the drillcore consists of intervals of light green and blue-green units which consist of hydrothermal breccia and less altered than the upper part (Figure 5D).

Drillcore CRO507

CRO507 was mapped from 300m to 350m. The upper part of the mapped drillhole is separated from the top lying unit with different alteration intensity and colour change. At 305m a light grey moderately altered argillic unit with silicic material is present which continues up to 317m (Figure 5E). This unit contains of disseminated pyrite with vuggy quartz veins. Interlayered units of different alteration intensities are present with alteration style gradually changing from argillic to propyllitic and massive quartz veins present at 324-325m and 327m-329m (Figure 5F). The lower part of the host rock again consists of more clay altered than the upper part from 345m to 350m.

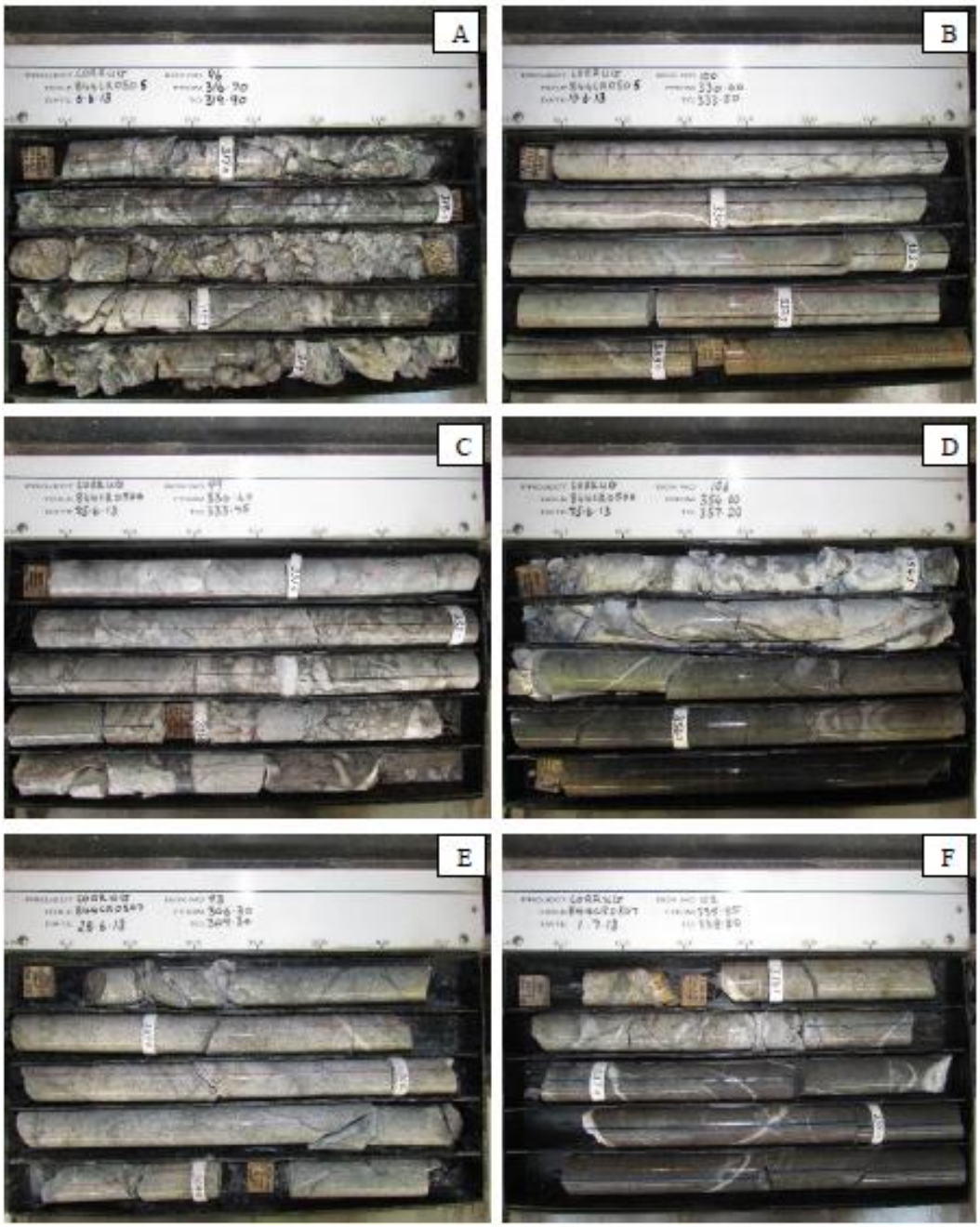

Figure 5.5. (A) Intensely altered colloform banded quartz vein at CRO505/319.6m (B) Clay altered andesite with vuggy and banded quartz veins present at CRO505/330.5m (C) Masive quartz veins with breccia clasts at CRO506/333m. (D) Quartz veins alongside less altered unit at CRO506/354 (E) Light grey moderately altered argillic unit with silicic material present at CRO507/306m (F) Gradual change of alteration style from argillic to propyllitic with quartz veins present CRO507/335m.

5.6. Alteration Intensity Map and Interpretation

The visual mapping results and Correnso data from Newmont Waihi was used to prepare alteration intensity map which was used to locate and interpret the alteration intensities throughout the system. The detailed colour code scheme and analytical methods used were already discussed in the sampling and analytical section. The map shows the zones of alteration zonations and areas of mineralization and location of drillcores and major veins.

The presence of highly altered and less altered (locally known as “hard bars”) units side by side in the upper and lower andesite units surrounding the vein system imply that hydrothermal fluids have migrated through the host rocks in a heterogeneous fashion. The complex alteration zonation around the Correnso vein suggests the migration of fluid in the system is possibly controlled by both primary permeability related to the properties (such as vesicularity) of the andesitic host rocks, as well as secondary permeability related to faulting and fracturing. The lower andesite unit contains more “hard bars” and appear to have more restricted hydrothermal fluid flow. The upper andesite unit on the other hand contains highly altered units, suggesting the zones of highly permeable volcaniclastic units. The alteration intensity pattern is also characterized in terms of change in colour of the core samples and identification of visible minerals. Both lower and upper andesite units exhibit a mix of strong argillic and propylitic alteration, propylitic being more widespread in the lower andesite unit when proximal to the Correnso vein. This is evident from the presence of greenish appearance of samples in the lower andesite unit indicating the presence of chlorite. The colour of samples range from light to dark grey, pale green to dark green (chlorite), black (hard bars), brown, and pale white. Host rock samples adjacent to the vein system contain abundant sulfide minerals, including sphalerite, pyrite and galena, whereas the veins contain quartz as most abundant mineral, followed by calcite, pyrite, and green clays (chlorite and/or correnSite).

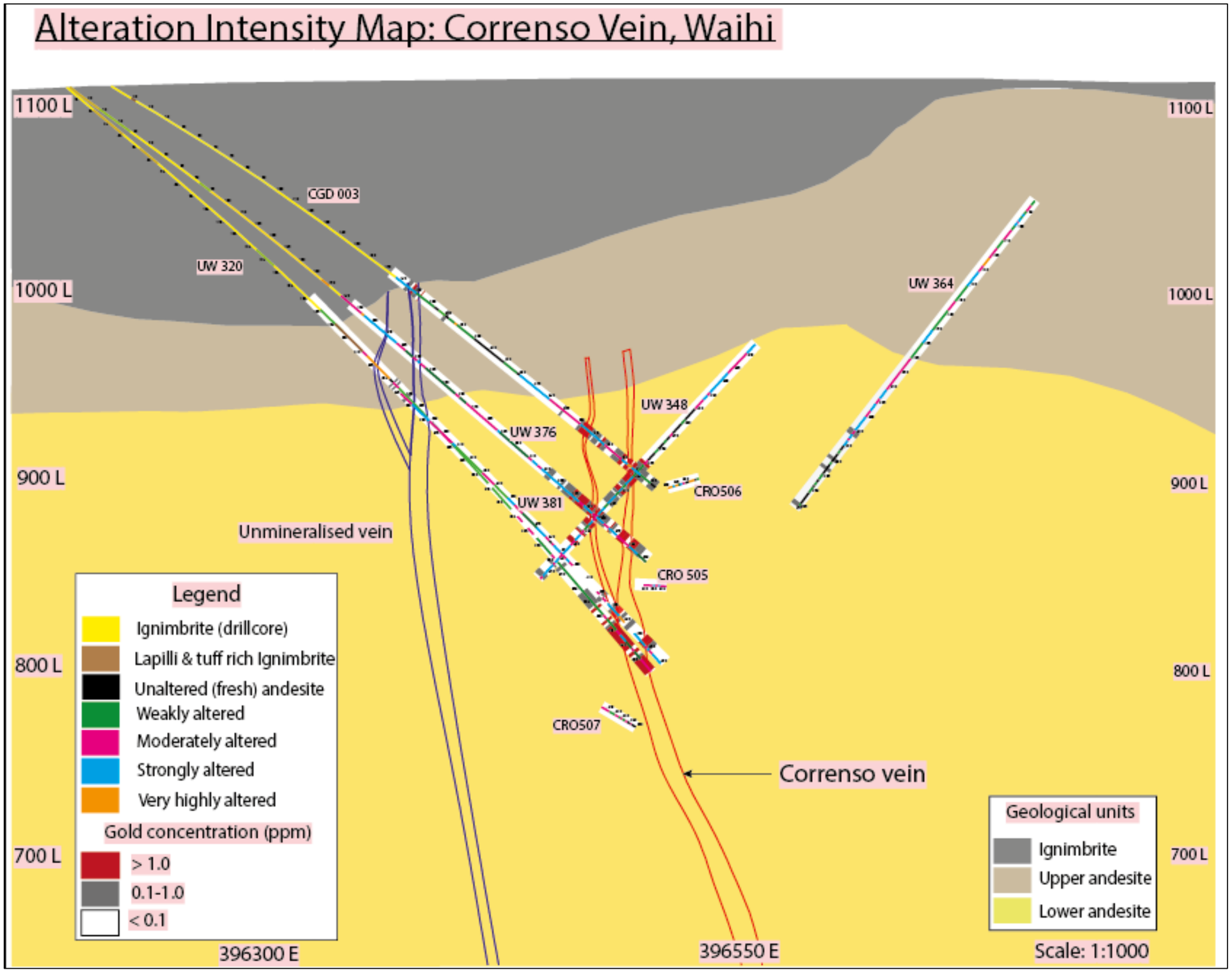

Figure 5.6. Map showing the alteration intensity pattern and geologic units. Drill cores are assigned colours on the basis of alteration intensity (Modified after Newmont Waihi Gold, 2013).

5.7. Geochemistry

Geochemistry is an important tool to quantify the hydrothermal alteration and identifying vectors by the presence or absence of certain anomalies which can help in effective exploration purposes. Geochemical data collected can be used to plot 2D and 3D diagrams and presented spatially which can help in analysing and evaluating results with ease. Major and trace element data is crucial for any exploration purposes as some elements tend to change chemically with respect to the mineralisation zones particularly, epithermal type of deposits. Low sulfidation epithermal deposit type show distinct geochemical signatures which can essentially vector towards the zones of high mineralisation. In general, low sulfidation epithermal systems are associated with higher concentrations of Au and Ag and other pathfinder elements like As, Sb, Zn, Pb, Se, and K and anomalously lower concentrations of Cu, Te and Se are also reported in such deposits (White & Hedenquist., 1995).

Circulating hydrothermal fluids can effectively result in the addition and removal of certain elements and transport metals to large areas. Hydrothermal activity can thus disperse trace minerals to considerable areas and create a zonation around the ore body and through geochemical analysis of these trace minerals, it is easy to vector towards the zones of mineralisation. Vertical zonation patterns in the low sulphidation epithermal deposits display a trend in which, from surface downwards, Hg, S, Sb, Au, Ag and base metals (Cu, Pb, Zn) are deposited. (Silberman and Berger, 1985). Neutral pH chloride fluids with dissolved gases act as transport agents in these type of deposits (Henley and Ellis, 1983). White (1981) discussed the deposition and transport of certain metals on the basis of their geochemical properties. Volatile metals (Hg and S) tend to deposit on or near the surface in the areas of low temperature advanced argillic alteration whereas non-volatile metals deposit in the areas altered by ascending neutral pH chloride waters. The relative mobility can force elements such as Hg, Tl, As, Sb to travel upward and outward thus creating near-surface haloes. Careful study of trace elements can thus give important clues about the location and extent of a precious metal deposit.

5.7.1. Geochemical results using pXRF

Introduction and working knowledge of pXRF has already been discussed in brief in the previous section of this chapter. 162 samples were collected from the core samples at regular intervals (approximately 10m) and crushed to fine powders for portable XRF (p-XRF) analysis using an Olympus Delta 50 KV portable XRF analyzer. Soil pXRF standards were used to monitor instrument drift and $Si0_2$ was used as a blank check. Values reported here have not been corrected for matrix affects. However, as the underlying rock type is either andesite, relative variations between samples should remain robust. The data here should be treated as a semi-quantitative and used to compare between samples to assess geochemical zonations only. Spatial 3-D plots were produced using the data acquired from the pXRF showing the geology and location of the drill cores using IoGas® software. The elemental concentrations of the major and trace element data with respect to the Correnso deposit are hereby discussed as follows.

5.7.2. Major Elements

Potassium (K)

K-rich mineral assemblages show proximity to the zones of mineralisation and can used as a vector towards the ore deposits in low sulphidation epithermal deposits. Potassium values at the Correnso deposit show increases in concentrations proximal to the vein system, particularly in the Lower Andesite unit (Figure 5.7A). Values range from 1335 ppm to 101,413 ppm. The upper and shallow parts of the system show depleted K concentrations suggesting clay-carbonate alteration was more prominent whereas in the deeper parts of the system, potassic alteration dominates the vein system as evident from the presence of adularia and K-feldspars identified by XRD analysis. Interestingly, K concentrations proximal to the vein also show some depleted zones which appear to be related to the presence of “hard bars” or less permeable and less altered units. Some samples in the Upper Andesite unit show elevated levels of K suggesting more intense alteration zones, which were also noted from the visual alteration mapping.

Calcium

Calcium is also found variable across the Correnso deposit which suggests the mobility during the hydrothermal alteration (Figure 5.7D). Calcium content is variable like iron and samples distal to the mineralisation show enrichment which is also documented from the presence of calcite more prominent in the upper parts of the system and distal from the vein system. Ca values range from 333 ppm to 77,758 ppm.

Iron

Iron content is variable across the ore body and concentrations range from 4879 ppm to 92,525 ppm. Fe is found in higher concentrations proximal to the main ore body in association with sulphides (Pyrite, chalcopyrite) and oxides (Haematite, magnetite). Elevated concentrations of Fe are also noted in the Upper andesite unit (Figure 5.7C) particularly in the drillcores UW348 and UW 364.

Manganese

Manganese is found in higher concentrations proximal to the mineralisation and only few samples were found containing elevated levels of Mn concentrations distal to the Correnso vein (Figure 5.7E). Mn values range from 48-9348 ppm. Drill core UW348 and CGD003 show very high concentrations of S in the Lower Andesite unit which is proximal to the Correnso vein.

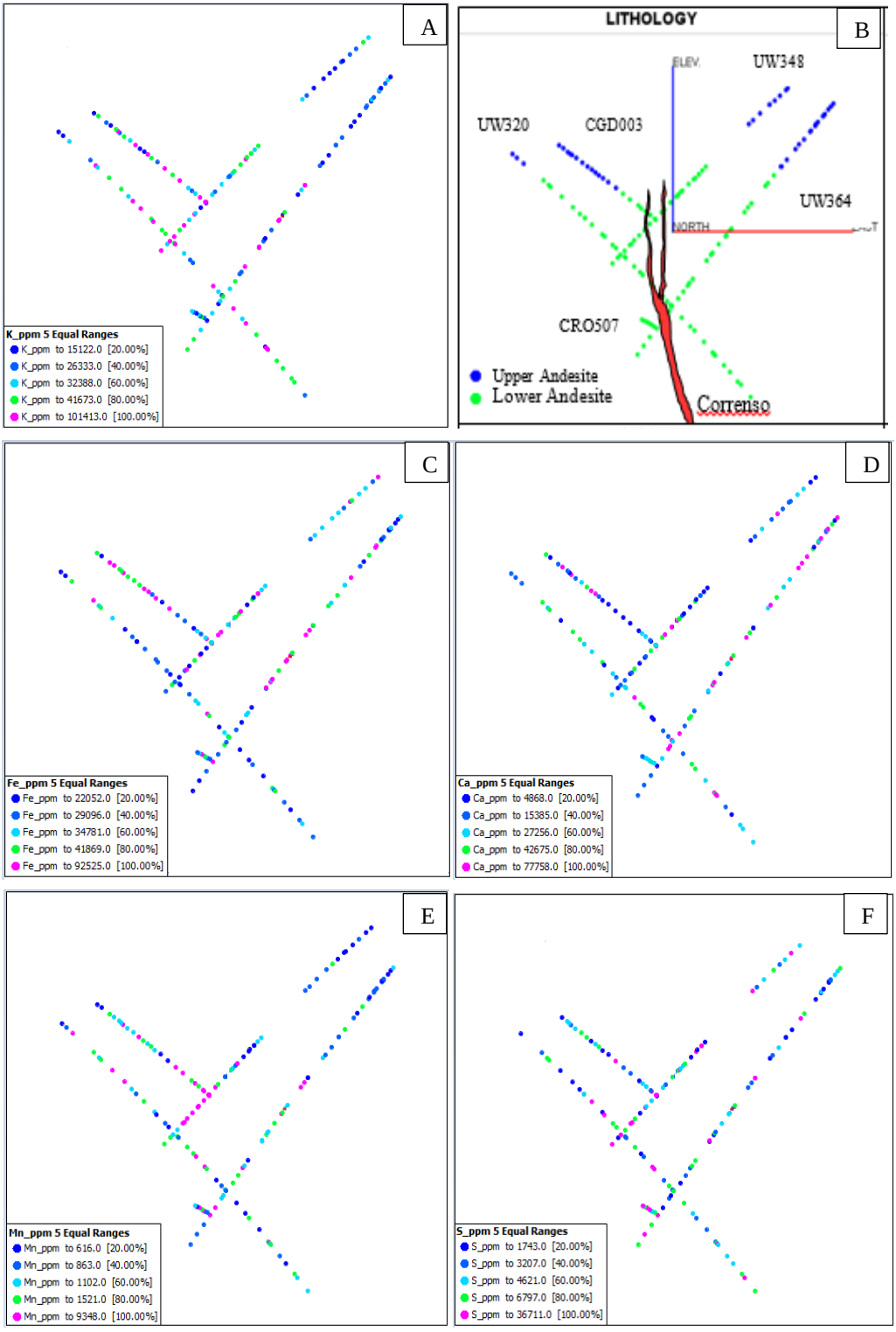

Figure 5.7. (A) Potassium. (B) Lithology and location of Correnso vein with drillcores. (C) Iron. (D) Calcium. (E) Manganese. (F) Sulphur.

Sulphur

Sulphur is found in the form of sulphide minerals in the Correnso deposit and is enriched proximal to the mineralisation (Figure 5.7F). It is found here in association with Fe, Pb, and Zn in the form of pyrite, galena, chalcopyrite and sphalerite. Sulphide minerals are found in higher concentrations in the veins as well as the host rocks. In the upper parts of the system it is found as pyrite whereas it is identified as galena, chalcopyrite and sphalerite proximal to the main ore body and in the veins. Sulphur concentrations here range from 435 ppm to 36,711 ppm.

5.7.3. Trace Elements

Zinc

Zinc is found associated with sulphur in the deeper parts of the system, particularly around the vein system. Zn concentrations range from 11.7 ppm to 73,338 ppm and surprisingly show high concentrations in the drillcores UW 364 and UW 348 proximal to the Correnso vein (Figure 5.8B). Also it shows depleted zones in the Lower Andesite unit away from the main ore body.

Arsenic

Arsenic concentrations range from 5-670 ppm and are highest proximal to the vein. As is also found in the deeper parts of the system but gradually depletes to the upper parts of the system where it is almost negligible (figure 5.8D). Arsenic is one of the important pathfinder elements and can vector towards the zones of high mineralisation.

Lead

Lead concentrations range from 6.9-14,921 ppm and is found enriched in the samples around the vein suggesting association with sulphide minerals. It is elevated in the samples close to the mineralisation where it forms galena with sulphides and is also found in the Upper Andesite unit (Figure 5.8C).

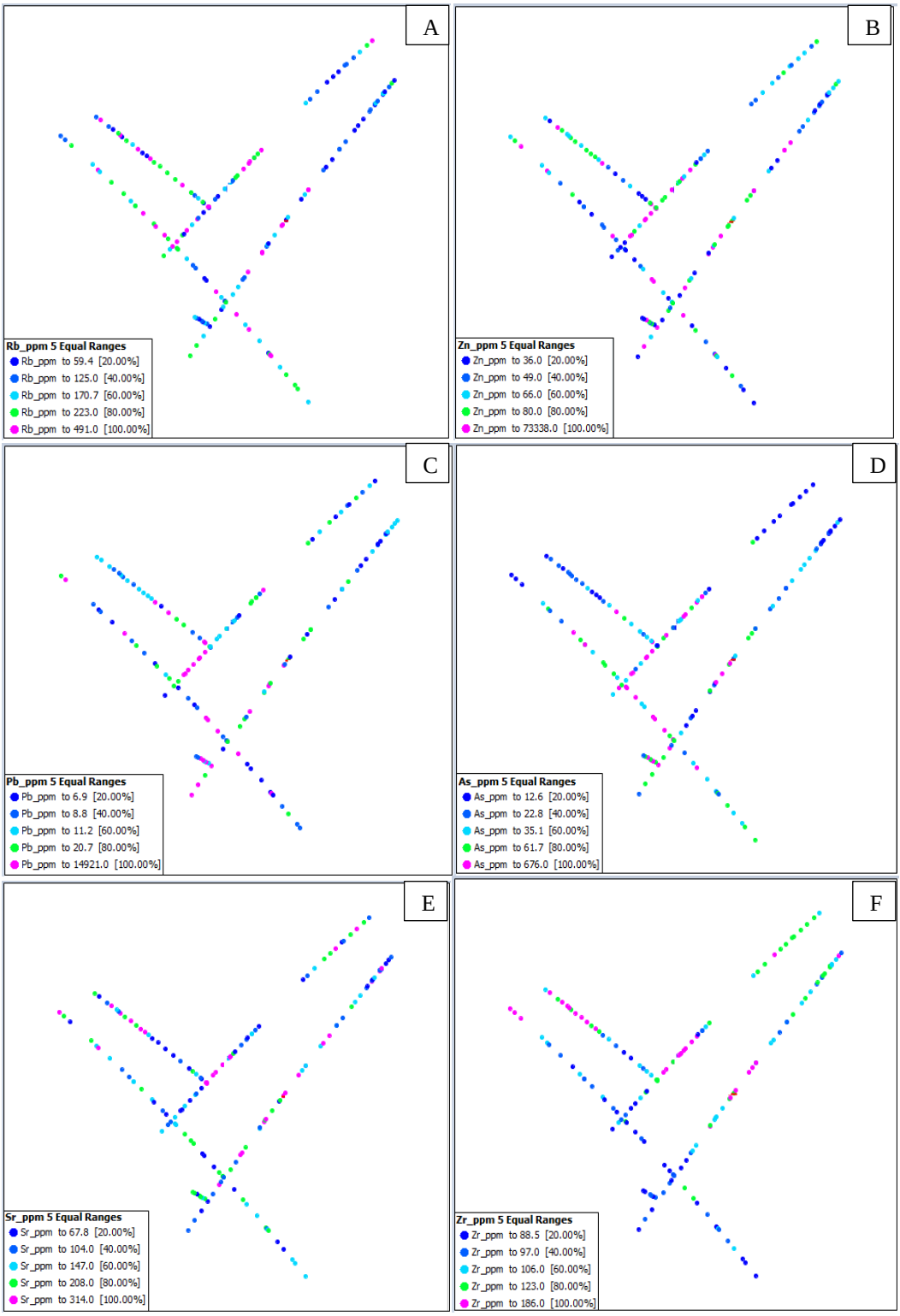

Figure 5.8. Spatial 3-D plots showing concentrations of selected elements in ppm. (A) Rb (B) Zn. (C) Lead. (D) Arsenic. (E) Niobium. (F) Zirconium.

Zirconium

Zirconium concentrations are more enriched in the ignimbrite unit, reflecting the more felsic nature of these rocks and in the middle part of the Correnso deposit. The concentrations range from 88-105 ppm. Zirconium is almost depleted in the lower parts of the system and being immobile is restricted to the rhyolite unit and the Upper Andesite.

Rubidium

Rubidium enrichment is largely restricted to the proximity of the Correnso veins with few samples containing elevated levels distal to the mineralisation. It replaces K in mica, muscovite here, and K-feldspar minerals and appears to follow the K trend. Upper parts of the drillcores UW348 and UW364 show depleted levels of Rb.

Strontium

Sr concentrations in the Correnso deposit range from 67.8 to 314 ppm. Elevated levels of Sr largely follow the Ca trend and appear to be depleted in the lower parts of the system which suggests its close association with calcite found in the parts of the system around the zones of boiling.

5.7.4. Other Trace Elements (Figure5.9)

Other trace elements identified by pXRF at the Correnso deposit were Selenium (Se), Titanium (Ti), Yttrium (Y), Tin (Sn), and Thorium (Th). Se, a pathfinder element, is totally depleted in the upper parts of the system and is found proximal to the vein and in the lower andesite unit. The concentrations range from 2.1-36.1 ppm and its elevated values proximal to the ore body suggests its association with the sulphide minerals. Titanium concentrations range from 2785-7209 ppm and again is enriched mostly in the upper parts of the system. Drillcore UW 348 and UW364 contain elevated concentrations of Ti proximal to the Correnso vein (Figure but otherwise it is depleted in the Lower Andesite unit. It is largely an immobile element and can withstand alteration and is found here in intensely altered zones.

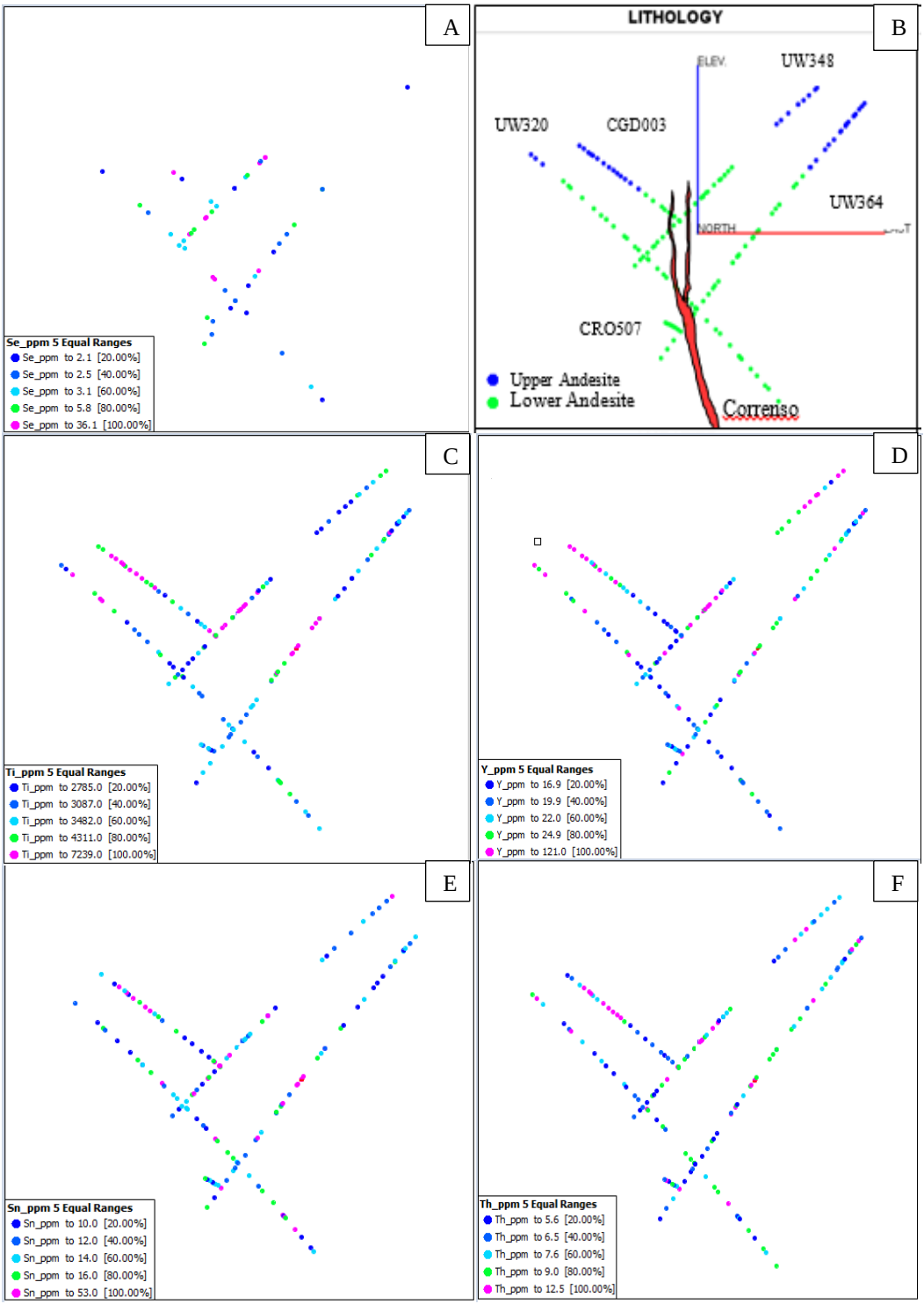

Figure 5.9. Spatial 3-D plots showing concentrations of selected elements in ppm. (A) Selenium (B) Lithology and location of Correnso vein with drillcores. (C) Titanium. (D) Yttrium (E) Tin (F) Thorium.

Yttrium is another immobile element which is found mostly distal to the mineralisation except few samples and the concentrations range from 16.9 to 121 ppm. Drillcore UW348 contains elevated levels of the Y concentrations distal and proximal to the vein. Thorium and Tin almost follow the same trend and are enriched in the upper parts of the system and away from the mineralisation zone but some samples are found scattered proximal to the vein. Drillcore CGD003 contains elevated levels of Th and Ti concentrations in the Upper andesite unit

5.8. Aqua-Regia ICP-MS Analysis and Results

Aqua-Regia ICP-MS analysis is an effective method used in the mining industry for determination of multiple elements in the geochemical samples. Sixty samples were send to SGS Waihi laboratory for Aqua Regia analysis to determine and identify the elements and their concentrations. The selected elements for which this test was carried out were Ag, As, Ba, Be, Bi, Co, Ce, Cu, Ga, In, Mn, Mo, Ni, Sb, Se, Sn, Th, Ti, U, and Zn. The methodology used for this analysis is described in brief as requested from the SGS Waihi laboratory. The samples were already been pulverised at the University of Waikato earth science laboratory. 0.3 grams of each sample was weighed into the test tubes. The powdered samples were then digested in the two acid/aqua regia. The combination of two acids HNO_3 and HCl were used for this analysis with the ratios of 2:1:HNO3: HCl. These acids combine to form Aqua Regia (Nitrosol Chloride) which dissolves the mineral matrix and holds the metal in solution. The digest methodology DIG12R was used in which the reaction was assisted by heating at temperature of 90°C +/- 5°C for 2.5hours within a water bath. The final digest volume of the sample came out to be 15ml each. Digest solution from DIG12R was then analysed by inductively coupled plasma-mass spectrometry (ICP-MS). The Two-acid digests are the weakest of the digestions and are thus not helpful for identifying silicate minerals, but are most useful for looking at elements housed in sulphide, carbonate and oxides. The results are presented in the table 5.1.

5.8.1. Results

Aqua-Regia analysis data from SGS Waihi was analysed using iogas suite and presented spatially and graphically in this chapter. Table 5.1 shows the elemental concentrations of selected samples from different drillcores. Firstly the samples were used for pXRF analysis and were analysed and plotted spatially. To further analyse and compare data with pXRF to get robust and accurate results, selected samples for Aqua-Regia analysis were sent to the laboratory to find the trace element concentrations. The results and brief geochemical description is given in the next few pages.

Table 5.1. Aqua Regia/Two-Acid digest analysis rsults of selected samples from the Corresno deposit

METHOD	IMS12R	IMS12R	IMS12R	IMS12R	IMS12R	IMS12R	IMS12R	IMS12R	IMS12R	IMS12R	IMS12R	IMS12R	IMS12R	IMS12R	IMS12R	IMS12R	IMS12R	IMS12R	IMS12R	IMS12R
SAMPLE ID	Ag	As	Ba	Be	Bi	Co	Ce	Cu	Ga	In	Mn	Mo	Ni	Sb	Se	Sn	Th	Tl	U	Zn
UW320/226.00	0.1	24	24	0.8	X	20.3	30.7	16	7.59	X	>1000	0.1	6	0.5	X	0.8	1.32	0.1	0.12	82
UW320/259.00	0.3	51	21	0.7	X	28.2	24.9	47	9.3	X	>1000	0.3	27	1.2	X	0.6	1.09	0.2	0.11	58
UW320/290.60	0.2	21	15	0.5	0.8	20.1	29.1	20	10.5	X	>1000	0.7	17	1	X	0.5	2.18	0.1	0.12	34
UW320/321.50	0.3	81	17	0.5	0.8	23.1	21	28	8.07	X	>1000	0.6	18	0.9	X	0.4	0.94	0.1	0.07	36
UW320/340.90	1.7	39	12	0.4	0.3	32.9	15.9	21	7.19	X	>1000	0.9	48	1.3	X	0.4	0.61	0.2	0.06	24
UW320/397.00	0.5	105	22	0.6	0.9	23.7	29	33	10.2	X	>1000	0.8	27	0.6	X	0.6	2.02	0.1	0.08	41
UW320/415.60	0.6	172	19	0.6	0.3	33.4	14.7	61	6.15	X	>1000	0.4	68	0.8	X	X	0.7	0.1	0.07	20
UW320/445.40	77.3	892	1	X	0.1	52.6	0.16	146	12.6	X	>1000	0.3	X	3.4	12	2.4	X	X	X	>2500
UW320/483.50	0.4	83	18	0.5	2.2	36.5	12.7	33	7.17	X	697	1.3	31	1	1	0.6	1.39	0.1	0.18	72
UW320/523.80	0.2	121	12	0.3	1.3	35.3	21.4	33	8.07	X	>1000	1.6	75	0.5	X	0.8	1.35	X	0.14	82
UW320/561.60	0.5	29	18	0.4	0.5	27.4	14.3	32	7.31	X	>1000	0.6	73	0.8	X	0.4	0.87	0.1	0.07	121
UW320/592.40	2.1	43	36	0.5	0.2	27.2	26.7	8	3.1	X	241	1.5	42	0.7	X	X	1.61	0.1	0.1	96
UW320/607.20	1.1	52	9	0.3	0.2	23.1	17.8	12	4.62	X	>1000	0.6	63	0.6	X	X	0.65	0.1	0.06	49
UW320/633.00	0.1	87	22	0.4	X	27.4	15.3	39	6.25	X	834	0.6	83	0.4	X	X	0.86	X	X	26
UW348/94.650	X	8	66	0.4	X	19.5	23.2	19	7.02	X	598	1	18	0.9	X	0.7	1.67	X	0.31	59
UW348/129.90	0.2	51	47	0.5	X	27.3	18.8	18	5.03	X	604	0.4	18	3.3	X	0.4	1.61	0.3	0.11	54
UW348/204.80	1.8	16	17	0.7	36.7	15.9	23.2	39	5.29	X	732	1.3	13	0.8	X	2	1.61	0.2	0.11	62
UW348/224.35	0.3	63	21	0.4	3.4	15.3	34.9	3	0.89	X	25	0.6	3	0.5	2	0.5	2.3	0.2	0.08	17
UW348/267.10	0.3	33	19	0.5	0.5	21.5	23	13	6.4	X	802	0.6	6	1.3	X	1.8	1.2	0.2	0.12	122
UW348/296.50	0.2	36	24	0.6	0.2	37.2	30.2	6	9.02	X	>1000	0.4	6	0.8	X	1.3	1.84	X	0.22	71
UW348/314.40	4.3	166	11	0.2	3.7	47.5	3.93	16	2.57	X	>1000	0.4	5	1.5	5	0.4	0.34	X	X	384
UW348/339.00	9.9	895	1	0.2	X	20	0.2	122	40.7	X	>1000	0.1	X	12.9	2	0.3	X	X	X	2270
UW348/352.70	4.4	39	14	0.6	2.3	20.9	17.4	14	6.64	X	>1000	0.9	33	0.7	2	0.7	1.9	0.2	0.12	37
UW348/374.55	2.4	41	13	0.4	1	25	17	15	8.87	X	>1000	0.5	31	0.6	X	X	1.37	X	0.07	37
UW364/79.85	0.1	12	39	0.7	X	22.9	20.2	16	9.26	X	>1000	0.6	20	1	X	0.7	1.28	X	0.15	60
UW364/115.65	X	16	50	0.6	0.2	20.9	19.5	13	7.81	X	695	0.4	18	0.5	X	0.6	0.81	X	0.09	43
UW364/138.65	X	24	54	0.5	X	21.9	27.2	7	12.9	X	>1000	0.6	16	X	X	0.9	0.68	X	0.07	85
UW364/181.85	X	11	113	0.5	0.7	27.2	24.2	16	7.05	X	636	0.8	38	0.2	X	0.7	1.87	0.1	0.34	100
UW364/208.25	X	49	106	0.4	4.6	21.1	19	13	11.1	X	708	0.7	16	0.4	X	1.5	1.76	X	0.23	25
UW364/241.80	3	61	28	X	1.9	51.4	12.1	17	1.32	X	116	1.5	9	2.3	2	0.5	1.08	0.2	0.08	21
UW364/281.90	0.2	53	21	0.5	0.1	24.8	27.8	13	9.39	X	914	0.6	6	1.3	X	0.9	1.52	X	0.11	57
UW364/307.10	0.4	782	9	0.5	0.6	26.1	18.2	17	9.18	X	977	0.4	31	9.4	2	0.6	0.92	0.2	X	101
UW364/333.40	0.1	17	15	0.6	X	23.7	25.5	10	8.24	X	931	0.9	15	0.4	1	0.7	4.17	0.1	0.16	91
UW364/360.70	0.2	12	27	0.3	0.3	36.1	20.5	12	4.16	X	543	0.8	20	1.3	6	0.7	2.56	0.2	0.13	68
UW364/437.05	30	420	2	0.1	0.1	51.4	0.13	747	6.39	X	>1000	0.2	X	14.5	5	0.5	X	X	X	>2500
UW364/478.00	0.6	36	24	0.5	3.3	25.8	19	11	3.68	X	722	0.3	31	0.4	X	0.4	1.6	0.1	0.08	81
CRO507/316.30	0.8	23	14	0.5	1.7	26.9	19.4	15	7.11	X	801	0.6	60	0.6	X	0.3	0.83	X	0.12	60
CRO507/334.10	0.7	72	23	0.5	6	34.8	17.2	29	7.63	0.1	>1000	0.4	54	0.5	X	0.6	0.89	X	0.21	146
CRO507/351.05	0.6	97	26	0.5	0.6	21.6	13.1	55	7.31	X	714	0.3	60	1	X	0.6	0.77	X	0.2	33
CGD003/222.30	0.3	21	17	0.7	0.5	21.7	31.8	16	8.5	X	782	0.3	6	0.8	1	0.9	0.96	0.1	0.08	78
CGD003/244.80	0.2	12	36	0.5	X	23.9	29.6	14	12.8	X	>1000	0.4	6	0.6	X	1.2	1.64	X	0.2	78
CGD003/256.45	0.2	9	12	0.6	0.2	23.6	32.3	6	7.74	X	937	0.3	6	0.3	X	0.6	1.42	0.1	0.09	80
CGD003/292.95	0.9	56	22	0.7	0.4	19.4	14.8	15	11.3	X	>1000	0.3	17	0.7	X	0.6	0.67	0.1	X	47
CGD003/315.80	0.2	29	18	0.7	0.3	16.3	21.4	5	4.38	X	>1000	0.6	8	0.7	X	1.4	2.5	0.2	0.11	18
CGD003/343.40	0.1	103	37	0.5	0.3	21.9	28.4	18	12.7	X	>1000	0.3	6	0.8	X	1.4	1.49	X	0.11	85

5.8.2. Elemental Concentrations and Interpretation

Aqua-Regia ICP-MS analysis did find variations in trace elements which pXRF failed to resolve as it is far more sensitive analytical technique. Figure 5.10 shows the elemental concentrations of selected trace metals. Elevated concentrations of barium are found, although not of significant quantity (12-113 ppm), distal to the mineralisation zone in the upper and lower parts of the system. Arsenic follows exactly the same trend as observed from the pXRF analysis and thus validates the accuracy of the pXRF results for As, and indicates that pXRF analysis of epithermal samples for As could add value as an exploration tool. As values for the selected samples here range from 17-895 ppm and are depleted distal to the ore body. Bi concentrations are found to be in the range of 0.2-36 ppm and show elevated levels only around the vein and almost absent or depleted distal to the mineralisation. Cobalt (20.3-52.6 ppm), like bismuth, is also found proximal to the mineralisation and depleted in the outer parts of the system.

Cerium is a rare earth element which is likely relative immobile, and Ce concentrations range between 14.7 to 34.9 ppm. It is more prominent in the Upper Andesite unit and three samples around the vein show elevated levels of Ce. Ce in Aqua-Regia analysis is most likely hosted in calcite and it appears to follow a pattern as more samples around the vein contain lower concentrations of Ce than the distal samples from the mineralisation, except samples from the drillcore UW348. Silver (Figure 5.11A) is found to show highly variable anomalies with maximum concentration of 77.3 ppm and minimum concentration of 0.1 ppm. Completely absent in the upper parts of the system, it is only found close to the main Correnso vein although few samples in the Lower Andesite unit contain elevated concentrations of Ag, particularly UW364 and UW320. The Gold (Au) results shown here are from the Newmont Au Assay data and not from the Aqua-Regia analysis. Au concentrations range from 0.01 ppm to 89.11 ppm. Au is almost negligible in the Upper Andesite unit but interestingly drillcore UW364 and UW348 show significant amounts of anomalies in the upper parts of the system. Otherwise, Au is restricted to the Correnso vein and the proximal areas around the

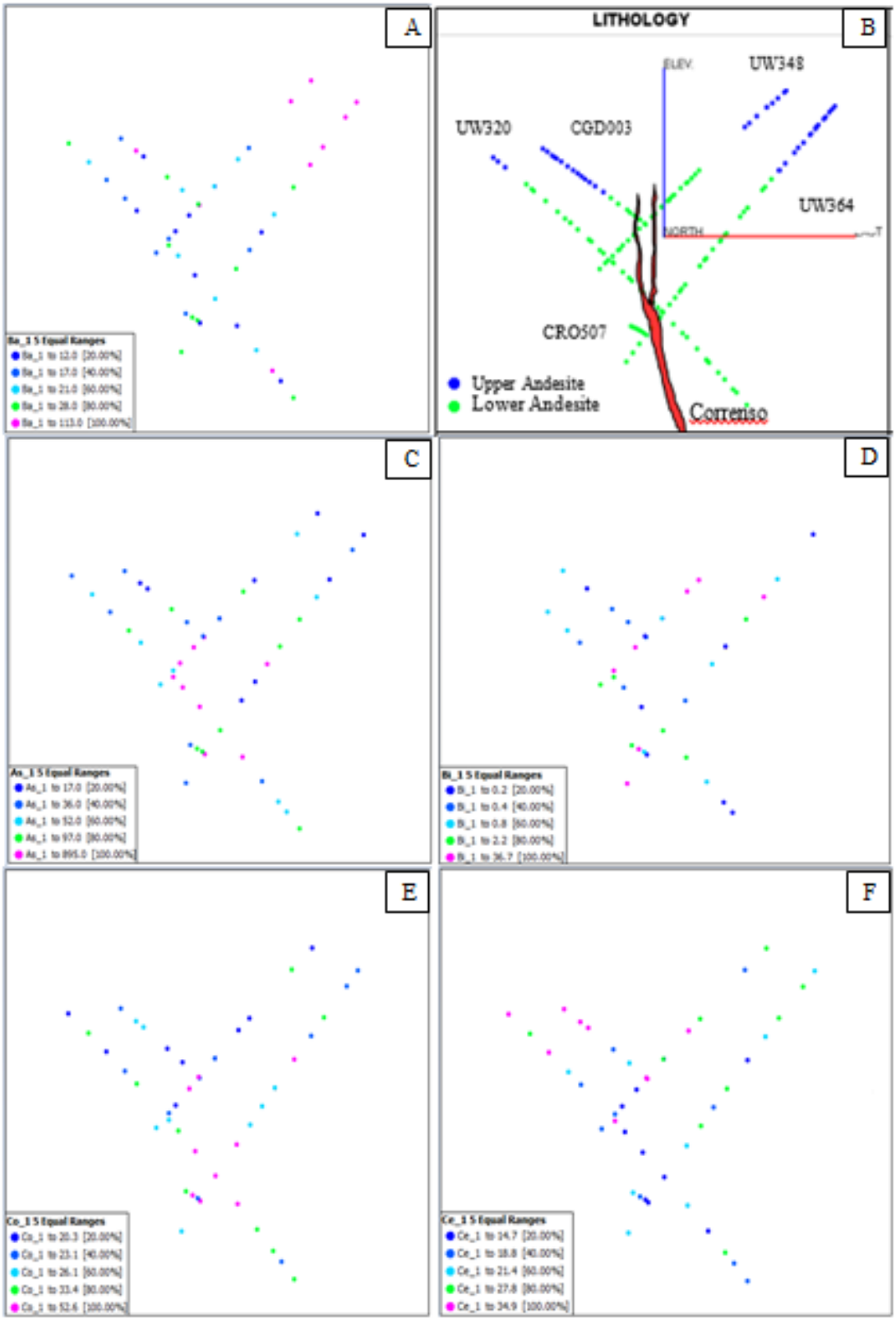

Figure 5.10. Spatial 3-D plots showing concentrations of selected elements in ppm. (A) Barium (B) Lithology and location of Correnso vein with drillcores. (C) Arsenic (D) Bismuth (E) Cobalt (F) Cerium.

vein system. The lower part of the drillcore UW320 shows discontinuous Au anomalies following the base of the main vein. Thallium concentrations appear to be very low and only one sample contains 0.3 ppm of Tl. Though they appear to follow a pattern with higher concentration samples found around the vein system. Zinc shows highly variable anomalies ranging from 33-2270 ppm and elevated concentrations are found proximal to the vein and follow the sulphur trend. Antimony appears to follow a pattern with anomalies more prominent to the mineralisation zone than the outer parts of the system. The values range from 0.5 ppm to 14.5 ppm. Copper shows significant difference in its anomalies with values ranging from 11 to 747 ppm.

Other trace elements found in the Aqua-regia analysis are Beryllium, Gallium, Manganese, Molybdenum and Nickel shown in figure 5.12. Beryllium concentrations are very low (0.3-0.8 ppm) but appear to follow a pattern. Elevated elemental concentrations of Be are found in the upper parts of the system, particularly in the Upper Andesite unit and ignimbrite unit whereas it is depleted in the deeper parts of the system. Gallium (5.07-40.7 ppm) values are higher proximal to the mineralisation but elevated concentrations are also found in the drillcore Uw364, especially in the upper parts. Mn figure here appears to show some missing data but is consistent with the anomalies stronger around the Correnso vein.

Mo values range from 0.3-0.8 ppm and does not seem to follow any pattern as it is found mostly in all the drillcore samples but depleted in the upper parts of UW320 and CGD003 drillcores. Nickel values are significantly higher in the deeper parts of the system suggesting its occurrence as the base metal. Its elemental concentrations range from 6-83 ppm and is depleted in the upper parts.

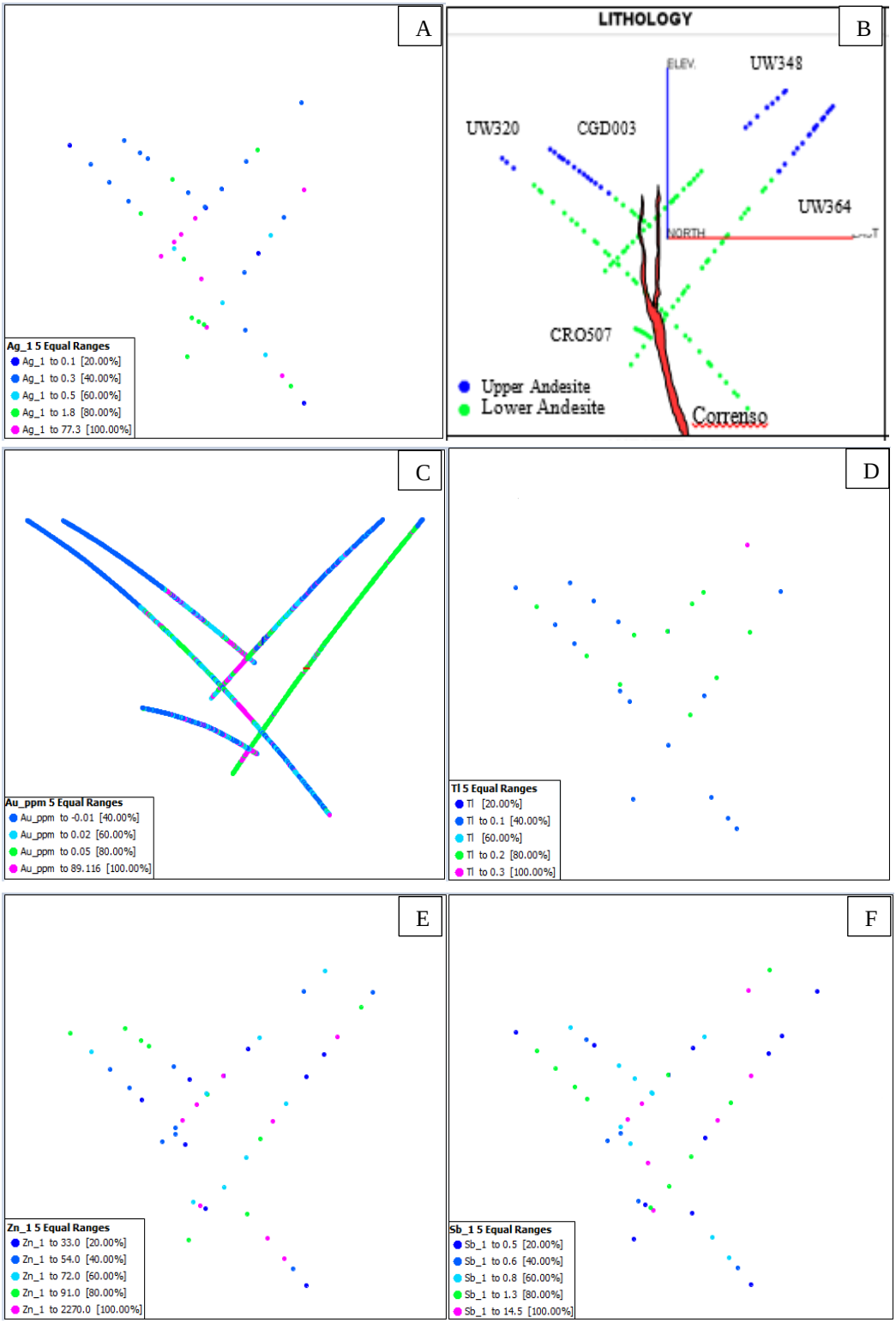

Figure 5.11. Spatial 3-D plots showing concentrations of selected elements in ppm. (A) Silver (B) Lithology and location of Correnso vein with drillcores. (C) Gold (D) Thallium (E) Zinc (F) Antimony.

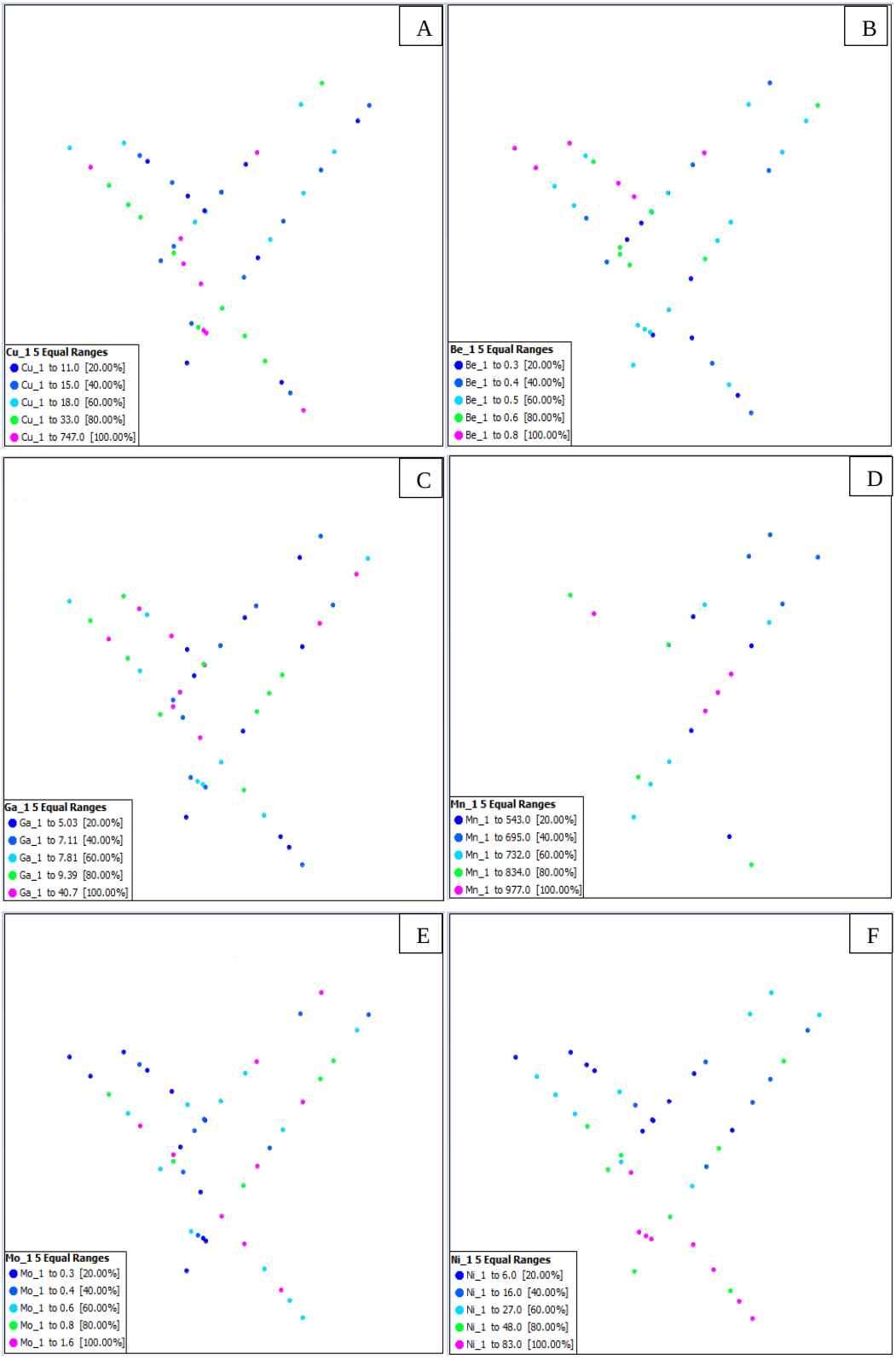

Figure 5.12. Spatial 3-D plots showing concentrations of selected elements in ppm. (A) Copper (B) Beryllium (C) Gallium (D) Manganese (E) Molybdenum (F) Nickel

5.9. Summary and Interpretation

Geochemical study of hydrothermal systems can help significantly in studying the litho-geochemical variations and provide better understanding of the geochemical patterns around the ore bodies. Low sulphidation epithermal deposits exhibit distinct geochemical signatures which can potentially vector towards the zones of mineralisation and can thus be helpful for exploration purposes. These signatures come in the form of addition or depletion of certain "pathfinder" elements. Also, anomalies of K-metasomatism can extend to considerable distances which can be studied to identify the areas containing mineralised ore bodies.

A map was prepared by corporating all the mineralogical, geochemical and visual alteration data (Figure 5.13). Hydrothermal alteration mineralogical assemblages displayed in the figure 5.13 show a clear mineralogical alteration zonation pattern. Potassic alteration, the result of K-metasomatism, has been identified through thin section petrography and XRD analysis. Potassic alteration asemblages are found to be confined to the proximity of the mineralisation. Alteration mineral assemblages found here, mainly orthoclase and adularia; suggest the zone of high temperature. The samples distal to the vein lack in K-feldspars which have been documented from geochemical and mineralogical analysis to occur proximal to the vein. This is confirmed from the zonation pattern of K and Rb-metasomatism which reveal K and Rb enrichment at distances in hundreds of metres. Mineralogical data on the other hand shows potassic zonation (as potassium feldspars) only proximal to the vein.

Sericitic alteration is mainly zoned around the vein and consists primarily of sericite (illite) and quartz ± chlorite in the outward zones and other clay minerals. Argillic alteration is widespread in the Correnso deposit and consists of clay minerals which have been identified as illite, smectite, chlorite and interstratified clays. It overprints all the other alteration types and is found both distal and proximal to the mineralisation. Also, the presence or absence of certain clays change laterally and vertically with respect to the vein.

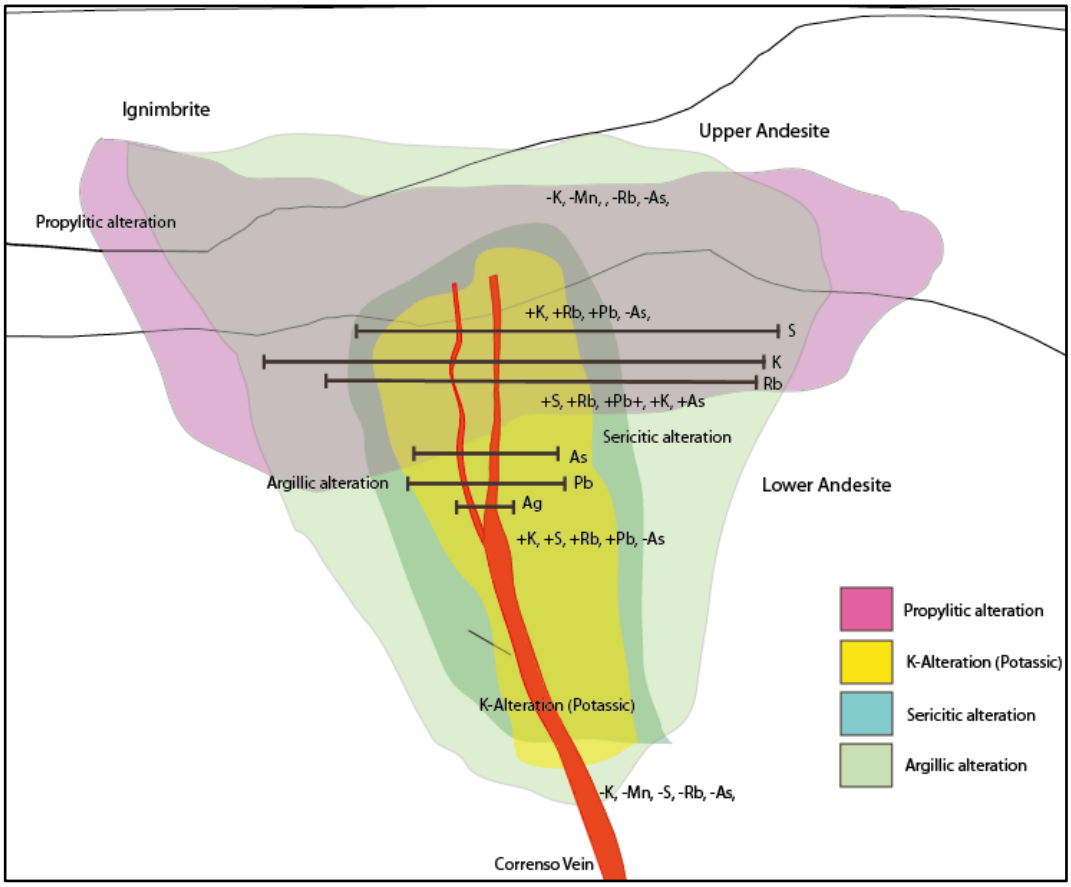

Figure 5.13. Lateral and vertical variations in trace elements at Correnso deposit. Addition (+) and depletion (-) of selected elements vertically are mentioned in the diagram which have been inferred from the Aqua-Regia (ICP-MS) and pXRF analysis. Hydrothermal alteration zonation pattern and alteration assemblages are estimated on the basis of XRD analysis, thin section petrography and visual logging.

In earlier chapters, these variations have been described in detail and certain clay minerals are found to show a clear mineralogical zonation. For example, corrensite is found in the deeper parts of the system and is present only proximal to the mineralisation. It is not found elsewhere apart from the vein proximity which suggests it to be considered as an important vector towards the mineralisation. Illite is also found close to the veins and is depleted in the outer zones whereas smectite is ubiquitous. Propylitic alteration is found to be present in the outward zones and in some drillcores close to the vein overprinting other alteration types especially in the upper parts of the system. It is also present in the peripheries of the vein system which is evident from its presence in the form of chlorite and albite in the drillhole UW320 at depths of more than 600m.

Mineralogical data and visual logging proved to be helpful in identifying specific mineralogical anomalies in this study which essentially vector towards the ore body but the size and extent of the visible and mineralogicalalteration haloes is not same as geochemical alteration haloes. Some of the vectors to mineralisation were identified using the geochemical tools with K-metasomatism extending considerably further than potassium feldspars identified from XRD data or thin section petrography. The figure 5.13 shows the trace and major elements and their variations across the system. K, Rb, Mn, As, S and Pb are key pathfinder elements and their addition can suggest the location and extent of orebody and can constrain the zones of high mineralisation from the barren one. Enrichment of these elements proximal to the vein has the potential to be useful vectors to help improve exploration, and identify potential “near misses” during drilling.

Mineralogical analysis is good for initial analysis purposes and can provide useful and important background for further exploration purposes but for accurate and robust interpretation, geochemistry provides valueable information which can validate and provide confidence with the results. However, both techniques should be used side by side for effective and robust results.

6. Summary and Conclusions

The Au-Ag rich Correnso deposit is a low sulphidation epithermal deposit located east of Waihi adjacent to the Martha and Favona deposits. It is part of the Coromandel Volcanic Zone (CVZ) which contains approximately 50 low-sulphidation (adularia-sericite) epithermal Au-Ag vein deposits and porphyry Cu deposits. The deposit is a high grade, "blind" Au-Ag deposit, discovered recently in 2009 and is named after the clay mineral correnside. Hydrothermally altered andesitic and dacitic host rocks of Waipupu Formation contain Au-Ag rich quartz veins. Mineralogical and geochemical analysis of drillcore samples from the Correnso deposit in this study provide an insight into the nature and extent of the alteration zonation. This is helpful in understanding the alteration pattern and geochemical anomalies identified as vectors towards the similar types of ore bodies of economic consideration. Correnso deposit is a classic example of low sulphidation epithermal deposit where hot near neutral chloride rich waters have interacted with the host rocks and resulted in the mineralogical and geochemical changes. These changes, in the form of alteration haloes spread to considerable distances, can be identified, analysed and quantified to better understand these deposits.

Visual core logging and petrographical study of the core samples in this study show the visual and mineralogical variations brought upon by hydrothermal alteration of host rocks. The core samples exhibit variable features visually which are identified and analysed for the extent and intensity of alteration and incorporated further with XRD and petrographical study. Drillcore logging shows a clear alteration zonation pattern around the vein system. Host rocks of variable alteration intensities are found to be adjacent to one another inferring heterogeneity of the fluid flow which implies that these fluids have been controlled by primary and secondary permeabilities. Primary and alteration minerals identified suggest quartz being the ubiquitous followed by chlorite and

feldspars. The vein mineralogy consists of pyrite, chalcopyrite, galena and sphalerite. Breccia zones occur in the upper parts of the system, proximal to the mineralisation, with same mineralogy as host rocks. Also, paleo-boiling zones were identified by the presence of platy calcite and hydrothermal breccia textures.

The overall alteration pattern identified at Correnso deposit consists of quartz-chlorite-adularia-sericite-calcite-pyrite alteration assemblage inferring formation of these minerals from near neutral chloride waters. Three main alteration assemblages were identified where propylitic alteration is confined predominantly to the outward zones and upper parts of the system. Potassic alteration is found enveloping the vein and proximal to the mineralisation with sericitic alteration also found close to the Correnso vein. Argillic alteration overprints both the alteration types and consists mainly of clay minerals illite, smectite, and interstratified clays.

Host rock geochemistry at the Correnso deposit shows a very clear geochemical pattern and the results obtained through pXRF and Aqua-Regia ICP-MS analysis demonstrate geochemical zonation around the main Correnso deposit. Lithogeochemical anomalies outline zones of mineralization and pathfinder elements such as Rb, As, K, Pb, Sb, and Zn are enriched proximal to the mineralisation and appear to follow a trend. Low concentrations of Cu, Se, and Te are measured in this study which also is in par with the geochemical signatures of the low sulphidation epithermal deposits (White and Hendenquist, 1995).

Further, spatially detailed and more extensive geochemical analysis using whole rock geochemistry to quantify hydrothermal alteration and study differences in the mass changes is required to fully understand the hydrothermal alteration intensity and zonation.

References

Adams, C.J., Wodzicki, A., and Weissberg, B.G., 1974. K-Ar dating of hydrothermal alteration at the Tui Mine, Te Aroha, New Zealand. *NZ Journal of Science,* 17:193-199.

Adams, C.J., Graham, I.J., Seward, D., and Skinner, D.N.B., 1994. Geochronological and geochemical evolution of the late Cenozoic volcanism in New Zealand. *NZ Geological Survey Bulletin*. v. 37, p. 359-379.

Arribas, A., 1995. Characteristics of high-sulphidation epithermal deposits and their relation to magmatic fluids. In: Thomson JFH (ed) Magmas, fluids, and ore deposits. *Miner Association Canada Short Course*, v. 23, p. 419-454.

Booden, M.A., Smith, I.E.M., Mauk, J.L., and Black, P.M., 2012. Geochemical and isotopic development of the Coromandel Volcanic Zone, northern New Zealand, since 18 Ma. Journal of Volcanology and Geothermal Research, 219-220: p. 15-35.

Brathwaite, R.L., and Christie, A.B., 1996. Geology of the Waihi area, scale 1:50,000. *Institute of Geological and Nuclear Sciences of New Zealand.* Geological Map 21.

Brathwaite, R.L., and Skinner, D.N.B., 1997. The Coromandel epithermal gold province: a result of collision of the Northland and Colville arcs in the northern New Zealand. *Proceedings New Zealand Minerals and Mining Conference, Ministry of Commerce, Wellington, New Zealand*, p. 111-117.

Brathwaite, R.L., 1989. Geology and exploration of the Karangahake gold-silver deposit. *Mineral Deposit of New Zealand Monograph*, 13: 73-78

Briggs, R.M., and Krippner, S.J.P., 2006. The control by caldera structures on epithermal Au-Ag mineralization and hydrothermal alteration at Kapowai, central Coromandel volcanic zone. *Australasian Institute of Mining and Metallurgy,* Monograph 25, p. 101–107.

Briggs, R.M., Houghton, B.F., McWilliams, M., and Wilson, C.N.J., 2005. 40Ar/39Ar ages of silicic volcanic rocks in the Tauranga-Kaimai area, New Zealand: Dating the transition between volcanism in the Coromandel arc and the Taupo Volcanic Zone. *New Zealand Journal of Geology and Geophysics*, v. 48, p. 459–469.

Britten, R.M., 1981. The geology of the Frieda River Copper prospect, Papua New Guinea. *Unpublished Ph.D. thesis, Canberra, The Australian National University,* 395 p.

Browne, P.R.L., Ellis, A.J., 1970. The Ohaaki-Broadlands hydrothermal area, New Zealand: mineralogy and related geochemistry. *American Journal of Science.* 269: 97-131.

Browne, P.R.L., 1970. Hydrothermal alteration as an aid in investigating geothermal fields. *Geothermics Special Issue* 2 : 564-70.

Browne, P.R.L., 1978. Hydrothermal alteration in active geothermal fields. *Annual Reviews of Earth and Planetary Science* 6: 229-250.

Buchanan, L.J., 1981. *Precious metal deposits associated with volcanic environments in the southwest. Arizona Geological Society Digest,* v. 14, p. 237-262.

Burnham, C.W., and Ohmoto, H., 1980. Late stage processes of felsic magmatism; in Ishihara, S., and Takenouchi, S. (eds). Granite magmatism and related mineralisation. *Mining Geology Special Issue*, 8: p.1-11.

Carr, R., Zhang, C., Moles, N., and Harder, M., 2008. Identification and mapping of heavy metal pollution in soils of a sports ground in Galway City, Ireland, using a portable XRF analyser and GIS. *Environmental Geochemistry and Health*, 30, 45–52.

Carter, L., Shane, P., Alloway, B., Hall, I.R., Harris, S.E., and Westgate, J.A., 2003. Demise of one volcanic zone and birth of another—a 12 m.y. marine record of major rhyolitic eruptions from New Zealand. *Geology*, v. 31, p. 493–496.

Christie, A.B., Simpson, M.P., Brathwaite, R.L., Mauk., J.L., and Simmons, S.F., 2007. Epithermal Au-Ag and related deposits of the Hauraki goldfield, Coromandel Volcanic Zone, New Zealand. *Economic Geology*, v. 102, p. 785–816.

Christie, A.B., Brathwaite., R.L., Mauk, J.L., and Simpson, M.P., 2006. Hauraki goldfield: regional exploration databases and prospectivity studies; in Christie, A.B., and Brathwaite, R.L., eds., Geology and Exploration of New Zealand Mineral Deposits. *Australasian Institute of Mining and Metallurgy Monograph*, v. 25, p. 73–84.

Cole, J.W., 1978. Distribution, petrography and chemistry of Kiwitahi and Maungatautari Volcanics, North Island, New Zealand. *NZ Journal of Geology and Geophysics* 21 (2): 143-154.

Corbett, G. J., and Leach, T.M., 1998. Southwest Pacific Rim gold-copper systems: structure, alteration, and mineralization. *Society of Economic Geologists*, Special Publication.

Corbett, G., 2002. Epithermal Gold for Explorationists: Applied geoscientific practiceand research in Australia. *Australian Institute of Geoscientists Jour*nal, Paper 01, p. 26.

Craig, H., 1963. The isotopic geochemistry of water and carbon in geothermal areas. In: E. Tongiorgi (Editor), Nuclear Geology on Geothermal Areas, Spoleto, 1963. *Cons. Naz. Ric. (C.N.R.), Lab. Geol. Nucl., Pisa*, p. 17-53.

Cox, S.F., Knackstedt, M.A., and Braun, J., 2001. Principles of structural control on permeability and fluid flow in hydrothermal systems. *Reviews in Economic Geology*, v. 14, p. 1−24.

Cox, S.F., 2005. Coupling between deformation, fluid pressures and fluid flow in ore-producing hydrothermal environments. *Economic Geology 100th Anniversary Volume*, p. 39−75.

Craig, N., Speakman, R.J., Popelka-Filcoff., R.S, Glascock., M.D, Robertson., D.J, Shackley, M.S., and Aldenderfer, M.S., 2007. Comparison of XRF and pXRF for analysis of archaeological obsidian from southern Perú. *Journal of Archaeological Science,* 34:2012-2024.

Fenner, C. N., 1934. *Trans. Am. Geophys. Union, 15th Meet*., Washington, Pl. 1, p. 240-43.

Fenner, C.N., 1936. Bore-hole investigations in Yellowstone Park. *Journal of Geology*. 44 : 225-315

Gazley, M.F., 2011. Metamorphism, geochronology and stratigraphy of an amphibolite-facies greenstone-hosted gold deposit: Plutonic Gold Mine, Marymia Inlier, Western Australia, PhD thesis (unpublished). *Victoria University of Wellington,* Wellington.

Gazley, M.F., and Fisher, L.A., 2014. A review of the reliability and validity of portable X-ray fluorescence spectrometry (pXRF) data. In: Mineral Resource and Ore Reserve Estimation – The AusIMM Guide to Good Practice. Second edition. *The Australasian Institute of Mining and Metallurgy*, Melbourne, p. 69–82.

Gazley, M.F., Vry, J.K., du Plessis, E. and Handler, M.R., 2011. Application of hand-held X-ray fluorescence analyses to metabasalt stratigraphy, Plutonic Gold Mine, Western Australia. *Journal of Geochemical Exploration*, 110, 74–80.

Gifkins, C.C., Allen, R.L., and McPhie, J., 2005. Apparent welding textures in altered pumice-rich rocks. *Journal of Volcanology and Geothermal Research,* v. 142, p. 29-47

Giggenbach, W.F., 1991. Redox processes accompanying the deposition of minerals in volcanic magmatic-hydrothermal systems: in Matsuhisa, Y., Aoki, M., and Hedenquist, J.W., eds., High temperature acid fluids and associated alteration and mineralization. *Geological Survey of Japan Report,* v. 277, p. 91-96.

Guilbert, J.M., and Park, C.F., 1985. The Geology of Ore Deposits. Waveland Press Inc.IL.

Harvey, C.C., and Browne, P.R.L., 1991. Mixed layered clay geothermometry in the Wairakei geothermal field, New Zealand. *Clay and Clay Minerals*, v. 39, p. 614-621.

Hayward, B.W., and Brook, F.J., 1984. Lithostratigraphy of the basal Waitemata Group, Kawau Subgroup, Auckland, New Zealand. *NZ Journal of Geology and Geophysics.* 27(2):101-124.

Heald, P., Foley, N.K., and Hayba, D.O., 1987. Comparative anatomy of volcanic-hosted epithermal deposits: Acid-sulfate and adularia-sericite types. *Economic Geology*, v. 82, p. 1–26.

Healy, J., Schofield, J.C., and Thompson, B.N., 1964. Sheet 5 Rotorua (1st Ed.). Geological Map of New Zealand, scale 1:250,000. *Dept of Scientific and Industrial Research, Wellington.*

Hedenquist, J.W., and Henley, R.W. (1985) The importance of CO_2 on freezing point measurements of fluid inclusions; evidence from active geothermal systems and implications for epithermal ore deposition. Econ. Geol. 80, 1379- 1406.

Hendenquist, J.W., and Lowenstern, J.B., 1994. The role of magmas in the formation of hydrothermal ore deposits. *Nature.* 370,p. 519-527.

Hedenquist, J.W., Izawa, E., Arribas, A., and White, N.C., 1996. Epithermal gold deposits: Styles, characterstics, exploration: Society of Resource Geology, Tokyo, Japan, Resource Geology Special Publication 1, p. 18.

Hedenquist, J.W., 1986. Geothermal systems of the Taupo Volcanic Zone, New Zealand: Their characteristics and relation to volcanism and mineralisation ;in Smith, I.M., ed., Late Cenozoic volcanism in New Zealand. *Royal Society of New Zealand Bulletin,* v. 23, p. 134- 138.

Hemley, J.J., Montoya, J.W., Marinenko, J.W., and Luce, R.W., 1980. Equilibria in the systems Al_2O_3-SiO_2-H_2O and some general implications for alteration/mineralization processes. Economic Geology, v. 75, p. 210-228.

Henley, R.W., and Ellis, A.J., 1983. Geothermal systems ancient and modern: A geochemical review. *Earth Science Reviews*, v. 19, p. 1-50

Henley, R.H., and Hedenquist, J.W., 1986. Introduction to the geochemistry of active and fossil geothermal systems: Berlin-Stuttgart, Gerbruder Borntrager, Monograph Series. *Mineral Deposits*, v. 26, p. 1–22.

Henley, R.W., and McNabb, A., 1978. Magmatic vapour plumes and ground water interaction in porphyry copper emplacement. Economic Geology, v. 73, p. 1-19.

Henley, R.W., Truesdall, A.H., and Barton, and P.B. Jr., 1984. Fluid mineral equilibria in hydrothermal systems. *Reviews in Economic Geology*, v. 1, p. 267.

Henley, R.W., 1985. The geothermal framework for epithermal deposits. *Reviews in Economic Geology*, v. 2, p. 1–24.

Hobbins, J.M., Torckler, L.K., Rhys, D.A., Ross, K.V., Mauk, J.L., 2012. The Correnso Epithermal Gold-Silver Deposit, a New Blind Discovery in Waihi, New Zealand. *Annual General Meeting and Conference - The Australasian Institute of Mining and Metallurgy*, New Zealand Branch 45: 227-240

Hochstein, M.P., and Nixon, I.M., 1979. Geophysical study of the Hauraki Depression, North Island, New Zealand. *NZ Journal of Geology and Geophysics*. 22:1-19.

Hochstein, M.P., Tearney, K., Rawson, K., Davey, F.J., Davidge, S., Henrys, S., and Backshall, D., 1986. Structure of the Hauraki rift, New Zealand. *Royal Society of New Zealand Bulletin,* v. 24, p. 333–348.

Hollinger, E., and Mauk, J.L., 2001. Low-sulfidation epithermal veins at the Gladstone Hill prospect, Waihi, New Zealand. *The Australasian Institute of Mining and Metallurgy New Zealand Branch 34th Annual Conference*, p. 165-174.

Hürkamp, K., Raab, T., and Völkel, J., 2009. Two- and three-dimensional quantification of lead contamination in alluvial soils of a historic mining area using field portable X-ray fluorescence (pXRF) analysis, *Geomorphology*, 110:28-36.

Jang, M., 2010. Application of portable X-ray fluorescence (pXRF) for heavy metal analysis of soils in crop fields near abandoned mine sites. *Environmental Geochemistry and Health*, 32:207-216.

Jia, P., Weiming, T., Doelman, C., Chen, H., Zhao, S., Lin, R., and Torrence Glascock, M.D., 2010. Moving sources: a preliminary study of volcanic glass artifact distributions in northeast China using pXRF. *Journal of Archaeological Science*, 37:1670-1677.

John, D.A., Wallace, A.R., Ponce, D.A., Fleck, R.J., and Conrad, J.E., 2000. New perspectives on the geology and origin of the northern Nevada rift: *Geological Society of Nevada, Geology and Ore Deposits 2000: the Great Basin and Beyond Symposium*, May 15–18, 2000, Reno-Sparks, Nevada, Proceedings, p. 127–154.

John, D.A., Hofstra, A.H., Fleck, R.J., Brummer, J.E., and Saderholm, E.C., 2003. Geologic Setting and Genesis of the Mule Canyon Low-Sulfidation Epithermal Gold-Silver Deposit, North-Central Nevada. *Economic Geology*, v. 98, pp. 425–463

Kalnicky, D.J. & Singhvi, R., 2001. Field portable XRF analysis of environmental samples. *Journal of Hazardous Materials*, 83, 93–122.

Kato, N., Kakai, I., and Shindo, Y., 2009. Change in chemical composition of early Islamic glass excavated in Raya, Sinai Peninsula, Egypt: on-site analysis using a portable X-ray fluorescence*, Journal of Archaeological Science*, 36:1698-1707.

Keith, T.E.C., and Muffler, L.J.P., 1978. Minerals produced during cooling and hydrothermal alteration of ash flow tuff from Yellowstone drill holeY-5. *Journal of Volcanology and Geothermal research*, V. 3, P. 373-402.

Kilbride, C., Poole, J., and Hutchings, T.R., 2006. A comparison of Cu, Pb, As, Cd, Zn, Fe, Ni and Mn determined by acid extraction/ ICP-OES and ex situ field portable X-ray fluorescence analyses. *Environmental Pollution*, 143:16-23.

King, P.R., 2000, Tectonic reconstruction of New Zealand: 40 Ma to the present. *New Zealand Journal of Geology and Geophysics*, v. 43, p. 611–638.

Kristmannsdotter, H., 1984, Types of clay minerals in hydrothermally altered basaltic rocks: Reykjanes, Iceland. *Jokull*, v. 26, p. 30-39.

Lindgren, W., 1933. *Mineral Deposits.* New York, McGraw Hill, p.930.

Markey, A.M., Clark, C.S., Succop, P.A., and Roda, S., 2008. Determination of the feasibility of using a portable X-ray fluorescence (pXRF) analyzer in the field for measurement of lead content of sieved soil, *Journal of Environmental Health,* 70:24-29

Mauk, J.L., and Simpson, M.P., 2007. Geochemistry and stable isotope composition of altered rocks and the Golden Cross epithermal Au-Ag deposit, New Zealand: *Economic Geology*, v. 102, p. 841−871.

Mauk, J.L., and Hall, C.M., 2003. 40Ar/39Ar age determinations from the Waihi and Favona deposits, North Island, New Zealand. *Australasian Institute of Mining and Metallurgy New Zealand Branch Annual Conference. 36th, Proceedings,* p. 231–239.

Mauk, J.L., and Hall, C.M., 2004. 40Ar/39Ar age of adularia from the Golden Cross, Neavesville and Komata epithermal deposits, Hauraki gold field, New Zealand. *New Zealand Journal of Geology and Geophysics*, v. 47, p. 227–231.

Mauk, J.L., Simpson, M.P., Hollinger, H., Morrell, A.E., Smith, N., Locke, C.A. and Cassidy, J., 2006. The Favona epithermal Au-Ag deposit, Hauraki goldfield—mineralogy, geochemistry and geophysics. *Australasian Institute of Mining and Metallurgy Monograph 25*, p. 185–190.

Meyer, C., and Hemley, J.J., 1967. Wall Rock Alteration. Pp. 166-235 in: Geochemistry of Hydrothermal Ore Deposits (H. L. Barnes, editor). Holt Rinehart and Winston, New York.

Mitchell, A.H.G., and Garson, M.S., 1981. *Mineral deposits and global tectonic settings.* London, Academic Press, p. 421.

Moore, C.R., 1983. Rhyolite domes and pyroclastic rocks (Whitianga Group) of the Hahei Area, Coromandel Peninsula. *Journal of the Royal Society of New Zealand*, 13 (1/2): 79-92.

Morris, P.A., 2009. Field-portable X-ray fluorescence analysis and its application in GSWA. *Geological Survey of Western Australia*, Record 2009/7.

Muffler, I.I.P., White, D.E., 1969. Active metamorphism of Upper Cenozoic sediments in the Salton Sea geothermal field and the Salton Trongh, southeastern California. *Geological Society of America Bulletin*, 80: 1 57-82

Nazaroff, A.J., Prufer, K.M., Drake, B.L., 2010. Assessing the applicability of portable X-ray fluorescence spectrometry for obsidian provenance research in the Maya lowlands. *Journal of Archaeological Science,* 37: 885-895.

Parsons, C., Grabulosa, E.M., Pili, E., Floor, G.H., Roman-Ross, G., and Charlet, L., 2012. Quantification of trace arsenic in soils by field-portable X-ray fluorescence spectrometry: considerations for sample preparation and measurement conditions, *Journal of Hazardous Materials*, 262:1213-1222.

Peinado, F.M., Ruanon, S.M., González, M.G.B., and Molina, C.E., 2010. A rapid field procedure for screening trace elements in polluted soil using portable X-ray fl uorescence (pXRF), *Geoderma*, 159:76- 82.

Phillips, S.C., and Speakman, R.J., 2009. Initial source evaluation of archaeological obsidian from the Kuril Islands of the Russian Far East using portable XRF, *Journal of Archaeological Science, 39*:1256- 1263.

Pirajno, F., 2009. Hydrothermal Processes and Mineral Systems. *Geological Survey of Western Australia.* Springer. p. 121-123, 422,448.

Radu, T., and Diamond, D., 2009. Comparison of soil pollution concentrations determined using AAS and portable XRF techniques, *Journal of Hazardous Materials*, 171:1168-1171.

Reyes, A.G., 1995. Geothermal systems in New Zealand and the Philippines - why are they so different. *Pacific Rim Congress, Auckland, New Zealand, proceedings:* Carlton South, *Australasian Institute of Mining and Metallurgy,* p. 485-490.

Reyes, A.G., 1990. Petrology of Philippine geothermal systems and the application of alteration mineralogy to their assessment. *Journal of Volcanology and Geothermal Research,* 43, 279-309.

Rose, A.W., and Bart, D.M., 1979. Hydrothermal alteration, in Barnes, H.L., ed., *Geochemistry of hydrothermal ore deposits, 2nd edition*, New York, John Wiley & Sons, p. 173-227.

Rowland, J., and Simmons, S. F., 2012. Hydrologic, magmatic, and tectonic controls on hydrothermal flow, Taupo Volcanic Zone, New Zealand: Implications for the formation of epithermal vein deposits. *Economic Geology, v*.107, p. 427-457.

Schofield, J.C., 1967. Geological Map of New Zealand, scale 1:250,000. *Department of Scientific and Industrial Research*, Wellington.

Sibson, R.H., 1996. Structural permeability of fluid-driven fault-fracture meshes. *Journal of Structural Geology*, v. 18, p. 1031–1042.

Sillitoe, R.H., 1999. Styles of High-Sulphidation Gold, Silver and Copper Mineralisation in Porphyry and Epithermal Environments. *PACRIM*, Bali, Indonesia..

Sillitoe, R.H., Lorson, R.C., 1994. Epithermal gold-silver-mercury deposits at Paradise Peak, Nevada: Ore controls, porphyry gold association, detachment faulting and supergene oxidation. *Economic Geology*, 89: 1228-1248.

Sillitoe, R.H., 1994. Indonesian mineral deposits - introductory comments, comparisons and speculations; in van Leeuwen, T.M., Hedenquist, J.W., James, L.P., and Dow, J.A.S., eds., Mineral deposits of Indonesia - discoveries of the past 25 years. *Journal of Geochemical Exploration*, v. 50, p. 1-12.

Sillitoe, R.H., 1993. Epithermal models: Genetic types, geometrical controls and shallow features. *Geological Association of Canada Special Paper* 40, p. 403−417.

Silberman, M.L., Berger, B.R., 1985. Relationship of trace element patterns to alteration and morphology in epithermal precious-metal deposits. Reviews in economic geology, 2: 203-232.

Simmons, S.F., and Christenson, B.W., 1994. Origins of calcite in a boiling geothermal system. *American Journal of Science,* v. 294, p. 361–400.

Simmons, S.F., White, N.C., and John, D., 2005. Geological characteristics of epithermal precious and base metal deposits. *Economic Geology 100th anniversary Volume*, p. 485−522.

Simmons, S.F., White, N.C., John, D.A., 2005. Geological characteristics of epithermal precious and base metal deposits. *Economic Geology 100th anniversary Volume*, p. 485–522.

Simpson, M.P., Chambefort, I.S., 2014. Epithermal Au-Ag deposits of the Hauraki Goldfield and geothermal fields of the Taupo Volcanic Zone, New Zealand : are they analogous?. p. 533-544 In: Rendell, C. (convener) Australasian Institute of Mining and Metallurgy. *Annual conference / Australasian Institute of Mining and Metallurgy*, New Zealand Branch.

Simpson, M.P. and Mauk, J.L., 2001. Hydrothermal alteration in the Gladstone Hill lowsulfidation epithermal area, Waihi, New Zealand. *New Zealand Branch of the AusIMM Annual Conference, Proceedings*, Dunedin, New Zealand, p. 175-184.

Simpson, M.P., and Mauk, J.L., 2007. The Favona epithermal gold-silver deposit, Waihi, New Zealand. *Economic Geology,* v. 102, p. 817−839.

Simpson, M.P., Mauk, J.L., 2000. Geochemistry of wall rock alteration at the Golden Cross deposit, New Zealand: *New Zealand Minerals and Mining Conference, 2000, Proceedings*, p. 197–208.

Simpson, M.P., Simmons, S.F., and Mauk, J.L., 2001. Hydrothermal alteration and hydrologic evolution of the Golden Cross epithermal Au-Ag deposit, New Zealand*. Economic geology*, v. 96, p. 773–796.

Simpson et al., 2007. The Favona epithermal gold-silver deposit, Waihi, New Zealand: Hydrothermal alteration, hydrologic evolution and implications for exploration. *Economic Geology*, v. 102, p. 817–839.

Skinner, D.N.B., 1967. Geology of the Coromandel Region with emphasis on some economic aspects. Ph.D Thesis, University of Auckland.

Skinner, D.N.B., 1976. Geological Map of NZ, scale 1:63,360. *Department of Scientific and Industrial Research, Wellington.*

Skinner, D.N.B., 1979. Volcanic and Geothermal Geology, Coromandel and central north island, New Zealnd. *ANZSAAS Auckland*, Tour Guide. NZ Geological Survey Report G37.

Skinner, D.N.B., 1969. Colville Formation, a new formation possibly correlative with the Waitemata Group. *NZ Journal of Geology and Geophysics*. 12(2): 349-360.

Skinner, D.N.B., 1977. Major element, Rb and Sr geochemistry of the Mercury Basalts, Hauraki Volcanic Region. Abstract. *NZ Geochemical Group 11th Conference, Auckland.* p. 22-23.

Skinner, D.N.B., 1986. Neogene volcanism of the Hauraki Volcanic Region, in Smith, IEM, ed., Late Cenozoic Volcanism in New Zealand, *Royal Society of New Zealand Bulletin*, p. 21-47.

Skinner, D.N.B., 1993. Geology of the Coromandel Harbour area. *Institute of Geological and Nuclear Sciences Geological Map 4.*

Smith, N., Cassidy, J., Locke, C.A., Mauk, J.L., and Christie, A.B., 2006. The role of regional-scale faults in controlling a trapdoor caldera, Coromandel Peninsula, New Zealand*. Journal of Volcanology and Geothermal Research*, 149: 312–328.

Spörli, K.B., and Cargill, H., 2011. Structural evolution of a world-class epithermal orebody: The Martha Hill deposit, Waihi, New Zealand*. Economic Geology,* v. 106, p. 975–998.

Spörli, K.B., Begbie, M.J., Irwin, M.R., Rowland, J.V., 2006. Structural processes and tectonic controls in epithermal Au-Ag deposits of the Hauraki goldfield,

New Zealand; in Christie, A.B., and Brathwaite, R.L., eds., Geology and exploration of New Zealand mineral deposits, *Australasian Institute of Mining and Metallurgy Monograph,* v. 25, p. 85–94.

Spörli, K.B., 1987. Development of the New Zealand microcontinent, in Monger, J.W.H., and Francheteau, J., eds., Orogenic belts and evolution of the Pacific ocean basin. *American Geophysical Union, Geodynamics Series*, v. 19, p. 115–132.

Thrasher, G.P., 1986. Basement structure and sediment thickness beneath the continental shelf of the Hauraki Gulf and offshore Coromandel region, New Zealand. *New Zealand Journal of Geology and Geophysics*, v. 29, p. 41–50.

Tykot, R.H., 2010. Sourcing of Sardinian obsidian collections in the Museo Preistorico-Etnografi co 'Luigi Pigorini' using non-destructive portable XRF, Obsidian Monte Arci in the Mediterranean: new contributions on the diffusion, production systems and their history, in *Proceedings Fifth International Conference* (ed: C Lugliè), NUR, Ales, p. 85-97.

Utadu, M., 2001. Zeolites in Hydrothermally Altered Rocks. *Reviews in Mineralogy and Geochemistry*, v. 45. p. 305-322.

Ward, K.T., Mauk, J.L., and Hall, C., 2005. New 40Ar/39Ar dates of adularia from epithermal deposits in the Hauraki goldfield, New Zealand: New Zealand Minerals Conference, Crown Minerals, 2005, *Ministry of Economic Development and Australasian Institute of Mining and Metallurgy*, New Zealand Branch, Proceedings, p. 426–433.

White, D.E., 1955. Thermal springs and epithermal ore deposits. In: Bateman, A.M. (Ed.), *Economic Geology*, p. 99– 154.

White, D.E., 1981. Active geothermal systems and hydrothermal deposits. *Economic Geology 75th Anniversary Volume*, p.392-423.

White, N.C., and Hedenquist, J.W., 1995. Epithermal gold deposits: Styles, characteristics and exploration: *Society of Economic Geology Newsletter* 23, p. 1–13.

White, N.C., Hedenquist, J.W., 1990. Epithermal environments and styles of mineralization: variations and their causes, and guidelines for exploration. *Journal of Geochemical Exploration*, 36: 445-474.

Yang, S.K., Duuring, P., Kim, Y.S., 2013. Structural genesis of the Eunsan and Moisan low-sulphidation epithermal au-Ag deposits, Seongsan district, Southwest Korea. Miner Deposita, 48: 467–483.

Appendix A

Sample Catalogue

Sample ID	Depth (m)	X	Y	Z	Rock type	Alteration Intensity	Veins	Au_ppm
CGD003_177.95	177.95	396397.13	643255.36	1014.25	0.00	4.00	0.00	0.02
CGD003_184.50	184.5	396401.88	643255.68	1010.60	0.00	4.00	1.00	0.06
CGD003_192.80	195.8	396411.26	643256.23	1003.13	1.00	4.00	1.00	0.05
CGD003_202.30	202.3	396415.93	643256.49	999.37	1.00	2.00	1.00	<0.010
CGD003_209.20	209.2	396421.76	643256.81	994.67	1.00	2.00	1.00	<0.01
CGD003_212.20	212.2	396424.10	643256.94	992.79	1.00	2.00	0.00	<0.010
CGD003_215.10	215.1	396426.43	643257.07	990.91	1.00	2.00	0.00	<0.01
CGD003_222.30	222.3	396431.49	643257.36	986.84	1.00	2.00	0.00	<0.01
CGD003_230.0	230	396438.10	643257.73	981.52	1.00	2.00	1.00	<0.01
CGD003_238.0	238	396444.33	643258.07	976.50	1.00	3.00	1.00	0.02
CGD003_244.80	244.8	396449.37	643258.36	972.41	1.00	2.00	0.00	0.01
CGD003_250.75	250.75	396453.96	643258.61	968.56	1.00	2.00	1.00	<0.01
CGD003_256.45	256.45	396457.79	643258.83	965.35	1.00	2.00	0.00	0.05
CGD003_261.95	261.95	396462.39	643259.08	961.50	1.00	1.00	1.00	0.06
CGD003_270.30	270.3	396468.52	643259.43	956.37	1.00	4.00	0.00	<0.01
CGD003_281.20	281.2	396477.33	643259.92	948.99	1.00	4.00	1.00	0.01
CGD003_292.95	292.95	396486.13	643260.41	941.62	2.00	3.00	1.00	0.02
CGD003_303.0	303	396494.08	643260.94	934.77	2.00	3.00	0.00	0.07
CGD003_315.80	315.8	396503.53	643261.57	926.62	2.00	4.00	0.00	0.39
CGD003_321.30	321.3	396507.31	643261.82	923.36	2.00	3.00	1.00	<0.01
CGD003_326.20	326.2	396511.48	643262.10	919.78	2.00	3.00	1.00	0.18
CGD003_333.90	333.9	396517.18	643262.50	914.92	2.00	4.00	0.00	0.41
CGD003_335.40	335.4	396517.94	643262.55	914.27	2.00	4.00	1.00	40.90
CGD003_343.40	343.4	396524.02	643262.98	909.09	2.00	2.00	0.00	0.02
CRO507_316.30	316.3	396508.15	643247.63	782.23	2.00	4.00	0.00	<0.010
CRO507_319.80	319.8	396509.72	643251.18	781.28	2.00	3.00	0.00	0.02
CRO507_327.70	327.7	396512.85	643258.29	779.37	2.00	3.00	1.00	2.81
CRO507_334.10	334.1	396515.40	643264.07	777.82	2.00	3.00	0.00	0.01
CRO507_338.35	338.35	396516.77	643267.18	776.98	2.00	2.00	0.00	0.01
CRO507_344.35	344.35	396519.12	643272.51	775.54	2.00	2.00	0.00	<0.010
CRO507_351.05	351.05	396521.66	643278.28	773.96	2.00	3.00	0.00	0.02
UW320_208.25	208.25	396356.84	643294.66	992.25	1.00	4.00	0.00	<0.010
UW320_216.60	216.6	396362.20	643292.82	987.33	1.00	5.00	0.00	<0.010
UW320_226.0	226	396369.69	643290.24	980.44	1.00	5.00	0.00	0.02
UW320_259.0	259	396393.11	643282.34	958.57	2.00	2.00	1.00	0.02
UW320_267.40	267.4	396399.10	643280.39	952.87	2.00	4.00	0.00	0.03
UW320_272.0	272	396401.55	643279.64	950.49	2.00	4.00	0.00	0.02
UW320_290.60	290.6	396414.50	643275.71	937.87	2.00	2.00	0.00	<0.020
UW320_308.80	308.8	396427.66	643271.62	924.79	2.00	2.00	1.00	0.05

UW320_321.50	321.5	396435.94	643269.03	916.50	2.00	2.00	0.00	0.04
UW320_328.15	328.15	396441.09	643267.44	911.28	2.00	3.00	1.00	<0.020
UW320_330.70	330.7	396441.43	643267.34	910.93	2.00	3.00	1.00	0.03
UW320_340.90	340.9	396449.60	643264.90	902.49	2.00	3.00	1.00	<0.020
UW320_358.80	358.8	396461.84	643261.27	889.80	2.00	3.00	0.00	<0.020
UW320_362.25	362.25	396464.19	643260.58	887.30	2.00	2.00	0.00	0.05
UW320_376.85	376.85	396473.95	643257.73	876.96	2.00	3.00	0.00	<0.020
UW320_382.0	382	396477.65	643256.65	873.04	2.00	2.00	0.00	0.02
UW320_397.0	397	396487.64	643253.73	862.24	2.00	2.00	0.00	0.05
UW320_399.80	399.8	396489.28	643253.25	860.41	2.00	2.00	0.00	0.03
UW320_415.60	415.6	396499.12	643250.37	849.46	2.00	3.00	1.00	0.04
UW320_425.80	425.8	396505.67	643248.45	842.16	2.00	1.00	0.00	<0.020
UW320_430.60	430.6	396508.94	643247.50	838.50	2.00	Q_vein	1.00	0.27
UW320_445.40	445.4	396518.57	643244.81	827.31	2.00	Q_Vein	1.00	31.00
UW320_448.80	448.8	396521.14	643244.10	824.33	2.00	Q_vein	1.00	10.80
UW320_465.80	465.8	396532.04	643241.04	811.65	2.00	3.00	1.00	0.05
UW320_474.0	474	396537.45	643239.50	805.28	2.00	2.00	1.00	<0.020
UW320_480.50	480.5	396541.91	643238.23	800.04	2.00	2.00	0.00	<0.020
UW320_481.20	481.2	396541.59	643238.32	800.41	2.00	2.00	1.00	<0.020
UW320_481.90	481.9	396542.23	643238.14	799.66	2.00	2.00	0.00	<0.020
UW320_483.50	483.5	396542.87	643237.95	798.91	2.00	2.00	1.00	0.03
UW320_501.15	501.15	396554.63	643234.61	785.03	2.00	3.00	0.00	<0.020
UW320_517.0	517	396564.77	643231.72	772.99	2.00	3.00	0.00	<0.020
UW320_523.80	523.8	396568.85	643230.57	768.07	2.00	3.00	0.00	<0.020
UW320_541.90	541.9	396580.11	643227.42	754.39	2.00	3.00	0.00	<0.020
UW320_559.10	559.01	396590.70	643225.41	740.61	2.00	2.00	1.00	<0.020
UW320_561.60	561.6	396591.60	643225.27	739.42	2.00	4.00	1.00	<0.020
UW320_562.65	562.65	396592.51	643225.05	738.25	2.00	3.00	1.00	0.03
UW320_564.40	564.4	396593.44	643224.78	737.11	2.00	2.00	0.00	<0.020
UW320_581.60	581.6	396603.93	643221.77	724.07	2.00	3.00	0.00	<0.020
UW320_592.40	592.4	396610.62	643219.82	715.56	2.00	3.00	0.00	<0.020
UW320_607.20	607.2	396620.05	643217.08	703.57	2.00	4.00	1.00	0.02
UW320_613.50	613.5	396623.40	643216.11	699.31	2.00	3.00	0.00	<0.020
UW320_633.0	633	396635.05	643212.85	684.03	2.00	3.00	0.00	<0.020
UW348 94.650	94.65	396656.73	643214.071	1054.274	1	3	0	<0.020
uw348_109.85	109.85	396645.74	643218.03	1043.35	1.00	3.00	0.00	<0.020
uw348_122.30	122.3	396637.31	643221.00	1034.60	1.00	3.00	0.00	<0.020
uw348_129.20	129.2	396632.62	643222.66	1029.69	1.00	3.00	0.00	<0.020
uw348_204.80	204.8	396582.76	643240.71	975.94	2.00	3.00	0.00	<0.020
uw348_211.0	211	396578.50	643242.24	971.28	2.00	4.00	1.00	0.02
uw348_217.35	217.35	396574.57	643243.66	966.97	2.00	3.00	0.00	<0.020
uw348_217.35	217.35	396574.57	643243.66	966.97	2.00	3.00	0.00	<0.020
uw348_22.50	22.5	396706.80	643195.44	1102.54	1.00	3.00	0.00	<0.020
uw348_224.35	224.35	396569.99	643245.31	961.94	2.00	3.00	0.00	0.03
uw348_227.70	227.7	396568.35	643245.90	960.15	2.00	4.00	0.00	0.02
uw348_235.20	235.2	396562.78	643247.90	954.04	2.00	4.00	1.00	<0.020
uw348_247.20	247.2	396555.62	643250.43	946.08	2.00	3.00	1.00	0.03

uw348_250.0	250	396553.67	643251.11	943.91	2.00	2.00	0.00	0.03
uw348_254.20	254.2	396550.42	643252.26	940.29	2.00	2.00	0.00	0.03
uw348_254.70	254.7	396550.10	643252.37	939.93	2.00	2.00	1.00	0.03
uw348_258.65	258.65	396548.14	643253.06	937.75	2.00	2.00	0.00	0.02
uw348_267.10	267.1	396541.97	643255.24	930.87	2.00	2.00	0.00	0.03
uw348_267.75	267.75	396541.65	643255.36	930.51	2.00	2.00	0.00	0.03
uw348_279.0	279	396534.21	643258.02	922.15	2.00	2.00	1.00	0.04
uw348_285.50	285.5	396530.65	643259.29	918.16	2.00	1.00	1.00	0.03
uw348_29.90	29.9	396701.16	643197.54	1097.26	1.00	3.00	0.00	<0.020
uw348_295.90	295.9	396523.53	643261.84	910.16	2.00	2.00	1.00	0.03
uw348_296.90	296.9	396522.89	643262.07	909.44	2.00	3.00	1.00	0.03
uw348_305.20	305.2	396517.40	643264.04	903.25	2.00	4.00	1.00	1.05
uw348_314.40	314.4	396511.91	643266.00	897.06	2.00	4.00	1.00	1.14
uw348_316.65	316.65	396510.62	643266.47	895.61	2.00	4.00	1.00	0.11
uw348_325.10	325.1	396504.49	643268.66	888.69	2.00	4.00	1.00	0.04
uw348_333.85	333.85	396499.02	643270.61	882.48	2.00	4.00	1.00	<0.020
uw348_339.0	339	396495.49	643271.87	878.46	2.00	3.00	1.00	20.30
uw348_341.25	341.25	396494.20	643272.32	877.00	2.00	4.00	1.00	0.81
uw348_352.70	352.7	396487.46	643274.73	869.32	2.00	4.00	1.00	0.02
uw348_358.70	358.7	396482.96	643276.33	864.20	2.00	3.00	1.00	0.06
uw348_364.50	364.5	396479.75	643277.47	860.54	2.00	3.00	0.00	0.03
uw348_374.55	374.55	396473.32	643279.76	853.23	2.00	3.00	0.00	0.19
uw348_41.75	41.75	396692.71	643200.68	1089.34	1.00	3.00	0.00	<0.020
uw348_52.45	52.45	396685.76	643203.30	1082.65	1.00	4.00	0.00	<0.020
uw348_63.50	63.5	396678.14	643206.17	1075.25	1.00	4.00	0.00	<0.020
uw348_65.35	65.35	396676.41	643206.83	1073.57	1.00	2.00	0.00	<0.020
uw348_75.80	75.8	396669.15	643209.57	1066.50	1.00	2.00	0.00	<0.020
uw348_84.85	84.85	396662.94	643211.82	1060.39	1.00	2.00	0.00	<0.020
uw348_94.65	94.65	396656.73	643214.07	1054.27	1.00	3.00	0.00	<0.020
uw364_100.0	100	396719.26	643243.69	1040.20	1.00	1.00	0.00	<0.050
uw364_110.0	110	396713.26	643245.66	1032.45	1.00	3.00	0.00	0.06
uw364_114.50	114.5	396711.15	643246.34	1029.74	1.00	3.00	0.00	<0.050
uw364_115.65	115.65	396710.55	643246.54	1028.97	1.00	1.00	0.00	<0.050
uw364_116.45	116.45	396709.95	643246.74	1028.19	1.00	2.00	0.00	<0.050
uw364_123.75	123.75	396705.20	643248.32	1021.95	1.00	5.00	0.00	<0.050
uw364_125.20	125.2	396704.31	643248.62	1020.78	1.00	4.00	0.00	<0.050
uw364_138.65	138.65	396696.90	643251.10	1011.03	1.00	4.00	0.00	<0.050
uw364_146.85	146.85	396691.56	643252.88	1004.01	1.00	3.00	0.00	<0.050
uw364_154.40	154.4	396687.40	643254.24	998.54	1.00	3.00	0.00	<0.050
uw364_170.70	170.7	396677.30	643257.54	985.27	1.00	3.00	0.00	<0.050
uw364_181.80	181.8	396670.76	643259.68	976.69	1.00	4.00	1.00	<0.050
uw364_181.85	181.85	396670.46	643259.78	976.30	1.00	4.00	0.00	<0.050
uw364_197.50	197.5	396661.86	643262.52	964.95	2.00	3.00	1.00	<0.050
Sample ID	**Depth (m)**	**X**	**Y**	**Z**	**Rock type**	**Alteration Intensity**	**Veins**	**Au_ppm**
uw364_208.25	208.25	396655.05	643264.63	955.93	2.00	4.00	0.00	<0.050
uw364_213.30	213.3	396652.09	643265.54	952.00	2.00	4.00	0.00	<0.050

uw364_241.20	241.2	396635.59	643270.64	929.97	2.00	4.00	0.00	0.07
uw364_241.80	241.8	396635.31	643270.75	929.57	2.00	1.00	0.00	0.07
uw364_248.85	248.85	396631.34	643272.22	923.99	2.00	3.00	0.00	<0.050
uw364_255.90	255.9	396627.37	643273.70	918.42	2.00	1.00	1.00	<0.050
uw364_281.90	281.9	396612.42	643278.50	897.71	2.00	2.00	1.00	<0.050
uw364_285.10	285.1	396610.38	643279.04	894.92	2.00	1.00	0.00	<0.050
uw364_292.30	292.3	396606.58	643280.14	889.35	2.00	1.00	0.00	<0.050
uw364_294.65	294.65	396605.42	643280.37	888.15	2.00	1.00	0.00	<0.050
uw364_307.10	307.1	396597.65	643282.48	877.31	2.00	2.00	0.00	<0.050
uw364_319.90	319.9	396590.52	643284.43	867.23	2.00	2.00	0.00	<0.050
uw364_321.20	321.2	396589.67	643284.66	866.02	2.00	2.00	1.00	<0.050
uw364_323.0	323	396588.53	643284.98	864.40	2.00	3.00	0.00	<0.050
uw364_331.85	331.85	396583.72	643286.34	857.53	2.00	3.00	1.00	<0.050
uw364_333.40	333.4	396583.17	643286.51	856.71	2.00	2.00	0.00	<0.050
uw364_360.70	360.7	396567.60	643291.30	833.94	2.00	3.00	1.00	<0.050
uw364_368.60	368.6	396563.71	643292.38	828.22	2.00	2.00	0.00	<0.050
uw364_371.20	371.2	396561.77	643292.92	825.36	2.00	2.00	0.00	<0.050
uw364_381.25	381.25	396556.21	643294.46	817.19	2.00	2.00	2.00	<0.050
uw364_391.90	391.9	396550.36	643296.05	808.62	2.00	2.00	1.00	<0.050
uw364_410.20	410.2	396539.91	643298.69	793.58	2.00	3.00	0.00	<0.050
uw364_414.40	414.4	396537.94	643299.19	790.73	2.00	2.00	0.00	<0.050
uw364_427.0	427	396530.39	643301.12	779.70	2.00	2.00	1.00	<0.050
uw364_437.05	437.05	396524.84	643302.54	771.51	2.00	Q_vein	1.00	9.68
uw364_450.80	450.8	396517.40	643304.43	760.41	2.00	3.00	0.00	0.08
uw364_464.10	464.1	396510.05	643306.25	749.23	2.00	2.00	0.00	<0.050
uw364_478.0	478	396502.48	643308.11	737.61	2.00	2.00	1.00	<0.050
uw364_79.85	79.85	396731.62	643239.61	1056.04	1.00	3.00	0.00	<0.050
uw364_84.30	84.3	396728.89	643240.53	1052.58	1.00	3.00	0.00	<0.050
uw364_89.0	89	396725.87	643241.53	1048.73	1.00	3.00	0.00	<0.050
uw364_97.30	97.3	396721.06	643243.10	1042.53	1.00	1.00	0.00	<0.050
uw364_97.35	97.35	396721.37	643243.01	1042.92	1.00	1.00	0.00	<0.050
uw364_99.75	99.75	396719.56	643243.59	1040.59	1.00	2.00	0.00	<0.050
uw364_99.75	99.75	396719.56	643243.59	1040.59	1.00	2.00	0.00	<0.050

Appendix B

List of Data in the DVD enclosed with this thesis.

4. Thin section microscopy pictures.
5. XRD data.
6. pXRF data.
7. Aqua-Regia analysis results.
8. Thesis copy
9. Maps and Figures
10. Newmont Waihi drillcore photos
11. Newmont Waihi drill logs
12. Assay results from Newmont Waihi
13. Pictures and Maps from Newmont Waihi
14. Other miscellaneous data.